LEVEL

RADC-TR-81-215
Final Technical Report
August 1981

SPACE-BASED RADAR ARRAY
SYSTEM SIMULATION AND VALIDATION

Atlantic Research Corporation

Harvey K. Schuman
Donald R. Pflug
Larry D. Thompson

AD A106996

DTIC
SELECTED
NOV 4 1981
A

ROME AIR DEVELOPMENT CENTER
Air Force Systems Command
Griffiss Air Force Base, New York 13441

81 11 02 208

This report has been reviewed by the RADC Public Affairs Office (PA) and is releasable to the National Technical Information Service (NTIS). At NTIS it will be releasable to the general public, including foreign nations.

RADC-TR-81-215 has been reviewed and is approved for publication.

APPROVED: *Russell C. Steenrod*

RUSSELL C. STEENROD, Captain, USAF
Project Engineer

APPROVED: *Frank J. Rehm*

FRANK J. REHM
Technical Director
Surveillance Division

FOR THE COMMANDER: *John P. Huss*

JOHN P. HUSS
Acting Chief, Plans Office

If your address has changed or if you wish to be removed from the RADC mailing list, or if the addressee is no longer employed by your organization, please notify RADC.(OCSA) Griffiss AFB NY 13441. This will assist us in maintaining a current mailing list.

Do not return copies of this report unless contractual obligations or notices on a specific document requires that it be returned.

REPORT DOCUMENTATION PAGE

READ INSTRUCTIONS
BEFORE COMPLETING FORM

1. REPORT NUMBER	2. GOVT ACCESSION NO.	3. RECIPIENT'S CATALOG NUMBER
RADC-TR-81-215	AD-A106 996	

4. TITLE (and Subtitle)	5. TYPE OF REPORT & PERIOD COVERED
SPACE-BASED RADAR ARRAY SYSTEM SIMULATION AND VALIDATION	Final Technical Report. 7 Mar 79—7 Mar 81
	6. PERFORMING ORG. REPORT NUMBER
	N/A

7. AUTHOR(s)	8. CONTRACT OR GRANT NUMBER(s)
Harvey K. Schuman Donald R. Pflug Larry D. Thompson	F30602-79-C-0116

9. PERFORMING ORGANIZATION NAME AND ADDRESS	10. PROGRAM ELEMENT. PROJECT, TASK AREA & WORK UNIT NUMBERS
Atlantic Research Corporation 1721 Black River Blvd Rome NY 13440	62702F 45061437

11. CONTROLLING OFFICE NAME AND ADDRESS	12. REPORT DATE
Rome Air Development Center (OCSA) Griffiss AFB NY 13441	August 1981
	13. NUMBER OF PAGES
	95

14. MONITORING AGENCY NAME & ADDRESS(if different from Controlling Office)	15. SECURITY CLASS. (of this report)
Same	UNCLASSIFIED
	15a. DECLASSIFICATION/DOWNGRADING SCHEDULE
	N/A

16. DISTRIBUTION STATEMENT (of this Report)

Approved for public release; distribution unlimited.

17. DISTRIBUTION STATEMENT (of the abstract entered in Block 20, if different from Report)

Same

18. SUPPLEMENTARY NOTES

RADC Project Engineer: Russell C. Steenrod, Captain, USAF (OCSA)

19. KEY WORDS (Continue on reverse side if necessary and identify by block number)

Space Fed Lens	Space-Based Radar
Infinite Arrays	Antenna
Moment Methods	RF Lens

20. ABSTRACT (Continue on reverse side if necessary and identify by block number)

The present status of the space-based radar phased array lens simulator is discussed. Huge arrays of thin wire radiating elements on either side of a ground screen are modeled by the simulator. Also modeled are amplitude and phase adjust modules connecting radiating elements between arrays, feedline to radiator mismatch, and lens warping. A successive approximation method is employed. The first approximation is based on a plane wave expansion (infinite array) moment method especially suited →

DD FORM 1473 EDITION OF 1 NOV 65 IS OBSOLETE
1 JAN 73

UNCLASSIFIED

to large array analysis. The first approximation results then facilitate higher approximation computations that account for effects of nonuniform periodicities (lens edge, lens section interfaces, failed modules, etc.). The programming to date is discussed via flow diagrams. An improved theory is presented in a consolidated development. The use of the simulator is illustrated by computing active impedances and radiating element current distributions for infinite planar arrays of straight and "swept back" dipoles (arms inclined with respect to the array plane) with feedline scattering taken into account.

TABLE OF CONTENTS

i

A

LIST OF ILLUSTRATIONS

SECTION 1

INTRODUCTION

This report describes the present status of a computer program for sim-
ulating the RF behavior of space-based radar (SBR) phased array lens antennas.
A typical SBR candidate lens is shown in Figure 1. The transmitter provides
the space feed that illuminates the lens during radar transmit. The space
feed may be in the form of several independently controlled beams that pro-
vide lens radiation pattern shaping, adaptive nulling, and time delayed lens
sector illumination. (The time delayed compensation is required because of
significantly different transmitter-to-lens path lengths to different points
on the lens). Beam steering and, possibly, amplification are performed by
the lens.

A lens comprising two arrays of thin wire radiators separated by a
ground screen currently is modeled in the simulator. The theory, with
straightforward modifications, can be extended to apply to other lens types
such as those composed of microstrip arrays.

A typical wire radiator lens section, that can be analyzed by the sim-
ulator, is shown in Figure 2. For simplicity, dipole radiating elements are
indicated. The simulator also is capable of analyzing other element types;
e.g., folded dipole, turnstile, and parasitic. The array lattices may be
skewed. Focusing and scanning of the lens-transmitted main beam is accom-
plished by electronic modules interconnecting the radiating elements between
the illuminated and nonilluminated arrays (Figure 3). These modules also
may provide power amplification.

A successive approximation method is employed whereby infinite array
analysis provides a first approximation of array currents and patterns.
Higher approximations then are obtained, with relative ease, by methods that
draw upon these first approximation currents. The higher approximations pro-
vide corrections to the currents on elements in the vicinity of discontinui-
ties in periodicities; e.g., lens edges, lens section interfaces, and failed
modules. A section of uniform periodicity of a lens is called a cell.

The first approximation patterns, although involving large numbers of
elements, are computed from closed form expressions. Since the number of
elements with currents perturbed from their infinite array values is expected

1

LENS

TRANSMITTER/RECEIVER

MAST

SOLAR COLLECTOR
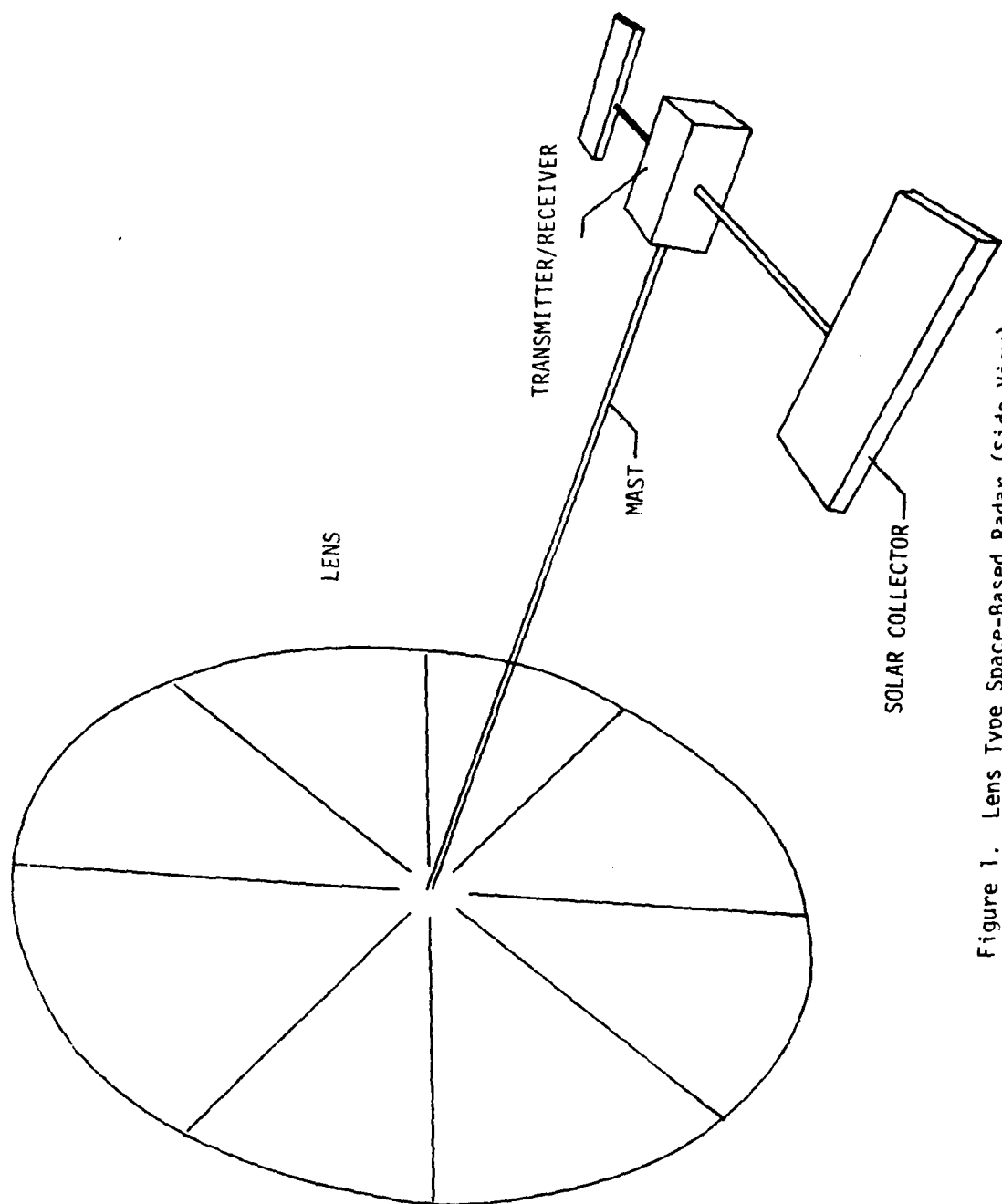
Figure 1. Lens Type Space-Based Radar (Side View)

2

GROUND SCREEN

ARRAY b
ELEMENT

ARRAY a
ELEMENT

AXES x,y,e LIE IN GROUND
SCREEN; z NORMAL TO GROUND
SCREEN
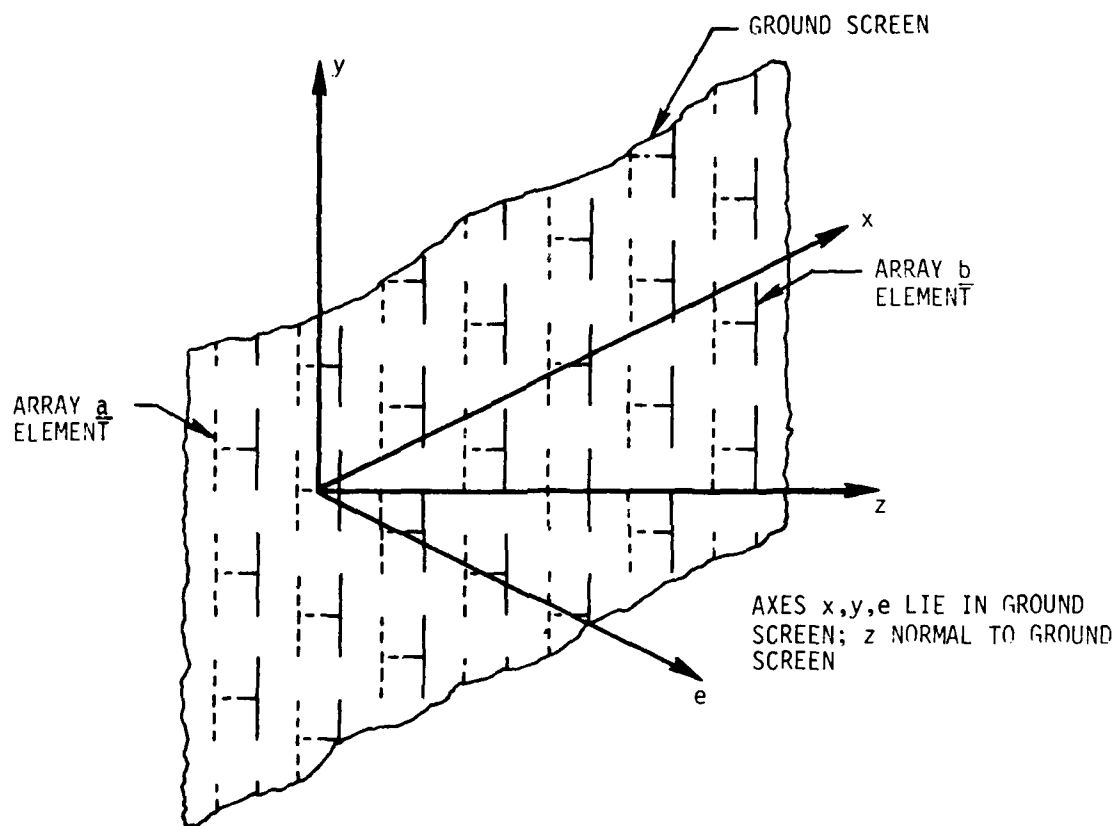
Figure 2. Skewed Lattice Dipole Lens

3
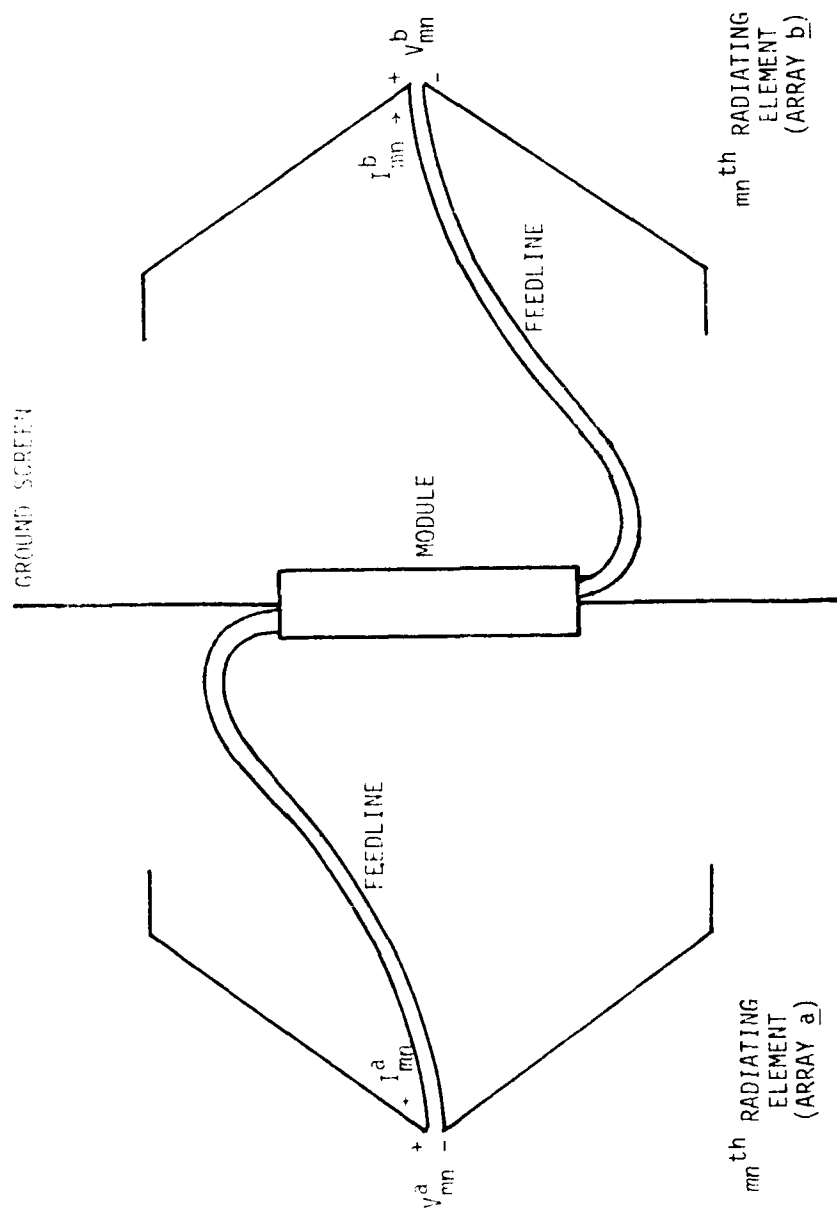
Figure 3. Lens Cross Section

to be relatively small, higher approximation "correction patterns" may be computed by direct summation of the field from each element. The superposition of the first approximation and correction patterns results in the overall pattern. This approach takes maximum advantage of the nominal periodicities and largeness of the arrays. It is as computationally manageable in the radar receive mode as in the radar transmit mode without resorting to reciprocity. This is important since the modules may be nonreciprocal. This approach also may avoid the need for a Fast Fourier Transform (FFT) for pattern computation. An FFT is not practical if, for example, fine angular pattern resolution in the vicinity of a null is required.

An infinite array analysis usually assumes plane wave excitation. During radar transmit, the illuminating field is expected to differ smoothly from a plane wave across the face of the lens. This difference is taken into account by expanding the beamformer field illuminating a cell in plane waves and analyzing the cell separately for each plane wave component.

The first approximation method is an extension of a moment method, plane wave expansion technique recently suggested by Munk and Burrell [1]. It is applicable to lens arrays composed of arbitrarily shaped wire radiating elements. The elements may be inclined with respect to the array plane. Feedline scattering, a nonflat lens, amplitude and phase adjust modules between the arrays, and an imperfect ground screen also are taken into account. (The nonflat lens is modeled in "piecewise" fashion by allowing the cells to be tilted with respect to each other.) The plane wave expansion technique facilitates computing the array-to-array coupling through the imperfect ground screen and suggests straightforward extensions, not discussed here, applicable to dielectric support sheets (e.g., Kevlar and Kapton) on which the radiators may be mounted.

The infinite array lens analysis facilitates computation by providing the first approximation solution to a finite array lens. It also provides clues to the performance of several important finite (but large) lens characteristics. For example, the array active impedance variation with module phase setting, an important parameter for module designers, can be assessed directly. The effect of imperfect ground screen "feedback" from the target side to the feed side of the lens also can be observed, and lens warping (nonflat lens) treated.

The application and generation of infinite array theory and the moment method in arriving at a first approximation to the lens radiating element currents has been detailed in [5]. This theory has since been improved and corrected and the development consolidated. The revision is given in Section 2. The principal improvement lies in replacing a pulse expansion-pulse matching moment method with a pulse expansion-point matching-finite difference operator moment method. Section 4 shows, through comparison with another method, that the "finite difference" method is computationally more accurate and efficient than the "pulse matching" method. Also, radiator arms inclined with respect to the array plane are modeled far simply with the "finite difference" method.

The theory underlying the higher approximations current computation and the first and higher approximations pattern computation is essentially unchanged from that in [5] and not repeated here.

The main computer programs and subprograms are described in Section 3. A general module model in terms of two-port scattering parameters is not yet implemented but should be available shortly. Two limited module models – an S parameter transmission line passive phase shifter model and the impedance representation described in [5] – presently are implemented and are included in the program descriptions. Data input is described in Section 3.3.11.

Section 4 gives results of applying the first approximation plane wave expansion (infinite array) moment method to active impedance and current distribution computations for dipole array elements with feedline scattering accounted for. Results for "swept back"-dipole arrays also are given. This is the first time theoretical active impedance and current computations of infinite planar arrays of radiating elements inclined with respect to the array plane have been reported.

SECTION 2

IMPROVEMENT AND CONSOLIDATION OF FIRST APPROXIMATION THEORY

A combined plane wave expansion moment method technique is applied in obtaining a first approximation of the radiating element currents in a lens. It is applicable to lens sections (cells) composed of many identical arbitrarily bent wire radiating elements in each of two parallel arrays. It also accounts for amplitude and phase adjust modules interconnecting the arrays and an imperfect ground screen between the arrays. In particular, the technique permits the modules to be progressively phased although the module amplitude adjustments must be uniform throughout each cell.

A lens formed by two planar, periodic infinite dipole arrays, $\underline{a}$ and $\underline{b}$ on either side of a finitely conducting infinite ground screen is shown in Figure 2. An exciting plane wave, $\vec{E}^{ex}$, that is arriving from the negative z side is directly incident on array $\underline{a}$ (Figure 3). Amplitude and phase adjust modules connect array $\underline{a}$ to array $\underline{b}$. Array $\underline{a}$ faces the radar transmitter during radar transmit and faces the target during receive. Array $\underline{a}$ thus is always on the illuminated side and array $\underline{b}$ is always on the nonilluminated side. Each array lattice may be general rectilinear (skewed) of which "rectangular" is a special case. Array $\underline{a}$ elements may differ from array $\underline{b}$ elements; however, each element within an array is assumed identical.

The following analysis of this lens is not restricted to dipole array elements. Each element can be a collection of thin bent wires; e.g., folded dipole or dipole with parasitic scatterers. The elements can be inclined with respect to the array plane. Also feedline scattering is considered.

The analysis is structured around a port representation. Each pair of terminals entering an array element is assumed to be a port. The port voltages and currents are shown in Figure 3. The superscript (a or b) indicates the array. The subscript indicates the element location with reference to Figure 4 where mn denotes the mth element along a line parallel to the lattice e coordinate and n^{th} element along a line parallel to the lattice y coordinate. The mn = 00 elements lie on the z axis and are referred to as the reference elements.

7
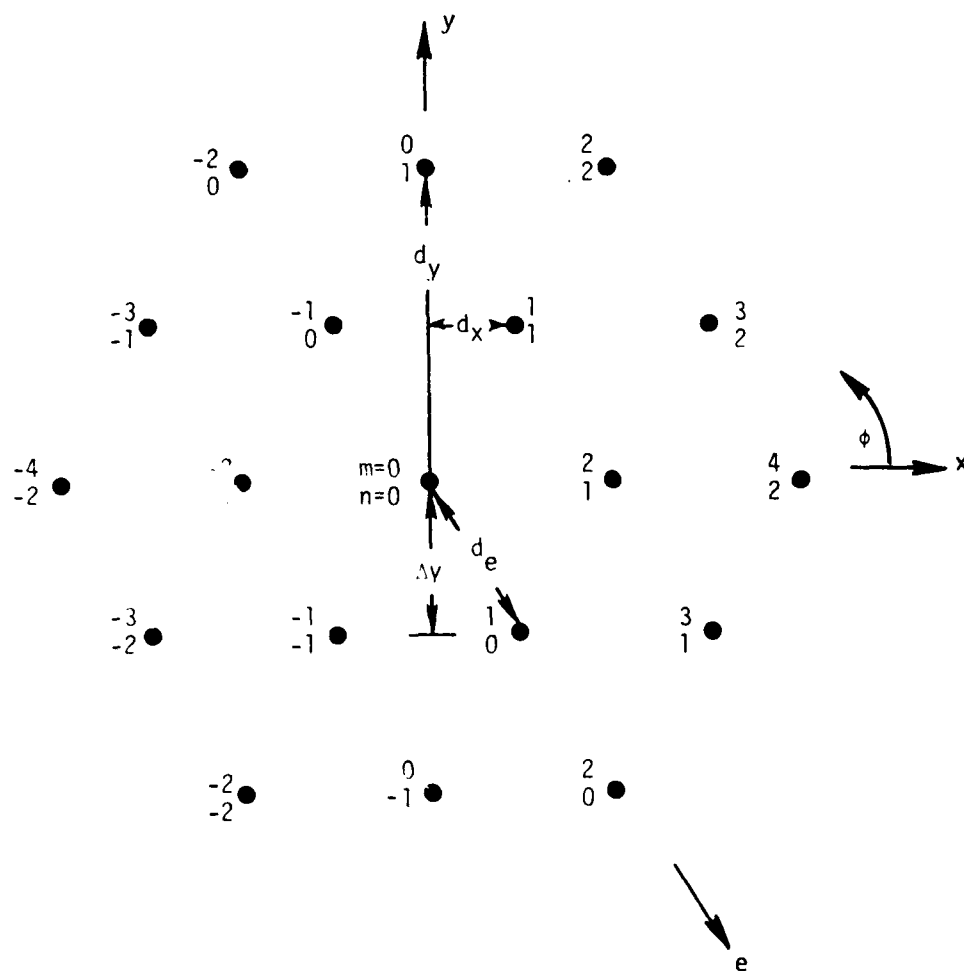
Figure 4. General Rectilinear (Skewed) Lattice

8

Balanced mode transmission line theory, applied to the mn^{th} elements' feedlines and module, is employed in relating the mn^{th} element array $\underline{a}$ port current and voltage to the mn^{th} element array $\underline{b}$ port current and voltage. This relationship is combined with a second relationship between the port voltages and currents in achieving a solution for all port voltages and radiating element current distributions. The second relationship employs a plane wave expansion moment method technique that accounts for all radiation coupling including field penetration through the ground screen and feedline (unbalanced mode) scattering. The feedlines, whether coaxial or twin wire, are modeled (Figure 5) as single thin wires. If the actual feedline is twin wire, the radius of the feedline model wire is chosen such that the model and the actual twin wire exhibit approximately the same scattering.

The Figure 5 model assumes zero unbalanced mode feedline currents at the element ports. The model also does not allow unbalanced feedline currents to flow through the modules. These assumptions can be removed by employing more general, but more complicated, models, e.g., treating modules as four-ports instead of two-ports and permitting multiple wire junctions at the feed ports.

2.1 PORT REPRESENTATION AND SOLUTION

Array $\underline{a}$ and array $\underline{b}$ port currents are determined by requiring that they satisify the port boundary conditions*

$$V_{mn}^{a} = V_{mn}^{aa} + V_{mn}^{ab} + V_{mn}^{ex} \tag{1}$$

$$V_{mn}^{b} = V_{mn}^{bb} \tag{2}$$

where

V_{mn}^{a} and V_{mn}^{b} , the total port voltages, are related to I_{mn}^{a} and I_{mn}^{b} via the mn^{th} module (including feedlines) two-port parameters;

V_{mn}^{aa} is the array $\underline{a}$ mn^{th} element port voltage with $\vec{E}^{ex} = 0$, the ground screen assumed perfectly conducting, and the array $\underline{a}$ ports excited with the I_{mn}^{a} as ideal current sources (Figure 6);

---

* A suppressed $\exp[j\omega t]$ temporal variation is assumed throughout the development.
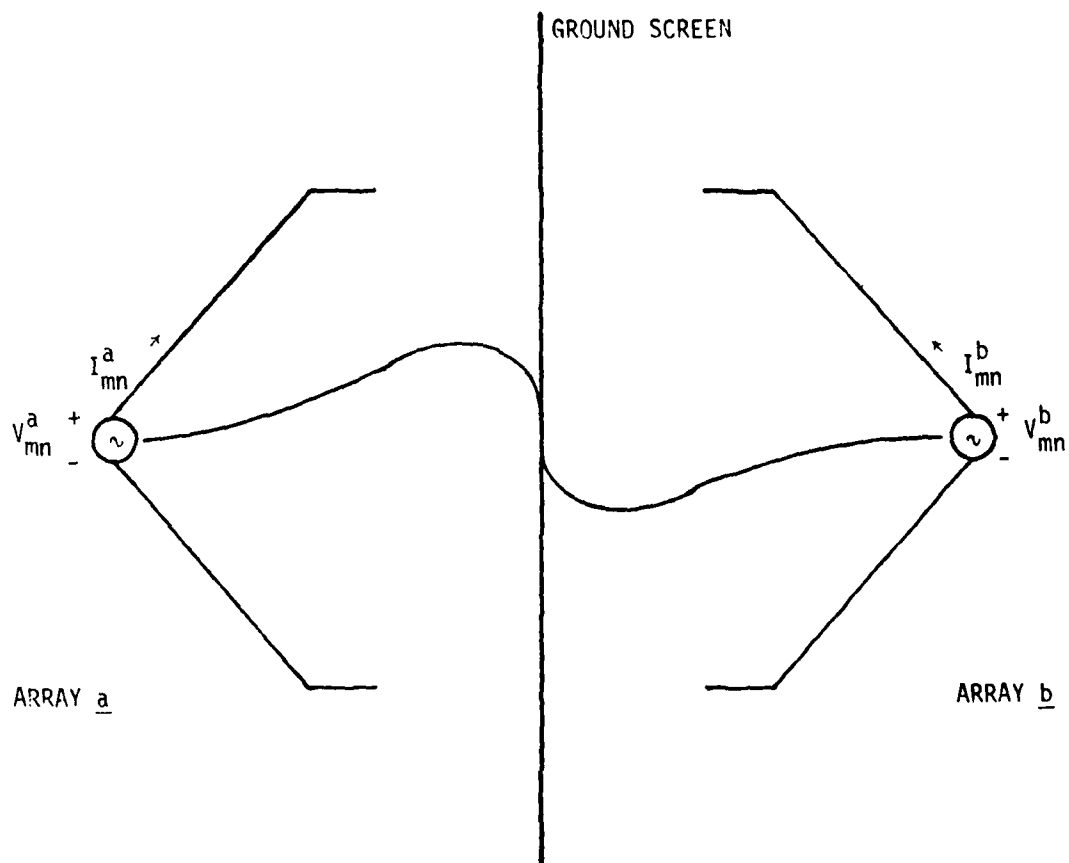
Figure 5. Model for Including Feedline Scattering
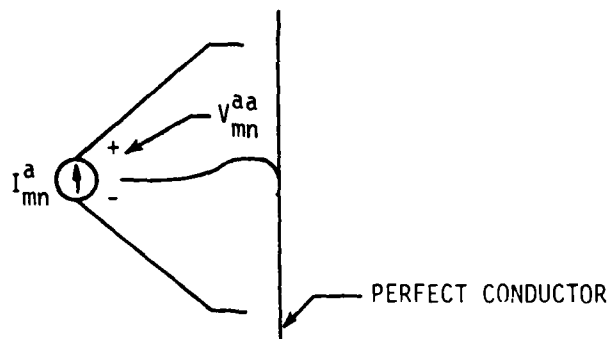
Figure 6. Problem Defining V_{mn}^{aa}
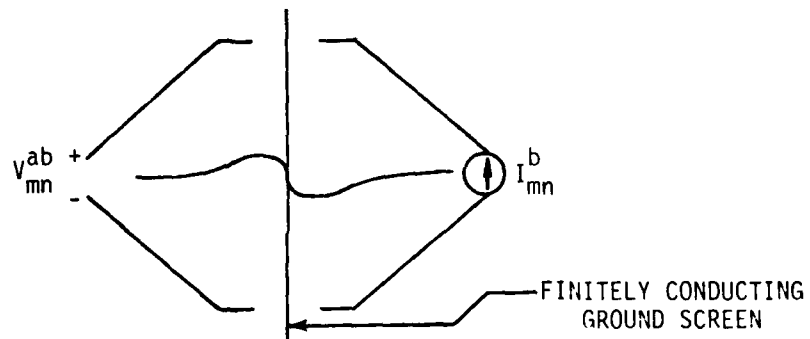
Figure 7. Problem Defining V_{mn}^{ab}
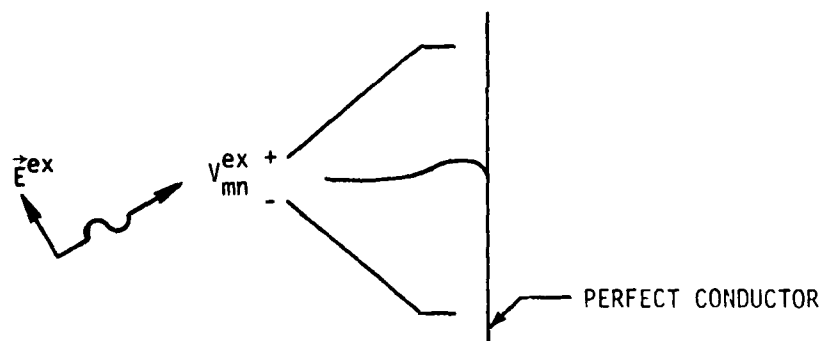
Figure 8. Problem Defining V_{mn}^{ex}

11

V_{mn}^{bb} is the array b counterpart to V_{mn}^{aa};

V_{mn}^{ab} is the array a mn^{th} element port voltage with $\vec{E}^{ex} = 0$, all

array a ports open-circuited, and the I_{mn}^{b} as ideal current

sources exciting the array b ports (Figure 7);

V_{mn}^{ex} is the array a mn^{th} element port voltage with all array a

ports open-circuited and the ground screen assumed perfectly

conducting (Figure 8).

In arriving at (1) and (2), the finite conductivity of the ground screen
is considered significant with regard to feedback from array b to array a.
Severe pattern degradation may result if the module amplification is compara-
ble to the ground screen attenuation; therefore, it is important to preserve
this effect in the model.

Since the excitation is assumed to be a plane wave, the relationship of
the current on the mn^{th} element to the reference (00th) element current is
known. It therefore is necessary to solve (1) and (2) for the reference ele-
ment current only. Each array element is modeled as piecewise linear and the
array is viewed as a collection of infinite arrays, each one corresponding to
one linear segment. A moment method procedure is applied where each expansion
function is one of the infinite arrays. The field from each "expansion array"
is expressed as a doubly infinite sum of plane waves. One advantage of this
plane wave expansion is that penetration through imperfect ground screens
becomes straightforward.

The method presented here is an extension of Munk and Burrell's work in
that interconnecting modules are introduced between arrays and, more impor-
tantly, the modules may differ from element to element. In particular, the
modules may introduce a linear progressive phase and thus differ in a well-
defined manner. If the modules are identical, the incident plane wave

$$\vec{E}^{ex} (\vec{r}) = \vec{E}^{ex} (\vec{0}) \exp[-jks_x x -jks_y y -jks_z z]$$

12

excites port currents of the form

$$I_{mn}^a = I_{00}^a \exp [-jkmd_e s_e - jknd_y s_y] \qquad (3)$$

$$I_{mn}^b = I_{00}^b \exp [- jkmd_e s_e - jknd_y s_y] \qquad (4)$$

where

$\vec{r} = x\hat{x} + y\hat{y} + z\hat{z}$ is a field point position vector;

$\hat{x}, \hat{y}, \hat{z}$ are the rectangular coordinate system unit vectors;

k is the propagation constant;

s_x, s_y, s_z are the rectangular coordinate directional cosines of the propagation direction of $\vec{E}^{ex}$;

d_e and i_y are the lattice e and y interelement spacings; (Figure 4);

I_{00}^a and I_{00}^b are the reference element port currents.

The directional cosine s_e is given in terms of s_x and s_y by [5 (Section 3.2.4)]

$$s_e = \frac{d_x s_x - \Delta y s_y}{d_e}$$

where d_x and Δy are defined in Figure 4.

The justification for (3) and (4) can be demonstrated from linearity considerations; a similar form applies to the induced port voltages. Equations (3) and (4) are not sufficiently general if the modules are progressively phased. If the phase imparted by the mn^{th} module with respect to the reference module is $-k(md_e \alpha_e + nd_y \alpha_y)$, the feedback phenonmenon due to the imperfect ground screen and impedance mismatch suggests port currents of the forms

$$I_{mn}^a = \sum_{u=-\infty}^{\infty} I_{00(u)}^a \exp [-jkmd_e (s_e + u\alpha_e) - jknd_y (s_y + u\alpha_y)] \qquad (5)$$

$$I_{mn}^b = \sum_{u=-\infty}^{\infty} I_{00(u)}^b \exp [- jkmd_e (s_e + u\alpha_e) - jknd_y (s_y + u\alpha_y)] \qquad (6)$$

13

where u is referred to as a feedback mode number. The $I^a_{00(u)}$ and $I^b_{00(u)}$ are the uth mode coefficients of array $\underline{a}$ and array $\underline{b}$ reference element port currents determined as described below, by satisfying (1) and (2) with (5) and (6).

With port currents expressed by (5) and (6), V^{aa}_{mn}, V^{bb}_{mn}, V^{ab}_{mn} in (1) and (2) become

$$V^{aa}_{mn} = \sum_{u=-\infty}^{\infty} z^{aa} [s_e + u\alpha_e, s_y + u\alpha_y] \, I^a_{00(u)} \exp [-jkmd_e (s_e + u\alpha_e)$$
$$- jknd_y (s_y + u\alpha_y)]$$

$$V^{bb}_{mn} = \sum_{u=-\infty}^{\infty} z^{bb} [s_e + u\alpha_e, s_y + u\alpha_y] \, I^b_{00(u)} \exp [-jkmd_e (s_e + u\alpha_e)$$
$$- jknd_y (s_y + u\alpha_y)]$$

$$V^{ab}_{mn} = \sum_{u=-\infty}^{\infty} z^{ab} [s_e + u\alpha_e, s_y + u\alpha_y] \, I^b_{00(u)} \exp [-jkmd_e (s_e + u\alpha_e)$$
$$- jknd_y (s_y + u\alpha_y)]$$

where , for u = 0,

$z^{aa} [s_e, s_y]$ is the array $\underline{a}$ active impedance when driven by port
currents (3) and the ground screen perfectly conducting;

$z^{bb} [s_e, s_y]$ is the array $\underline{b}$ active impedance when driven by port
currents (4) and the ground screen perfectly conducting;

$z^{ab} [s_e, s_y]$ is the active mutual impedance from array $\underline{b}$ ports to
array $\underline{a}$ ports with array $\underline{b}$ excited by port currents (4) and
array $\underline{a}$ open-circuited (feedlines removed).

14

Specifically,

$$z^{aa}[s_e, s_y] = \frac{V^{aa}_{00}}{I^{a}_{00}} \Bigg|_{\text{perfect ground screen}}$$

$$z^{bb}[s_e, s_y] = \frac{V^{bb}_{00}}{I^{b}_{00}} \Bigg|_{\text{perfect ground screen}}$$

$$z^{ab}[s_e, s_y] = \frac{V^{ab}_{00}}{I^{b}_{00}} \Bigg|_{\substack{\text{imperfect ground screen, array } \underline{a} \text{ ports} \\ \text{open-circuited}}}$$

where I^{a}_{00} and I^{b}_{00} are reference element port currents with the arrays excited by port currents related by (3) and (4). A moment method technique for computing $z^{aa}[s_e, s_y]$, $z^{bb}[s_e, s_y]$, and $z^{ab}[s_e, s_y]$ is described in Section 2.2. Similar relations hold for $u \neq 0$.

A means for determing the short-circuit array $\underline{a}$ port currents

$$I^{ex}_{mn} = I^{ex}_{00} \exp\left[- jkmd_e s_e - jknd_y s_y\right]$$

due to $\vec{E}^{ex}$ with the ground screen perfectly conducting, is described in Section 2.2. The V^{ex}_{mn} in (1) then are given by [5, Eq. (3-20)]

$$V^{ex}_{mn} = - z^{aa}[s_e, s_y] \, I^{ex}_{00} \exp\left[-jkmd_e s_e - jknd_y s_y\right] \tag{7}$$

where the reference direction for I^{ex}_{mn} is the same for I^{a}_{mn} in Figure 5.

In column vector notation, (5) and (6) can be represented as

$$\bar{I}_{mn} = \sum_{u=-\infty}^{\infty} \bar{I}_{00(u)} \exp\left[-jkmd \, (s_e + u\alpha_e) - jknd_y (s_y + u\alpha_y) \right] \tag{8}$$

15

where

$$\bar{I}_{00(u)} = \begin{bmatrix} I^a_{00(u)} \\ \\ I^b_{00(u)} \end{bmatrix}$$

$$\bar{I}_{mn} = \begin{bmatrix} I^a_{mn} \\ \\ I^b_{mn} \end{bmatrix}$$

The port conditions that must be satisfied are

$$\bar{V}_{mn} = \begin{bmatrix} V^{aa}_{mn} + V^{ab}_{mn} \\ \\ V^{bb}_{mn} \end{bmatrix} + \begin{bmatrix} V^{ex}_{mn} \\ \\ 0 \end{bmatrix}$$

where

$$\bar{V}_{mn} = \begin{bmatrix} V^a_{mn} \\ \\ V^b_{mn} \end{bmatrix}$$

This may be written

$$\bar{V}_{mn} = \sum_{u=-\infty}^{\infty} \left[[z_u] \, I_{00(u)} \, \exp \, [-jkmd_e(s_e+u\alpha_e) - jknd_y(s_y+u\alpha_y)] \right.$$
$$\left. + \exp \, [-jkmd_e s_e - jknd_y s_y] \, \bar{V}^{ex}_{00} \right] \tag{9}$$

16

where

$$[z_u] = \begin{bmatrix} z^{aa}[s_e+u\alpha_e, s_y+u\alpha_y] & z^{ab}[s_e+u\alpha_e, s_y+u\alpha_y] \\ \\ 0 & z^{bb}[s_e+u\alpha_e, s_y+u\alpha_y] \end{bmatrix}$$

$$\bar{V}_{00}^{ex} = \begin{bmatrix} -z^{aa}[s_e, s_y] \; I_{00}^{ex} \\ \\ 0 \end{bmatrix}$$

Let the mn^{th} module (plus feedlines) scattering parameter matrix be denoted $[S_{mn}]$. If the scattering parameter normalizing impedances are R^a and R^b for the array a and b sides respectively,

$$\bar{V}_{mn} = [R]^{1/2}([U] + [S_{mn}])\bar{C}_{mn} \tag{10}$$

$$\bar{I}_{mn} = -[R]^{-1/2}([U] - [S_{mn}])\bar{C}_{mn} \tag{11}$$

where

$$[U] = \begin{bmatrix} 1 & 0 \\ 0 & 1 \end{bmatrix}$$

$$[R] = \begin{bmatrix} R^a & 0 \\ 0 & R^b \end{bmatrix}$$

$$\bar{C}_{mn} = \begin{bmatrix} C_{mn}^a \\ C_{mn}^b \end{bmatrix}$$

17

and c_{mn}^a and c_{mn}^b are the "incident" scattering variables. Assume that $\bar{C}_{mn}$ may be expanded in "feedback" modes, as is $\bar{I}_{mn}$, according to

$$\bar{C}_{mn} = \sum_{u=-\infty}^{\infty} \bar{C}_{00(u)} \exp\left[-jkmd_e(s_e+u\alpha_e) - jknd_y(s_y+u\alpha_y)\right] \qquad (12)$$

Then (9), (10), and (12) combine to yield

$$\sum_{u=-\infty}^{\infty} \exp\left[-jkmd_e u\alpha_e - jknd_y u\alpha_y\right] \left[[R]^{1/2}([U] + [S_{mn}])\bar{C}_{00(u)} \right. \qquad (13)$$

$$\left. - [z_c]\bar{I}_{00(u)} \right] = \bar{V}_{00}^{ex}$$

Another equation in $\bar{C}_{00(u)}$ and $\bar{I}_{00(u)}$, obtained from (8), (11), and (12), is

$$\sum_{u=-\infty}^{\infty} \exp\left[-jkmd_e u\alpha_e - jknd_y u\alpha_y\right] \left[[R]^{1/2}([U] - [S_{mn}])\bar{C}_{00(u)} \right. \qquad (14)$$

$$\left. + \bar{I}_{00(u)} \right] = \bar{0}$$

where $\bar{0}$ is the null column vector. A set of simultaneous equations is formed from (13) and (14). The module "phase settings", α_e and α_y, will be of such magnitude that $[S_{mn}]$ repeats every M x N elements. Premultiplication of (13) and (14) by $\exp[j2\pi mvM'/M + j2\pi nvN'/N]$, where v is an integer, summation over one "progressive phase period," 1_m_M and 1_n_N, and interchange of summations yields

18

$$\sum_{u=-\infty}^{\infty} ([F'_{vu}]\bar{C}_{00(u)} - [F_{vu}][z_u]\bar{I}_{00(u)}) = \begin{cases} NM \ \bar{V}_{00}^{ex} & v=0 \\ \\ \bar{0} & v=\pm1,\pm2,\ \ldots \end{cases} \quad (15)$$

$$\sum_{u=-\infty}^{\infty} ([F''_{vu}]\bar{C}_{00(u)} + [F_{vu}]\bar{I}_{00(u)}) = \bar{0} \quad v=0,\pm1,\pm2,\ \ldots \quad (16)$$

where

$$[F'_{vu}] = \sum_{n=1}^{N}\sum_{m=1}^{M} \exp\left[j2\pi m(v-u)M'/M + j2\pi n(v-u)N'/N\right]$$
$$[R]^{\frac{1}{2}}([U]+[S_{mn}]) \quad (17)$$

$$[F''_{vu}] = \sum_{n=1}^{N}\sum_{m=1}^{M} \exp\left[j2\pi m(v-u)M'/M + j2\pi n(v-u)N'/N\right]$$
$$[R]^{-\frac{1}{2}}([U]-[S_{mn}]) \quad (18)$$

$$[F_{vu}] = \sum_{n=1}^{N}\sum_{m=1}^{M} \exp\left[j2\pi m(v-u)M'/M + j2\pi n(v-u)N'/N\right][U]$$
$$= \begin{cases} MN[U] & u=v \\ 0 & \text{otherwise} \end{cases} \quad (19)$$

The simplications resulting in the right-hand sides of (15) and (19) assume
that $(v-u)M'/M$ and $(v-u)N'/N$ are never integers simultaneously. This condition
occurs whenever $(v-u)$ is an integer multiple of M and N simultaneously. This
condition is avoided by limiting (15) and (19) to only the lower valued

equations in $|v|$ and by limiting the infinite summations to only lower values of $|u|$. This is permissible if only lower-ordered "feedback" modes, u, are significant.

A special case of interest is a passive lens with modules replaced by transmission lines. The relative lengths of line determine the progressive phasing. The scattering parameters for the mn^{th} element become

$$[S_{mn}] = \exp\left[-j2\pi m \frac{M'}{M} -j2\pi n \frac{N'}{N}\right][W]$$

if $R^a = R^b = R_0$, where R_0 is the characteristic impedance of the transmission line and

$$[W] = \begin{bmatrix} 0 & \exp[-jk\ell_0] \\ \exp[-jk\ell_0] & 0 \end{bmatrix}$$

where ℓ_0 is the length of the reference element transmission line. Equations (17) and (18) reduce to

$$[F'_{vu}] = \begin{cases} \sqrt{R_0}\ MN\ [U] & v - u = 0 \\ \sqrt{R_0}\ MN\ [W] & v - u - 1 = 0 \\ 0 & \text{otherwise} \end{cases}$$

$$[F''_{vu}] = \begin{cases} (MN/\sqrt{R_0})\ [U] & v - u = 0 \\ (-MN/\sqrt{R_0})\ [W] & v - u - 1 = 0 \\ 0 & \text{otherwise} \end{cases}$$

Equations (15) and (16) then become

$$\sqrt{R_0}\ \bar{C}_{00(v)} + \sqrt{R_0}\ [W]\bar{C}_{00(v-1)} - [z_v]\bar{I}_{00(v)} = \begin{cases} \bar{V}^{ex}_{00} & v = 0 \\ \bar{0} & v = \pm 1, \pm 2, \ldots \end{cases} \quad (20)$$

$$-\frac{1}{\sqrt{R_0}}\ \bar{C}_{00(v)} - \frac{1}{\sqrt{R_0}}\ [W]\bar{C}_{00(v-1)} + \bar{I}_{00(v)} = \bar{0} \quad v = 0, \pm 1, \pm 2, \ldots \quad (21)$$

20

Finally, (20) and (21) can be combined to form

$$\left[\sqrt{R_0}[U] + \frac{1}{\sqrt{R_0}}[z_v]\right]\bar{C}_{00(v)} + \left[-\frac{1}{\sqrt{R_0}}[z_v] + \sqrt{R_0}[U]\right][W]\bar{C}_{00(v-1)}$$

$$= \begin{cases} \bar{V}_{00}^{ex} & v = 0 \\ \\ \bar{0} & v = \pm1,\pm2,\ldots \end{cases} \tag{22}$$

Equation (22) can be solved for $\bar{C}_{00(v)}$ under the previously stated

condition that only lower-ordered feedback modes are significant. Then

(21) can be solved for $I_{00(v)}$.

2.2 PLANE-WAVE EXPANSION MOMENT METHOD

The array $\underline{a}$ and $\underline{b}$ active impedances, $z^{aa}(s_e,s_y)$, $z^{bb}(s_e,s_y)$, array $\underline{b}$ to

array $\underline{a}$ mutual impedance $z^{ab}(s_e,s_y)$, and the array $\underline{a}$ reference element short-

circuit port current I_{00}^{ex}, are considered in this section. The development is

not limited to array radiating elements oriented in the plane of the array.

Scattering from element feedlines and radiation and scattering from elements

having arms inclined with respect to the array plane, thus, are accounted for.

Consider first array $\underline{b}$ with the ground screen absent. A port voltage

or current source array excitation that is uniform, except for the pro-

gressive phase $-jk(md_e s_e + nd_y s_y)$ imparted at the mn^{th} element with

respect to the reference element (m = n = 0), results in the current

$$\vec{I}_{mn}(\vec{r}'+\vec{r}_{mn}) = \vec{I}_{00}(\vec{r}') \exp[-jkmd_e s_e - jknd_y s_y] \tag{23}$$

along the mn^{th} element wire axis, where $\vec{r}'$ is a point along the reference ele-

ment wire axis (path C' of Figure 9) and $\vec{r}_{mn}$ is the vector from the reference

element feed to the mn^{th} element feed. This form for $\vec{I}_{mn}(\vec{r}'+\vec{r}_{mn})$ also will

arise if the array is excited by a plane wave with directional cosines

s_x, s_y, s_z for the propagation direction. Under this excitation, once $\vec{I}_{00}(\vec{r}')$

is determined, the current on any array element is given by (23).

21
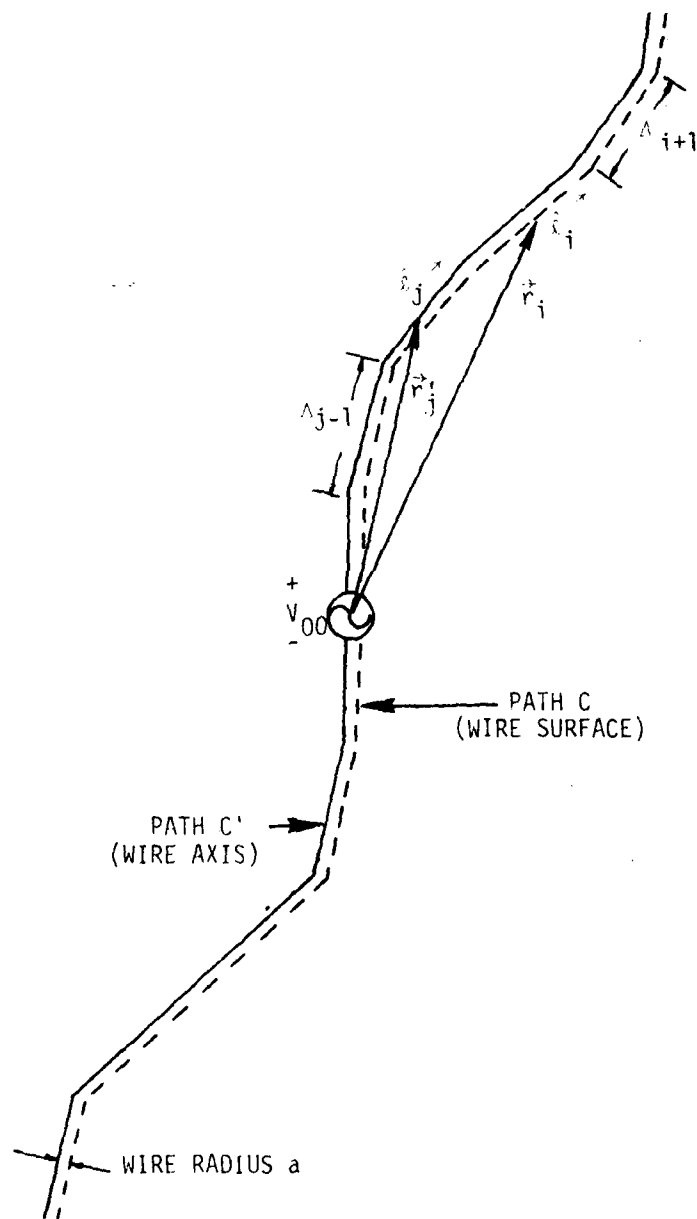
Figure 9. Curved Thin Wire Array Reference Element
Modeled by Linear Segments

The boundary condition from which $\vec{I}_{00}(\vec{r}')$ is determined is

$$-\vec{E}^s_{tan} = \vec{E}^{ex}_{tan} - \vec{E}_{tan} \qquad (24)$$

along the surface of the reference element, where $\vec{E}^s$ is the field radiated by all $\vec{I}_{mn}(\vec{r}'+\vec{r}_{mn})$, $\vec{E}^{ex}$ is an exciting plane wave in the absence of the array (impressed field), $\vec{E}$ is the total field, and the subscript "tan" denotes "component tangential to wire surface." Along perfectly conducting wires, $\vec{E}_{tan} = 0$ at all points except at a source port, where $\vec{E}_{tan}$ is the source field of an ideal port voltage source, V_{00}, and it is assumed that each mn^{th} element is excited by port voltage

$$V_{mn} = V_{00} \exp [-jkmd_e s_e -jknd_y s_y]$$

A partial difference operator, point matching moment method solution of the thin wire approximation of (24) results in an approximation of $\vec{I}_{00}(\vec{r}')$ [2]. In this procedure, the wire axis of the reference element is approximated by an N_s straight line segment fit (path C' of Figure 9) beginning half a segment in from wire ends where the current is zero. The reference element may be composed of disjoint wires (as with parasitics) and also may have multiple wire junctions (as with top-loaded dipoles). First, $\vec{I}_{00}(\vec{r}')$ is expanded as

$$\vec{I}_{00}(\vec{r}') = \sum_{j=1}^{N_s} I_j f_j(\vec{r}')\hat{\ell}_j \qquad (25)$$

where $f_j(\vec{r}')$ is a unit "pulse" of wire current traversing the jth segment of length Δ_j, $\hat{\ell}_j$ is the jth segment of path C' reference direction unit vector and I_j is an unknown coefficient to be determined. The substitution of (25) into (24) results in

$$-\sum_{j=1}^{N_s} I_j \vec{E}^s_{tan}(\vec{r},j) = \vec{E}^{ex}_{tan} - \vec{E}_{tan} \qquad (26)$$

23

where $\vec{E}^s(\vec{r},j)$ is the field radiated by the infinite array of jth segment expansion functions

$$f_j(\vec{r}')\hat{\ell}_j \exp [-jkmd_e s_e -jknd_y s_y]$$

A matrix equation, solvable for the I_j, results from (26) by a point matching procedure. Equation (26) is satisfied at the centers of each segment along a path C parallel to the segmented path C'. This is equivalently an impulse weighting moment method whereby the weighted average of (26) along C is taken with respect to each of the N_s weights

$$\vec{w}_i(\vec{r}) = \Delta_i \ \delta(\vec{r}-\vec{r}_i)\hat{\ell}_i$$

where $\delta(\vec{r}-\vec{r}_i)$ is the unit impulse function and $\vec{r}_i$ is the position vector of the center of the ith segment of path C. The result is

$$[Z]\bar{I} = \bar{V}^{ex} + \bar{V} \tag{27}$$

where the ith elements of the N_s x 1 column vectors $\bar{I}$, $\bar{V}^{ex}$, and $\bar{V}$ are, respectively, I_i

$$I_i$$

$$V_i^{ex} = \int_C \vec{E}^{ex}\cdot\vec{w}_i(\vec{r}) \ d\ell = \Delta_i \ \vec{E}^{ex}(\vec{r}_i)\cdot\hat{\ell}_i \tag{28}$$

$$V_i = \int_C \vec{E}\cdot\vec{w}_i(\vec{r}) \ d\ell = \Delta_i \ \vec{E}(\vec{r}_i)\cdot\hat{\ell}_i$$

and the ij^{th} element of the N_s x N_s moment matrix $[Z]$ is

$$Z_{ij} = - \int_C w_i(\vec{r})\cdot\vec{E}^s(\vec{r},j) \ d\ell = - \Delta_i \ \vec{E}^s(\vec{r}_i,j)\cdot\hat{\ell}_i \tag{29}$$

24

In determining Z_{ij}, the field $\vec{E}^s(\vec{r}_i,j)$ is represented in terms of a vector potential $\vec{A}$ and gradient of a scalar potential ϕ. Following the development in [2, Chapter 4], the scalar potential term is approximated by a partial difference for the gradient resulting in

$$Z_{ij} = j\omega\Delta_i\hat{\ell}_i\cdot\vec{A}(\vec{r}_i,j) + \phi(\vec{r}_{i_a},j) - \phi(\vec{r}_{i_b},j) \tag{30}$$

where

$$\vec{r}_{i_a} = \vec{r}_i + (\Delta_i/2)\hat{\ell}_i$$

$$\vec{r}_{i_b} = \vec{r}_i - (\Delta_i/2)\hat{\ell}_i$$

and ω is the radian frequency. The vector potential arises from the infinite array of progressively phased unit amplitude pulse segments

$$f_j(\vec{r}')\hat{\ell}_j \exp[-jkmd_es_e -jknd_ys_y]$$

and the scalar potentials from partial difference approximations to the linear charge densities associated with the infinite array of $f_j(\vec{r}')$. The reference element charge density $\sigma_j(\vec{r}')$ associated with $f_j(\vec{r}')$ becomes two "shifted" pulses of charge density, each of length Δ_j. Thus

$$\sigma_j(\vec{r}') = \frac{f_{j_a}(\vec{r}') - f_{j_b}(\vec{r}')}{j\omega\Delta_j} \tag{31}$$

where f_{j_a} is f_j shifted in the direction $\hat{\ell}_j$ to center at $\vec{r}'_{j_a} = \vec{r}'_j + (\Delta_j/2)\hat{\ell}_j$ ($\vec{r}'_j$ is the position vector of the center of the jth segment of path C') and f_{j_b} is f_j shifted in the direction $-\hat{\ell}_j$ to center at $\vec{r}'_{j_b} = \vec{r}'_j - (\Delta_j/2)\hat{\ell}_j$. Plane wave expansions for $\vec{A}(\vec{r}_\alpha,j)$ and $\phi(\vec{r}_\alpha,j)$ are derived below.

Munk and Burrell obtained the expression [1, Eq. 3] for the field from an infinite planar array of point current dipoles. They indicated that this

expression is valid for arbitrarily oriented dipoles; the dipoles need not be oriented parallel to the array plane. Munk and Burrell also mentioned that a moment method can be developed from this expression. However, the mutual impedance expression they derived [1, Eq. 19] restricts mutually coupled antenna segments to have disjoint z axis projections. The generalization of the moment method to handle "out of plane" elements necessitates more complicated expressions. These are derived here.

Consider two-dimensional arrays of incremental current dipoles and incremental linear charge densities having mn[th] elements given respectively by

$$\vec{f}_{mn}(\vec{r}'+\vec{r}_{mn})d\ell' = f_j(\vec{r}')d\ell' \, \hat{y}_j \exp[-jkmd_e s_e - jknd_y s_y]$$

$$\sigma_{mn}(\vec{r}'+\vec{r}_{mn})d\ell' = \sigma_j(\vec{r}')d\ell' \exp[-jkmd_e s_e - jknd_y s_y]$$

Following the work of Munk and Burrell [1, Appendix A] and Kornbau [4], the corresponding vector potential $d\vec{A}(\vec{r}_\alpha,j)$ and scalar potential $d\phi(\vec{r}_\alpha,j)$ at a point $\vec{r}_\alpha$ are given by the plane wave expansions

$$d\vec{A}(\vec{r}_\alpha,j) = \frac{d\ell' \eta \, f_j(\vec{r}') \hat{y}_j}{2j\omega d_x d_y} \sum_{p=-\infty}^{\infty} \sum_{q=-\infty}^{\infty} \frac{\exp[-jk(\vec{r}_\alpha-\vec{r}')\cdot\hat{g}_\pm]}{g_z} \tag{32}$$

$$d\phi(\vec{r}_\alpha,j) = \frac{d\ell' \sigma_j(\vec{r}')}{2jk\epsilon d_x d_y} \sum_{p=-\infty}^{\infty} \sum_{q=-\infty}^{\infty} \frac{\exp[-jk(\vec{r}_\alpha-\vec{r}')\cdot\hat{g}_\pm]}{g_z} \tag{33}$$

for $(\vec{r}_\alpha-\vec{r}')\cdot z \geq 0$ where

η = free space wave impedance

ϵ = free space permitivity

$\hat{g}_\pm = \hat{x}[s_x+p \frac{\lambda}{d_x} + q \frac{\lambda y}{d_x d_y}] + \hat{y}[s_y+q \frac{\lambda}{d_y}] \pm z g_z$

$g_z = \sqrt{1-[s_x+p \frac{\lambda}{d_x} +q \frac{\lambda y}{d_x d_y}]^2 - [s_y+q \frac{\lambda}{d_y}]^2}$

λ = free space wavelength

26

If the expression under the radical in g_z is negative, g_z is chosen to be negative imaginary; if the expression is positive, g_z is nonnegative real. This assures that all plane wave modal fields travel outward from the source array plane and nonpropagating modes attenuate. A plus sign subscript on $\hat{g}$ corresponds to field points $\vec{r}_\alpha$ in front of the array plane; i.e., $(\vec{r}_\alpha - \vec{r}') \cdot \hat{z} > 0$. A minus sign subscript corresponds to field points behind the array plane; i.e., $(\vec{r}_\alpha - \vec{r}') \cdot \hat{z} < 0$.

Since $f_j(\vec{r}')$ is the reference element j^{th} segment unit "pulse" and $\vec{r}' = \vec{r}'_j + \ell' \hat{\ell}_j$ (as defined in Figure 10), (31), (32), and (33) yield, after interchange of integrations and summations,

$$\vec{A}(\vec{r}_\alpha, j) = \int_{C'} d\vec{A}(\vec{r}_\alpha, j) = \frac{\hat{\ell}_j n \Delta_j}{2j\omega d_x d_y} \sum_{p=-\infty}^{\infty} \sum_{q=-\infty}^{\infty} \psi_{pq}(\alpha, j) \tag{34}$$

$$\Phi(\vec{r}_\alpha, j) = \int_{C'} d\Phi(\vec{r}_\alpha, j) = \frac{-\eta}{2k^2 d_x d_y} \left[\sum_{p=-\infty}^{\infty} \sum_{q=-\infty}^{\infty} (\psi_{pq}(\alpha, j_a) - \psi_{pq}(\alpha, j_b)) \right] \tag{35}$$

The $\psi_{pq}(\alpha, \beta)$ functions assume one of three different forms:

$$\psi_{pq}(\alpha, \beta) = \frac{\exp[-jk(\vec{r}_\alpha - \vec{r}'_\beta) \cdot \hat{g}_+)]}{g_z} \frac{\sin[k(\hat{\ell}_j \cdot \hat{g}_+)\Delta_j/2]}{k(\hat{\ell}_j \cdot \hat{g}_+)\Delta_j/2} \tag{36a}$$

$$\text{if } (\vec{r}_\alpha - \vec{r}'_\beta) \cdot \hat{z} \geq \frac{\Delta_j}{2} |\hat{\ell}_j \cdot \hat{z}|$$

$$\psi_{pq}(\alpha, \beta) = \frac{\exp[-jk(\vec{r}_\alpha - \vec{r}'_\beta) \cdot \hat{g}_-]}{g_z} \frac{\sin[k(\hat{\ell}_j \cdot \hat{g}_-)\Delta_j/2]}{k(\hat{\ell}_j \cdot \hat{g}_-)\Delta_j/2} \tag{36b}$$

$$\text{if } (\vec{r}_\alpha - \vec{r}'_\beta) \cdot \hat{z} \leq - \frac{\Delta_j}{2} |\hat{\ell}_j \cdot \hat{z}|$$
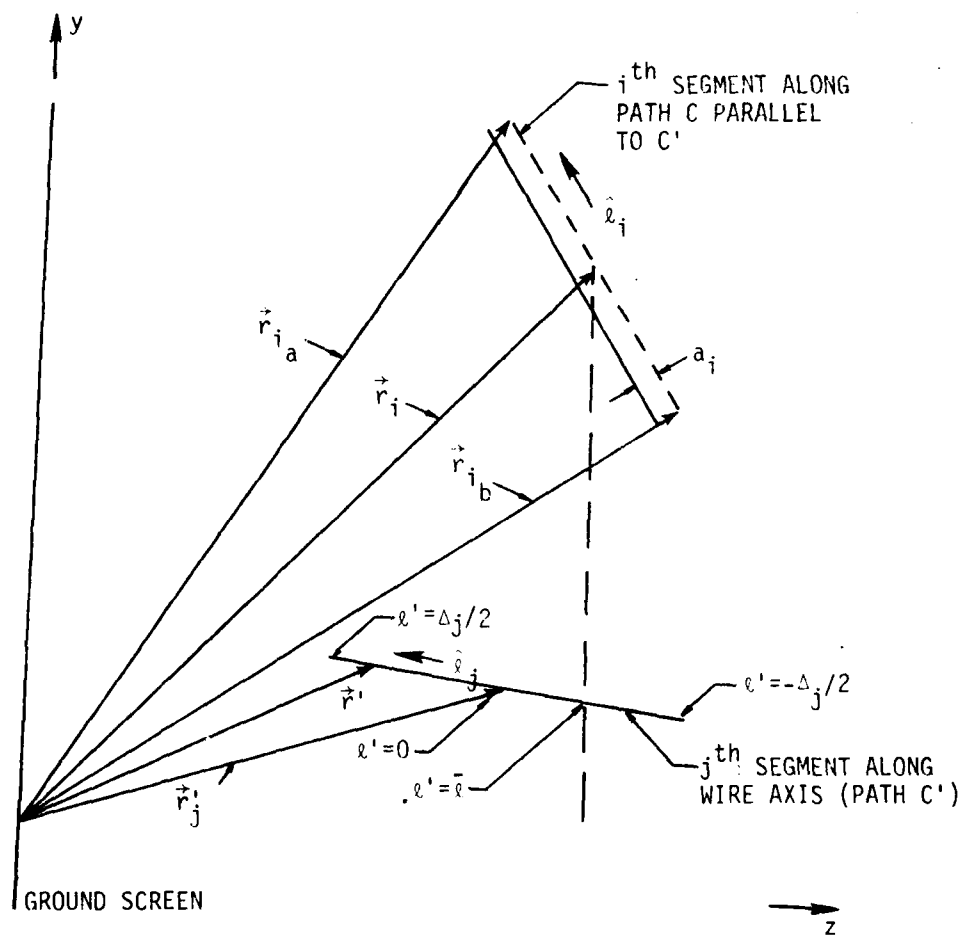
Figure 10. Expansion and Weighting Segments

28

$$\psi_{pq}(\alpha,\beta) = \pm \left[\frac{\exp[-jk(\vec{r}_\alpha-\vec{r}'_\beta)\cdot\hat{g}_+]}{jk\Delta_j g_z \ell_j \cdot \hat{g}_+} (\exp[jk\bar{\ell}(\hat{\ell}_j\cdot\hat{g}_+)] - \exp[\mp jk(\hat{\ell}_j\cdot\hat{g}_+)\Delta_j/2]) \right.$$

$$\left. - \frac{\exp[-jk(\vec{r}_\alpha-\vec{r}'_\beta)\cdot\hat{g}_-]}{jk\Delta_j g_z \ell_j \cdot \hat{g}_-} (\exp[jk\bar{\ell}(\hat{\ell}_j\cdot\hat{g}_-)] - \exp[\pm jk(\hat{\ell}_j\cdot\hat{g}_-)\Delta_j/2]) \right]$$

$$(36c)$$

$$\text{if} \quad |(\vec{r}_\alpha-\vec{r}'_\beta)\cdot\hat{z}| < \frac{\Delta_j}{2}|\hat{\ell}_j\cdot\hat{z} \quad \text{and} \quad \hat{\ell}_j\cdot\hat{z} \gtrless 0$$

where

$$\bar{\ell} = \frac{(\vec{r}_\alpha-\vec{r}'_\beta)\cdot\hat{z}}{\hat{\ell}_j\cdot\hat{z}}$$

Equation (36a) applies when the entire source segment is closer to the ground screen than is the field point $\vec{r}_\alpha$. The plus sign subscript is indicated since the plane waves then are propagating in the positive z direction. Equation (36b) applies when the entire source segment is further from the ground screen than is $\vec{r}_\alpha$. The negative sign subscript now appears since the plane waves are propagating in the negative z direction. Equation (36c) applies when $\vec{r}_\alpha$ defines a point common to a plane that simultaneously divides the source segment and is parallel to the array plane. The $\hat{\ell}$ coordinate along the source segment of this point is defined by equating $\hat{z}$ axis projections of $\vec{r}_\alpha$ and $\vec{r}'_\beta + \ell'\hat{\ell}_j$, yielding $\hat{\ell}$ given by (37) (Figure 10 with $\vec{r}_\alpha = \vec{r}_i$). For $\ell_j \cdot z < 0$, e.g., the ℓ_j direction indicated in Figure 10, integration with respect to ℓ' from $-\Delta_j/2$ to $\bar{\ell}$ involves plane waves propagating in the negative z direction; hence, the $-$ subscript is indicated for $\hat{g}$ in the second set of terms in (36c). For the integration from $\bar{\ell}$ to $\Delta_j/2$, the properly chosen plane waves propagate in the positive z direction; hence, the first set of terms in (36c). Equation (36c) also applies when $\hat{\ell}_j\cdot\hat{z} > 0$. The upper (lower) of the $\pm$ signs in (36c) applies for $\hat{\ell}_j\cdot\hat{z} > 0$ ($\hat{\ell}_j\cdot\hat{z} < 0$). If $\hat{\ell}\cdot\hat{z} = 0$ ($\bar{\ell}$ not defined), either (36a) or (36b) applies.

Equations (30), (34), and (35) yield

$$z_{ij} = \frac{\Delta_i \Delta_j n \; \hat{\ell}_i \cdot \hat{\ell}_j}{2 d_x d_y} \sum_{p=-\infty}^{\infty} \sum_{q=-\infty}^{\infty} \psi_{pq}(i,j)$$

$$- \frac{1}{2k^2 d_x d_y} \left[\sum_{p=-\infty}^{\infty} \sum_{q=-\infty}^{\infty} \left(\psi_{pq}(i_a, j_a) - \psi_{pq}(i_a, j_b) \right. \right.$$

$$\left. \left. - \psi_{pq}(i_b, j_a) + \psi_{pq}(i_b, j_b) \right) \right] \tag{38}$$

In (38), the field point vectors $\vec{r}_i$, $\vec{r}_{i_a}$, and $\vec{r}_{i_b}$ occur (note defining equations following (30)). These vectors define the midpoint and endpoints of the ith weighting segment along path C as shown in Figure 10. Thus

$$\vec{r}_i = \vec{r}'_i + \vec{a}_i$$

where $|\vec{a}_i|$ is the wire radius a_i along the ith segment. The vector direction of $\vec{a}_i$ is, of course, normal to $\hat{\ell}_i$. The vector $\vec{a}_i$ is defined fully by requiring that $\vec{a}_i$ also lie in the plane formed by $\hat{\ell}_i$ and $\hat{z}$. This speeds convergence of the infinite summations in (38) for segments oriented nearly parallel to the xy plane. This condition is satisfied for

$$\vec{a}_i = a_i \hat{\ell}_i \times (\hat{z} \times \hat{\ell}_i) / |\hat{\ell}_i \times (\hat{z} \times \hat{\ell}_i)|$$

If a ground screen is present a distance d behind the array, image fields must be considered in each impedance element computation. Let double primed position vectors and segment path lengths refer to those for image currents and associated charge densities. Then, since the coordinate origin lies on the ground screen,

$$\vec{r}''_j = \hat{x}(\hat{x} \cdot \vec{r}'_j) + \hat{y}(\hat{y} \cdot \vec{r}'_j) - \hat{z}(\hat{z} \cdot \vec{r}'_j)$$

$$\hat{\ell}''_j = \hat{x}(\hat{x} \cdot \hat{\ell}_j) + \hat{y}(\hat{y} \cdot \hat{\ell}_j) - \hat{z}(\hat{z} \cdot \hat{\ell}_j)$$

30

and the ij^{th} element of the moment matrix for an infinite array over a perfect ground screen becomes

$$Z_{ij}^{gs} = Z_{ij} - Z_{ij}^{image} \qquad (39)$$

where Z_{ij} is given by (38) and Z_{ij}^{image} is Z_{ij} of (38) with $\psi_{pq}(\alpha,\beta)$ of (38) computed by (36) with $\vec{r}_j'$ replaced with $\vec{r}_j''$, and $\hat{\ell}_j$ replaced with $\hat{\ell}_j''$.

For plane wave incidence, the voltage column vector elements given by (28) must be appropriately modified to account for reflection. If

$$\vec{E}^{ex} = E_x^{ex}\,\hat{x} + E_y^{ex}\,\hat{y} + E_z^{ex}\,\hat{z}$$

(where E_x^{ex}, E_y^{ex}, and E_z^{ex} are, by the plane wave condition, constrained by $s_x E_x^{ex} + s_y E_y^{ex} + s_z E_z^{ex} = 0$), the ith element of the voltage column vector including reflection from the perfect ground screen is given by

$$V_i^{ex,gs} = \Delta_i \hat{\ell}_i \cdot e^{-jk(s_x x + s_y y)} \left[-2j\sin(ks_z z)(E_x^{ex}\,\hat{x} + E_y^{ex}\,\hat{y}) + 2\cos(ks_z z)E_z^{ex}\,\hat{z} \right]$$

$$(40)$$

Equation (27) then becomes

$$[Z^{gs}]\bar{I} = \bar{V}^{ex,gs} + \bar{V} \qquad (41)$$

Equations (36),(38), and (39) simplify if the radiating elements lie in the array plane. For this special case, (36) and (38) reduce to

$$Z_{ij} = \frac{\eta}{2d_x d_y} \sum_{p=-\infty}^{\infty} \sum_{q=-\infty}^{\infty} (\Delta_i \Delta_j (\hat{\ell}_i \cdot \hat{\ell}_j) \qquad (42)$$

$$- \frac{4}{k^2} \sin[k(\hat{\ell}_i \cdot \hat{g}_+)\Delta_i/2] \sin[k(\hat{\ell}_j \cdot \hat{g}_+)\Delta_j/2]) \psi_{pq}(i,j)$$

$$\psi_{pq}(i,j) = \frac{\exp[-jk(\vec{r}_i - \vec{r}_j') \cdot \hat{g}_+]}{g_z} \; \frac{\sin[k(\hat{\ell}_j \cdot \hat{g}_+)\Delta_j/2]}{k(\hat{\ell}_j \cdot \hat{g}_+)\Delta_j/2} \qquad (43)$$

31

Only the "+" sign for $\hat{g}_+$ appears in (42) and (43) because of the simplifying assumption of wires lying parallel to the xy plane and the path C is chosen to lie a wire radius in front (positive z direction) of C'.

The progressive phasings, s_x and s_y, which, for a particular p and q, cause g_z to be zero, can result in an infinite Z_{ij}. These progressive phasings correspond to "grating lobe singularities" since they correspond to grating lobes just entering the visible range; i.e., nonattenuating plane waves propagating along the array plane. This is one possible source of "blind spots" and rapidly varying active impedances with scan. This is only a "potential" condition for infinite Z_{ij} since, although g_z is in the denominator of ψ_{pq}, in some situations a compensating effect occurs. Such is th case, for example, in E-plane scans with periodic infinite arrays of y directed dipoles where E-plane grating lobe singularities are suppressed. This is clear from (42) for small $k\Delta_i/2$ since, in the E-plane, $\hat{g}_\pm \cdot \hat{x} = 0$, $\hat{\ell}_i \cdot \hat{g}_+ = 1$ as $g_z \to 0$, and the parenthetical term multiplying $\psi_{pq}(i,j)$ vanishes.

The presence of a perfect ground screen also inhibits blind spots due to grating lobe singularities if the radiating elements lie parallel to the array plane. If d is the height of the array above the ground screen and the positive z axis is directed from the ground screen to the array as for array $\underline{b}$, Z_{ij}^{gs} of (39) is given by Z_{ij} of (42) with $\psi_{pq}(i,j)$ given by

$$\psi_{pq}\ (i,j)\ =\ \frac{2j\ \sin(kdg_z)}{g_z}\ \exp\left[-jk\left((\vec{r}_i-\vec{r}_j')\cdot\hat{g}_++dg_z\right)\right]\ \frac{\sin[k(\hat{\ell}_i\cdot\hat{g}_+)\Delta_i/2]}{k(\hat{\ell}_j\cdot\hat{g}_+)\Delta_j/2}\ \ (44)$$

in place of (43). It is apparent from (44) that ψ_{pq} is bounded at a grating lobe singularity since $\dfrac{\sin\ kdg_z}{g_z}$ is bounded as $g_z \to 0$. This ground screen suppression of a blind spot at a grating lobe singularity assumes the radiating elements lie in the array plane. If, for example, the dipole arms are inclined with respect to the array plane or feedline scattering is present, the ground screen may enhance the blind spot effect at a grating lobe singularity above what it would be if the ground screen is absent; thus, consideration of out-of-plane radiating elements via the general expressions (36), (38), and (39) is important.

32

The array $\underline{b}$ active impedance, $z^{bb}(s_e, s_y)$, then can be determined by solving (41) for the source segment, $i = i_s$, current coefficient, I_{i_s}, with $V_i^{ex,gs} = 0$ for all i and $V_i = 0$ for all $i \neq i_s$. Then

$$z^{bb}(s_e, s_y) = \frac{V_{i_s}}{I_{i_s}}$$

The array $\underline{a}$ active impedance, $z^{aa}(s_e, s_y)$, can be obtained in the same manner.

The array $\underline{a}$ reference element short-circuit current, I_{00}^{ex}, can be determined by solving (41) for I_i. Now, however, $V_i = 0$ for all i and the elements of $\bar{V}^{ex,gs}$ are given by (40).

The array $\underline{b}$ to array $\underline{a}$ ground screen penetration coupling, $z^{ab}(s_e, s_y)$, fect ground screen can be determined from (41) where $[Z^{gs}]$ is the array $\underline{a}$ ground screen present moment matrix, $\bar{V}^t = \bar{V}^{ex,gs} + \bar{V}$, and the elements of $\bar{V}^t$ are given by (28) with $\vec{E}^{ex}$ replaced by the field $\vec{E}^t$ transmitted through the ground screen with array $\underline{b}$ excited by current sources given by (4). (A means for determining $\vec{E}^t$ is discussed below). The element I_{i_s} in the solution vector, $\bar{I}$ of (41), is then the short-circuit array $\underline{a}$ reference element port current. The reference element open-circuit voltage is

$$V_{00}^t = -z^{aa}(s_e, s_y) \, I_{i_s}^a$$

thus,

$$z^{ab}(s_e, s_y) = -\frac{z^{aa}(s_e, s_y) \, I_{i_s}^a}{I_{00}^b} \tag{45}$$

The field $\vec{E}^t$ is obtained readily from knowledge of the plane wave transmission coefficients of the ground screen and the plane wave decompostition of the field from array $\underline{b}$. The array $\underline{b}$ current is determined with array $\underline{b}$ excited with port current sources (4). The array $\underline{b}$ reference element current vector $\bar{I}^b$ is the solution $\bar{I}$ to (41) with $V_i^{ex,gs} = 0$ for all i and

$$
V_i = \begin{cases} 0 & i \neq i_s \\ z^{bb}(s_e, s_y) \, I_{00}^b & i = i_s \end{cases}
$$

The array $\underline{b}$ currents excite a field $\vec{E}^i(\vec{r})$ incident on the ground screen. The plane wave expansion

$$
\vec{E}^i(\vec{r}) = \sum_{j=1}^{N_s} I_j^b \frac{\Lambda_j \eta}{2 d_x d_y} \sum_{p=-\infty}^{\infty} \sum_{q=-\infty}^{\infty} \psi_{pq}^i (j) \, \vec{h}_- \tag{46}
$$

where

$$
\psi_{pq}^i (j) = \frac{\exp[-jk(\vec{r}-\vec{r}_j')\cdot \hat{g}_-]}{g_z} \frac{\sin[k(\hat{\ell}_j \cdot \hat{g}_-)\Delta_j/2]}{k(\hat{\ell}_j \cdot \hat{g}_-)\Delta_j/2}
$$

$$
\vec{h}_- = (\hat{\ell}_j \times \hat{g}_-) \times \hat{g}_-
$$

can be derived from [1, Eq. 3]. The subscripted negative signs indicate that (46) applies for $(\vec{r}-\vec{r}_j')\cdot z < 0$ as is appropriate since the ground screen is "behind" array $\underline{b}$. Since $\vec{E}^i$ is a superposition of plane waves, $\vec{E}^t$ is obtained by applying the proper transmission coefficients to each component plane wave. Each plane wave in (46) propagates in the $\hat{g}_-$ direction; thus, $\hat{g}_-$ and $\hat{z}$ (ground screen normal) form the corresponding "plane of incidence." A unit vector normal to the incidence plane is

$$
\hat{n}_\perp = \frac{\hat{g}_- \times \hat{z}}{|\hat{g}_- \times \hat{z}|}
$$

and a unit vector parallel to the incidence plane and normal to $\hat{g}_-$ is

$$
\hat{n}_{\parallel} = \hat{g}_- \times \hat{n}_\perp
$$

34

Any plane wave travelling in the $\hat{g}_-$ direction can be decomposed into two plane waves, one with an $\vec{E}$ field polarized along $\hat{n}_\perp$ and the other with an $\vec{E}$ field polarized along $\hat{n}_{||}$. If $T_\perp$ and $T_{||}$ are the corresponding transmission coefficients,

$$\vec{E}^t(\vec{r}) = \sum_{j=1}^{N_s} I_j^b \frac{\Delta_j \eta}{2d_x d_y} \sum_{p=-\infty}^{\infty} \sum_{q=-\infty}^{\infty} \left[\hat{n}_\perp T_\perp (\hat{n}_\perp \cdot \vec{h}_-) \right.$$

$$\left. + \hat{n}_{||} T_{||} (\hat{n}_{||} \cdot \vec{h}_-) \right] \psi_{pq}^i (j) \tag{47}$$

The substitution of (47) for $\vec{E}^{ex}$ in (28) yields

$$V_i^t = \sum_{j=1}^{N_s} I_j^b \frac{\Delta_i \Delta_j \eta}{2d_x d_y} \sum_{p=-\infty}^{\infty} \sum_{q=-\infty}^{\infty} \left[(\hat{\ell}_i \cdot \hat{n}_\perp) T_\perp (\hat{n}_\perp \cdot \vec{h}_-) + (\hat{\ell}_i \cdot \hat{n}_{||}) T_{||} (\hat{n}_{||} \cdot \vec{h}_-) \right] \psi_{pq}^i (i,j) \tag{48}$$

and $z^{ab}(s_e, s_y)$ is determined as previously discussed in the paragraph containing (45). In (48) $\psi_{pq}^i(i,j)$ is $\psi_{pq}^i(j)$ with $\vec{r}_i$ replacing $\vec{r}$.

SECTION 3

IMPLEMENTATION

The computer programming to date of the lens simulator is discussed below. Two main programs have been developed - FAM and HAM. The first approximation method is carried out in FAM (Section 3.1). The higher approximation method is carried out in HAM (Section 3.2). The program HAM relies on data generated by FAM that is stored in disk files. Several subprograms, discussed in Section 3.3, are used by both FAM and HAM. The discussions and flow diagrams follow closely the theory nomenclature of Section 2 and [5]. Computational considerations of several equations and convergence rational are discussed.

User data input is described in Section 3.3.11. Data is inputted in an interactive manner; the computer queries the user.

The general scattering parameter model derived in Section 2.1 is not yet implemented. This implementation is presently taking place. The specialized scattering parameter model that applies to passive phase shifters composed simply of lengths of transmission line is implemented. Also a specialized impedance parameter model [5, Section 3.2.1] is implemented. The user selects the model most suitable.

An efficient folded dipole radiator model, not discussed in the theoretical developments, is implemented as a user option. This model is described in Section 3.1.

Computer run time is consumed primarily in the computation of the infinite array moment matrices. Atlantic Research Corporation is investigating eliminating this computation from FAM. Instead, a third computer code would be constructed that generates the infinite array moment matrices for several scan angles. The program FAM, then, would read these matrices from data files and interpolate to arrive at the moment matrix for a specified scan angle. The moment matrix generating code would best be run in a batch-like mode and FAM and HAM in a user-interactive mode.

3.1 First Approximation Method

The first approximation method (FAM) implementation is discussed here. The radiating element currents and port impedances are computed for each cell assuming infinite periodic lattices. The first approximation lens radiation patterns are computed from these currents. The underlying theory is described in Section 2 and [5].

The subroutines called by FAM are listed in order of first invocation in Figure 11. Subroutines called by subroutines of FAM also are listed (indented) beneath their respective calling programs. A flow diagram of FAM is given in Figure 12.

Lens data are read in via LENSIN, cell data via CELLIN and cell illumination via FEED. Subroutine FEED assumes a point source located a global z axis distance behind the lens. The effective radiated power and $\vec{E}$-field x,y polarization components (global system) at the cell coordinate origin must be provided for each plane wave component of illumination. (The illumination is the field in the absence of the lens; the global coordinate origin is in the lens ground screen).

An option for modeling folded dipole radiating elements efficiently is available in FAM. If the option is exercised, the user supplies the folded dipole transmission line mode characteristic impedance Z_0 and dipole length (end to end) L. The transmission line mode impedance is computed in FAM as

$$Z_t = jZ_0 \tan(\tfrac{1}{2} kL)$$

This impedance is combined with the infinite array folded dipole radiation mode impedance z to yield the folded dipole scan impedance given by [6]

$$\text{folded dipole scan impedance} = \frac{4Z_t z}{Z_t + 2z}$$

The infinite array folded dipole radiation mode impedance z is the scan impedance, including scattering from feedlines, of an array of simple dipoles of equivalent folded dipole radii a_e. The wire geometry supplied by the user that specifies the radiating element must, therefore, treat the folded dipole as a simple dipole of radius a_e. A good approximation for a_e can be obtained through two dimensional analyses as indicated by Wolff [6, pg. 61]. A first

```
LENSIN

CELLIN
   ARAYIN
   CEXP
   GEOMET

FEED
   CEXP

ZMATG
   PERP
   PSIGEN
      PSIA

   OFFD
      PSIGEN
         PSIA

   GNDS
      PERP
      OFFD
         PSIGEN
            PSIA

SCAN
   LINEQ

TAN

ZCOL

SCIA
   EX
      CEXP
   CEXP

MUTUAL
   CEXP

CELPAT
   CEXP

TPLANE
   TPIN
```

Figure 11.   Program FAM Subprograms

BEGIN

SET UP FAM WORKING FILES AND
SPECIFY FILE UNIT NUMBERS

INPUT JOB TITLE

LENSIN
INPUT LENS SYSTEM DATA

BEGIN LOOP OVER
CELLS OF LENS

CELLIN
INPUT DATA FOR LENS CELL

TEST FOR MORE CELLS
ICELID > 0? —NO→ Ⓐ

YES

BEGIN LOOP OVER INCI-
DENT PLANE WAVES

CALCULATE DIRECTION COSINES (S_xG, S_yG, S_zG)
OF WAVE TRAVELING FROM FEED TO THE LENS CELLS

$$S_xG = \sin \theta_{ex} \cos \phi_{ex}$$
$$S_yG = \sin \theta_{ex} \sin \phi_{ex}$$
$$S_zG = \cos \theta_{ex}$$

FEED
INPUT FEED EXCITATION
OF LENS ARRAY a (IN
GLOBAL SYSTEM COORDINATE)

TRANSFORM THE WAVE DIRECTION COSINES INTO
THE CELL COORDINATE SYSTEM

$$S_x = S_xG \cos \phi_g + S_yG \sin \phi_g$$
$$S_y = -S_xG \sin \phi_g + S_yG \cos \phi_g$$
$$S_z = S_zG$$

ϕ_g IS THE ROTATION ANGLE OF THE CELL COORDI-
NATE SYSTEM RELATIVE TO THE GLOBAL
COORDINATE SYSTEM

CALCULATE NORMALIZATION CONSTANTS
FOR MODULE S-PARAMETERS.

CALCULATE PHASE DELAY AND CHARACTERISTIC IMPEDANCE
OF REFERENCE ELEMENT PASSIVE LINE PHASE SHIFTER

BEGIN LOOP OVER FEEDBACK
MODES U_a, U_b

IF IMPEDANCE PARAMETER MODULE MODEL,
DECREMENT ARRAY a FEEDBACK MODE NUMBER U_a

CALCULATE TOTAL PROGRESSIVE
PHASE FOR EACH ARRAY.

ZMATG
CALCULATE MOMENT MATRIX FOR ARRAY b
ABOVE INFINITE PERFECT GROUND SCREEN.

SCAN
CALCULATE ARRAY b MOMENT MATRIX
INVERSE AND SCAN IMPEDANCE z^{bb}.

ARE ARRAY b ELEMENTS
FOLDED DIPOLES? —NO→

YES

IS FOLDED DIPOLE A
HALF WAVE DIPOLE? —YES→

NO

CALCULATE TRANSMISSION
LINE LOADING OF FOLDED
DIPOLE OF LENGTH L^b
AND CHARACTERISTIC
IMPEDANCE Z_0^b AS

$$z_t^b = jZ_0^b \tan (\tfrac{1}{2} k L^a)$$

CALCULATE FOLDED
DIPOLE SCAN
IMPEDANCE AS
$4z^{bb}$

CALCULATE ARRAY b FOLDED
DIPOLE SCAN IMPEDANCE
$4z_t^b z^{bb}/(z_t^b + 2z^{bb})$

ZCOL
SAVE THE COLUMN IN ARRAY b INVERTED MOMENT
MATRIX THAT CORRESPONDS TO THE ARRAY b REF-
ERENCE ELEMENT CURRENT FOR UNIT PORT VOLTAGE
PROGRESSIVE PHASED ARRAY b EXCITATION.

ZMATG
CALCULATE MOMENT MATRIX FOR ARRAY a
ABOVE INFINITE PERFECT GROUND SCREEN

Ⓑ

Figure 12. Flow Diagram for FAM

39

B

SCAN

CALCULATE ARRAY a MOMENT MATRIX INVERSE AND SCAN IMPEDANCE z^{aa}

ARE ARRAY a ELEMENTS FOLDED DIPOLES? — NO

YES

IS FOLDED DIPOLE A HALF WAVE DIPOLE? — YES — CALCULATE FOLDED DIPOLE SCAN IMPEDANCE AS $4z^{aa}$

NO

CALCULATE TRANSMISSION LINE LOADING OF FOLDED DIPOLE OF LENGTH L^a AND CHARACTERISTIC IMPEDANCE Z_0^a AS

$$Z_t^a = jZ_0^a \tan(\tfrac{1}{2}kL^a)$$

CALCULATE ARRAY a FOLDED DIPOLE SCAN IMPEDANCE AS $(4Z_t^a z^{aa})(Z_t^a + 2z^{aa})^{-1}$

ZCOL

SAVE THE COLUMN IN ARRAY a MOMENT MATRIX THAT CORRESPONDS TO THE ARRAY a REFERENCE ELEMENT CURRENT FOR UNIT PORT VOLTAGE PROGRESSIVE PHASED ARRAY a EXCITATION

NO — ARE MODULES (PLUE FEEDLINES) REPRESENTED BY TWO PORT IMPEDANCE PARAMETERS?

YES

ADD MODULE DIAGONAL IMPEDANCE PARAMETERS TO ARRAY SCAN IMPEDANCES
$$\bar{z}^{aa} = z_{mod}^{aa} + z^{aa}$$
$$\bar{z}^{bb} = z_{mod}^{bb} + z^{bb}$$

BEGIN ELEMENT CURRENT CALCULATIONS

IS ZERO FEEDBACK LOOP PRESENT? — NO — **C**

YES

SCIA

CALCULATE ARRAY a REFERENCE ELEMENT PLANE WAVE EXCITATION COLUMN VECTOR $v^{ex,gs}$ SHORT CIRCUIT CURRENT COLUMN VECTOR $\bar{I}$ AND SHORT CIRCUIT PORT CURRENT I_{00}^{ex} FOR THE ARRAY ABOVE AN INFINITE PERFECT GROUND

IS MODULE IMPEDANCE PARAMETER REPRESENTATION USED? — YES

NO

CALCULATE ARRAY a AND ARRAY b REFERENCE ELEMENT PORT CURRENTS FOR ZERO FEEDBACK LOOP FROM

$$I_{00(0)}^a = \frac{z^{aa}}{z_0^{aa}}\, I_0^{ex}$$

$$I_{00(0)}^t = 0$$

TRANSMISSION LINE MODULE PHASE SHIFTERS ASSUMED. CALCULATE ARRAY a AND ARRAY b REFERENCE ELEMENT ZERO FEEDBACK MODE PORT CURRENTS $I_{00(0)}^a$; $I_{00(0)}^b$ AND SCATTERING VARIABLES $C_{00(0)}^a$, $C_{00(0)}^b$

IS GROUND SCREEN FEEDBACK PRESENT? — NO

C — YES

MUTUAL

CALCULATE GROUND SCREEN PENETRATION MUTUAL IMPEDANCE COUPLING z^{ab} BETWEEN ARRAY b AND ARRAY a. ALSO COMPUTE ARRAY a EXCITATION VOLTAGE AND SHORT CIRCUIT CURRENT COLUMN VECTORS DUE TO CURRENTS ON ARRAY b

IF MODULES (PLUS FEEDLINES) REPRESENTED BY TWO PORT IMPEDANCE PARAMETERS, FORM

$$\bar{z}^{ab} = z_{mod}^{ab} + z^{ab}$$

CALCULATE FEEDBACK MODE CONTRIBUTION TO ARRAY a AND ARRAY b REFERENCE ELEMENT PORT CURRENTS

FIRST FEEDBACK LOOP? — YES — **D**

NO

E

Figure 12. Continued

40

Figure 12. Concluded

E (connector)

IS MODULE IMPEDANCE PARAMETER REPRESENTATION USED? — YES / NO

CALCULATE ARRAY a AND ARRAY b PORT CURRENTS FOR IMPEDANCE PARAMETER REPRESENTATION

$$I^a_{00(u)} = -\frac{\bar{z}^{ab}_u}{\bar{z}^{aa}_u} I^b_{00(u-1)}$$

$$I^b_{00(u)} = -\frac{\bar{z}^{ba}_{mod}}{\bar{z}^{bb}_{u+1}} I^a_{00(u)}$$

TRANSMISSION LINE MODULE PHASE SHIFTERS ASSUMED. CALCULATE SCATTERING VARIABLE INTERMEDIATE QUANTITIES Q_{11}, Q_{12}, Q_{21}, AND Q_{22}

CALCULATE ARRAY a AND ARRAY b SCATTERING VARIABLES AS

$$c^a_{00(u)} = e^{-jk\ell_0} (n_{11} c^b_{00(u-1)} + n_{12} c^a_{00(u-1)})$$

$$c^b_{00(u)} = e^{-jk\ell_0} (n_{11} c^b_{00(u-1)} + n_{22} c^a_{00(u-1)})$$

CALCULATE ARRAY a AND ARRAY b REFERENCE ELEMENT PORT CURRENTS AS

$$I^a_{00(u)} = -\frac{1}{\sqrt{k_0}} \left[c^a_{00(u)} - e^{-jk\ell_0} c^b_{00(u-1)} \right]$$

$$I^b_{00(u)} = -\frac{1}{\sqrt{k_0}} \left[c^b_{00(u)} - e^{-jk\ell_0} c^a_{00(u-1)} \right]$$

D (connector)

CALCULATE ARRAY a AND ARRAY b REFERENCE ELEMENT PORT VOLTAGES

$$V^a_{00(u)} = z^{aa}_u I^a_{00(u)}$$

$$V^b_{00(u)} = z^{bb}_u I^b_{00(u)}$$

ADJUST ARRAY a AND ARRAY b VOLTAGE AND CURRENT COLUMN VECTORS FOR CORRECT ARRAY a AND ARRAY b PORT CURRENTS

WRITE ARRAY a AND ARRAY b CURRENTS AND VOLTAGES TO WORKING FILE — Fill

CELPAT

CALCULATE AND ACCUMULATE CELL PATTERN

END FEEDBACK MODE LOOP

WRITE ARRAY a REFERENCE ELEMENT VOLTAGES AND CURRENTS TO FILE — FILE

END LOOP OVER INCIDENT PLANE WAVES

END CELL LOOP

A (connector) — TPLANE

OUTPUT PATTERN AS A T-PLANE PLOT

END

41

approximation to a_e for a folded strip dipole with parallel strips separated a small distance with respect to the overall folded dipole width w is

$$a_e = w/4$$

The user may choose either an impedance parameter model or a scattering parameter model for the module (plus feedlines) two-port implementation. The impedance parameter model is based on the derivation in [5, Section 3.2.1]. It allows for active modules (amplifiers) but restricts the impedance parameters to an idealized model; impedance parameters must be uniform functions of progressive phase angle setting except for the phase of the forward mutual impedance parameter. That phase varies from module to module by a progressive phase increment. Be advised that the impedance parameter model described in [5] is based on [5, Eq. (3-12)] whereas the development in this report is based on (6). The two equations differ by a feedback mode offset, and the restriction to only nonnegative feedback modes in [5]. The offset implies that the $u = p$ mode computed using (6) is the $u = p-1$ mode computed using [5, Eq. (3-12)]. The mode incrementation loop in FAM follows the (6) convention. Thus, if impedance parameters are chosen, the $u = p$ mode computation of I_{mn}^b in FAM should be interpreted according to [5, Eq. (3-12)] as the $u = p+1$ mode.

If Mutual is bypassed (ground screen assumed perfectly conducting) only a scattering parameter module representation is allowed.

The scattering parameter representation for the module plus feedlines is presently implemented for the special case of modules composed simply of lengths of transmission line. The characteristic impedances of the module transmission line and feedlines are assumed equal ($=R_0$). Equations (21) and (22) then apply for determining the array $\underline{a}$ and array $\underline{b}$ reference element port scattering variables $\bar{C}_{00(u)}$ and currents $\bar{I}_{00(u)}$ for "feedback" modes $u = 0, \pm1, \pm2, \ldots$. Equations (22) generally are not decoupled. A simplification, employed in the present implementation, is that only nonnegative feedback modes u are significant. Equations (22) then decouple to yield the recursion relations

42

$$\bar{C}_{00(0)} = (\sqrt{R_0}[U] + \frac{1}{\sqrt{R_0}}[z_0])^{-1} \bar{V}_{00}^{ex}$$

$$\bar{C}_{00(u)} = (R_0[U] + [z_u])^{-1} ([z_u] - R_0[U]) [W]\bar{C}_{00(u-1)} \qquad u = 1, 2, \ldots$$

The corresponding port currents are found from

$$\bar{I}_{00(0)} = -\frac{1}{\sqrt{R_0}} \bar{C}_{00(0)}$$

$$\bar{I}_{00(u)} = -\frac{1}{\sqrt{R_0}} (\bar{C}_{00(u)} - [W]\bar{C}_{00(u-1)}) \qquad u = 1, 2, \ldots$$

A qualitative justification for omitting negative feedback modes is given in [5(pg. 3-4)]. The validity of this assumption lies in observing convergence in $\bar{I}_{00(u)}$ with increasing u.

The above four equations are implemented by first computing

$$Q_{11} = G_{11}(z_u^{aa} - R_0) + G_{12} z_u^{ba}$$

$$Q_{12} = G_{11} z_u^{ab} + G_{12}(z_u^{bb} - R_0)$$

$$Q_{21} = G_{21}(z_u^{aa} - R_0) + G_{22} z_u^{ba}$$

$$Q_{22} = G_{21} z_u^{ab} + G_{22}(z_u^{bb} - R_0)$$

where $z_u^{aa} = z^{aa}[s_e + u\alpha_e, s_y + u\alpha_y]$ and so forth for z_u^{bb}, z^{ab}, and z^{ba};

$$G_{11} = \frac{R_0 + z_u^{bb}}{(R_0 + z_u^{bb})(R_0 + z_u^{aa}) - z_u^{ab} z_u^{ba}}$$

$$G_{12} = \frac{-z_u^{ab}}{(R_0 + z_u^{aa})(R_0 + z_u^{bb}) - z_u^{ab} z_u^{ba}}$$

43

$$G_{21} \approx \frac{-z_u^{ba}}{(R_0 + z_u^{aa})(R_0 + z_u^{bb}) - z_u^{ab} z_u^{ba}}$$

$$G_{22} = \frac{R_0 + z_u^{aa}}{(R_0 + z_u^{aa})(R_0 + z_u^{bb}) - z_u^{ab} z_u^{ba}}$$

and provision for a feed "forward" imperfect ground screen penetration transfer impedance z_u^{ba}, in addition to the feedback term z_u^{ba}, is included. It is expected that z_u^{ba} will be set to zero during an actual lens analysis for the reasons cited in Section 2.1 concerning (1) and (2). During validation of the simulation program, however, provision for z_u^{ba} other than zero may be helpful. Then

$$C_{00(0)}^a = -\sqrt{R_0}\, G_{11}\, z_0^{aa}\, I_{00}^{ex}$$

$$C_{00(0)}^b = -\sqrt{R_0}\, G_{21}\, z_0^{aa}\, I_{00}^{ex}$$

$$I_{00(0)}^a = -\frac{1}{\sqrt{R_0}}\, C_{00(0)}^a$$

$$I_{00(0)}^b = -\frac{1}{\sqrt{R_0}}\, C_{00(0)}^b$$

and, for $u = 1, 2, \ldots$,

$$C_{00(u)}^a = e^{-jk\ell_0}(Q_{11}\, C_{00(u-1)}^b + Q_{12}\, C_{00(u-1)}^a)$$

$$C_{00(u)}^b = e^{-jk\ell_0}(Q_{21}\, C_{00(u-1)}^b + Q_{22}\, C_{00(u-1)}^a)$$

$$I_{00(u)}^a = -\frac{1}{\sqrt{R_0}}(C_{00(u)}^a - e^{-jk\ell_0}\, C_{00(u-1)}^b)$$

$$I_{00(u)}^b = -\frac{1}{\sqrt{R_0}}(C_{00(u)}^b - e^{-jk\ell_0}\, C_{00(u-1)}^a)$$

where ℓ_0 is the length of reference element transmission line (module plus feedlines).

If the ground screen is perfectly conducting,
$$z_u^{ab} = z_u^{ba} = G_{12} = G_{21} = Q_{12} = Q_{21} = 0 \text{ and}$$

$$I_{00(u)}^b = 0 \qquad u \text{ even}$$

$$I_{00(u)}^a = 0 \qquad u \text{ odd}$$

3.2 Higher Approximations Method

The theory underlying the higher approximations method (HAM) is given in [5, Section 3.3]. First approximation radiating element currents initialize an iterative procedure that updates the current distributions on elements near discontinuities in periodicity (lens edge, section interface, failed modules, etc.) The lens radiation pattern also is updated.

The present implementation of HAM, discussed here, computes only the second approximation. This is expected to yield accurate results for lattice spacings exceeding $\sim 0.25\lambda$.

The subroutines called by HAM are listed in order of first invocation in Figure 13. Subroutines called by subroutines of HAM also are listed (indented) beneath their respective calling programs. A flow diagram of HAM is given in Figure 14.

The combined module and feedlines (transmission line mode) two-port model can be specified in terms of the specialized impedance parameters used in FAM or general scattering parameters. When impedance parameters are specified, the array $\underline{a}$ and array $\underline{b}$ second approximation port currents $I_0^{(2)a}$ $I_0^{(2)b}$ for a 0th array element are computed by solving [5, Eqs. (3-139) (3-1..] When scattering parameters are specified,

$$\bar{I}_0 = \begin{bmatrix} I_0^{(2)a} \\ I_0^{(2)b} \end{bmatrix}$$

45

```
GEOMET

ZIMPS
    ZIMP3
    ZIMP2
        HAMPSI

LINEQ

ZCOL

ARAYIN

XYGCS

AOFI

VIDCJ
    ZIMP3

CELPAT

TPLANE
    TPIN
```

Figure 13. Program HAM Subprograms

Figure 14.   Flow Diagram for HAM

(B)

LOOP OVER COLUMNS, n_a, OF ARRAY
(n_a INCREASES ALONG THE e LATTICE COORDINATE)

CALCULATE i^{th} ELEMENT xy COORDINATES WITH RESPECT TO CELL COORDINATE ORIGIN

$$x_i = md_x + x_{aref} \qquad y_i = nd_y - m\Delta y + y_{aref}$$

XYGCS

CALCULATE i^{th} ELEMENT LOCATION IN GLOBAL COORDINATES

$$x_{ig} = x_{cref} + x_i \cos \phi_g - y_i \sin \phi_g$$

$$y_{ig} = y_{cref} + x_i \sin \phi_g + y_i \cos \phi_g$$

LOOP OVER CELLS

INPUT ELEMENT PLACEMENT DATA FOR ℓ^{th} CELL

LOOP OVER ARRAYS WITHIN CELL

AOFI

DEFINE REGION OF INFLUENCE OF RADIATING ELEMENTS IN ℓ^{th} ARRAY DESCRIPTION RELATIVE TO i^{th} RADIATING ELEMENT

ARE ANY ELEMENTS WITHIN REGION OF INFLUENCE?
$m_2 = n_2 = 0$? — NO — (C)

YES

INPUT RANDOM ACCESS FILE RECORD IDENTIFIERS FOR FEEDBACK MODE INFORMATION OF ℓth CELL

LOOP OVER "COLUMNS" IN REGION OF INFLUENCE, $m = m_1, m_2$

LOOP OVER "ROWS" IN REGION OF INFLUENCE, $n = n_1, n_2$

(D)

Figure 14.   Continued

(D)

CALCULATE j^{th} ELEMENT xy COORDINATES WITH
RESPECT TO ℓ^{th} CELL COORDINATE ORIGIN

$$x_j = md_x + x_{\ell aref}$$

$$y_j = nd_y - m\Delta y + y_{\ell ref}$$

XYGCS

COMPUTE j^{th} ELEMENT LOCATION IN GLOBAL COORDINATES

$$x_{jg} = x_{\ell cref} + x_j \cos \phi_{\ell g} - y_j \sin \phi_{\ell g}$$

$$y_{ig} = y_{\ell cref} + x_j \sin \phi_{\ell g} - y_j \cos \phi_{\ell g}$$

COMPUTE DISTANCE BETWEEN i^{th} AND j^{th} ELEMENTS

$$r_s = \sqrt{(x_{ig} - x_{jg})^2 + (y_{ig} - y_{jg})^2}$$

COMPUTE FIRST APPROXIMATION CURRENT DISTRIBUTION ON j^{th} ARRAY $\underline{a}$ ELEMENT

$$\bar{I}_j^{(1)a} = \sum_{\substack{\text{feedback} \\ \text{mode } u}} \bar{I}_{(u)}^{(1)a} \exp\left[-jk((s_x + u\alpha_x)\, x_j + (s_y + u\alpha_y)\, y_j)\right]$$

AND SAME FOR j^{th} ARRAY $\underline{b}$ ELEMENT

VIDCJ

COMPUTE GENERALIZED VOLTAGE (EXCITATION) COLUMN VECTOR FOR ARRAY
$\underline{a}$ i^{th} ELEMENT DUE TO ARRAY $\underline{a}$ j^{tn} ELEMENT. ACCUMULATE IN $\bar{V}^{aa}$.

(E)

Figure 14.   Continued

49

(E)

VIDCJ

COMPUTE GENERALIZED VOLTAGE COLUMN VECTOR FOR ARRAY $\underline{b}$ i^{th} ELEMENT DUE TO ARRAY $\underline{b}$ j^{th} ELEMENT. ACCUMULATE IN $\bar{V}_i^{b\bar{b}}$.

END OF LOOP OVER "ROWS" n

END OF LOOP OVER "COLUMNS" m

(C)

END OF LOOP OVER ARRAYS WITHIN CELL

END OF LOOP OVER CELLS

INPUT CELL REFERENCE ELEMENT ILLUMINATION VOLTAGE COLUMN VECTOR $\bar{V}^{ex}$ AND ILLUMINATION PROGRESSIVE "PHASING" s_x, s_y

COMPUTE i^{th} ELEMENT ILLUMINATION VOLTAGE COLUMN VECTOR
$$\bar{V}_i^{ex} = \exp\left[-jk(s_x x_i + s_y y_i)\right] \bar{V}^{ex}$$

INPUT FIRST APPROXIMATION REFERENCE ELEMENT CURRENT DISTRIBUTION, GROUND SCREEN PENETRATION VOLTAGE COLUMN VECTOR, $\bar{V}^{ab}$, AND MODULE PROGRESSIVE "PHASING," α_x, α_y, FOR ALL FEEDBACK MODES

COMPUTE i^{th} ELEMENT GROUND SCREEN PENETRATION VOLTAGE COLUMN VECTOR

$$\bar{V}_i^{ab} = \sum_{\substack{\text{feedback} \\ \text{modes } u}} \exp\left[-jk((s_x + u\alpha_x) x_i + (s_y + u\alpha_y) y_i)\right] \bar{V}^{ab}$$

COMPUTE ARRAY $\underline{b}$ i^{th} ELEMENT OPEN CIRCUIT PORT VOLTAGE

$$V_i^b = -Z^b \bar{Y}^b \bar{V}_i^{bb}$$

(Z^b = ARRAY $\underline{b}$ ISOLATED ELEMENT DRIVING POINT IMPEDANCE)

(F)

Figure 14. Continued

50

(F)

COMPUTE ARRAY a ith ELEMENT PORT VOLTAGE

$$V_i^a = -Z_i^a \bar{Y}^a (\bar{V}_i^{ex} + \bar{V}_i^{aa} + \bar{V}_i^{ab})$$

(Z^a = ARRAY a ISOLATED ELEMENT DRIVING POINT IMPEDANCE)

ARE MODULES (PLUS FEEDLINES) REPRESENTED BY TWO-PORT IMPEDANCE PARAMETERS?

NO

YES

CALCULATE SECOND APPROXIMATION PORT CURRENTS OF ith ARRAY a AND ARRAY b ELEMENTS $I_i^{(2)a}$, $I_i^{(2)b}$ VIA SCATTERING PARAMETER MODEL GIVEN BY EQUATIONS OF SECTION 3.2.

CALCULATE SECOND APPROXIMATION PORT CURRENTS OF ith ARRAY a AND ARRAY b ELEMENTS $I_i^{(2)a}$, $I_i^{(2)b}$ VIA SPECIALIZED IMPEDANCE PARAMETER MODEL GIVEN BY EQS. (3-139) AND (3-140) OF [5].

COMPUTE FIRST APPROXIMATION CURRENT DISTRIBUTION ON i^{th} ARRAY b ELEMENT

$$\bar{I}_i^{(1)b} = \sum_{\substack{\text{feedback} \\ \text{modes } u}} \bar{I}_{(u)}^{(1)b} \exp[-jk((s_x + u\alpha_x) x_i + (s_y + u\alpha_y) y_i)]$$

COMPUTE ARRAY b i^{th} ELEMENT CORRECTION CURRENT DISTRIBUTION

$$\bar{I}_i^c = \bar{I}_i^{(1)b} (I_i^{(2)b}/A - 1)$$

WHERE A = ELEMENT OF $\bar{I}_i^{(1)b}$ CORRESPONDING TO FEED PORT OF RADIATING ELEMENT

(G)

Figure 14.   Continued

51

Figure 14.   Concluded

52

is given by

$$\bar{I}_0 = - [R]^{\frac{1}{2}} ([U] - [S_0]) \, \bar{C}_0$$

where $[R]$ and $[U]$ are defined in the discussion following (11), $[S_0]$ is the zero[th] element's scattering parameter matrix, and $\bar{C}_0$ is the zero[th] element's incident scattering variable column vector. The vector $\bar{C}_0$ is the solution to
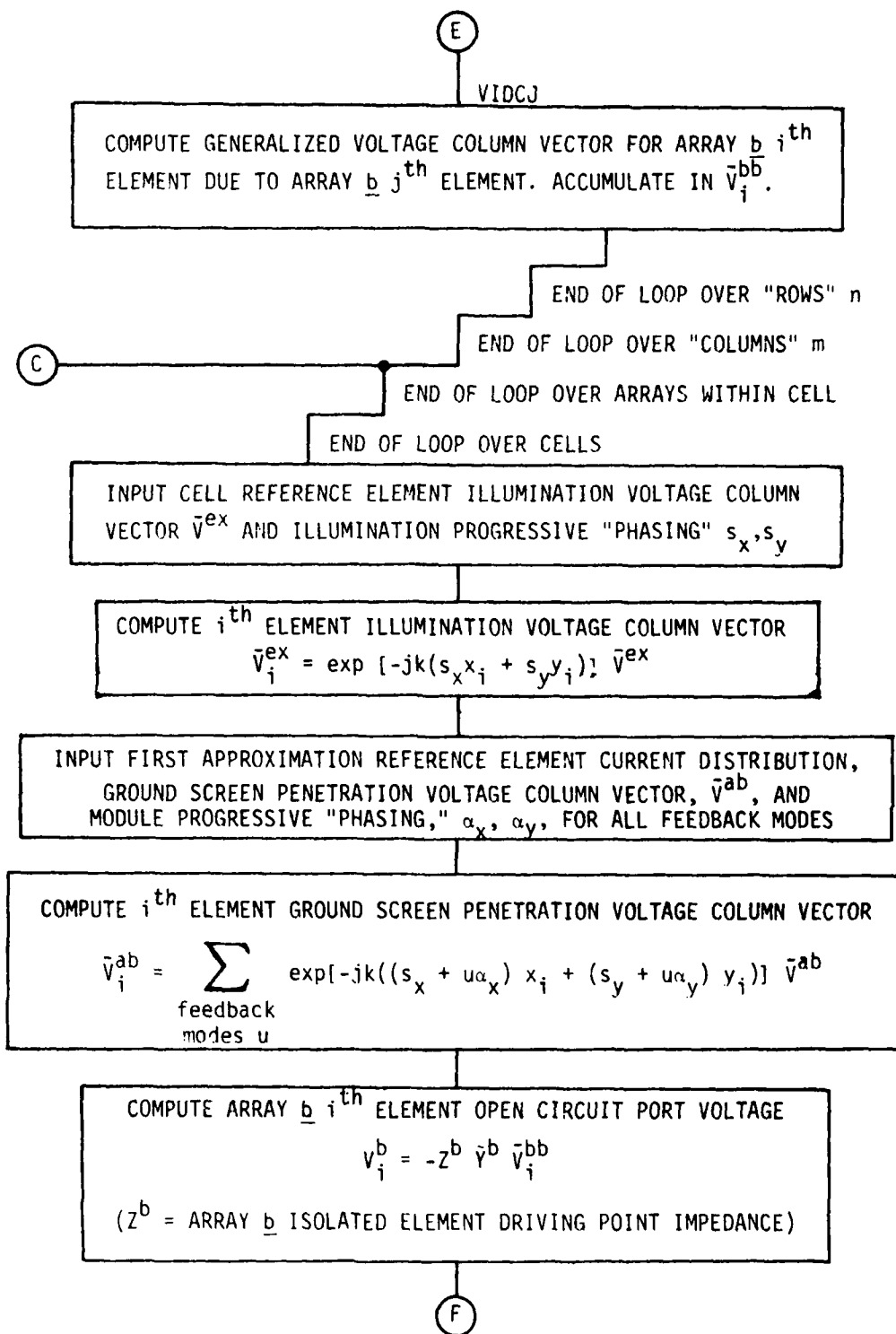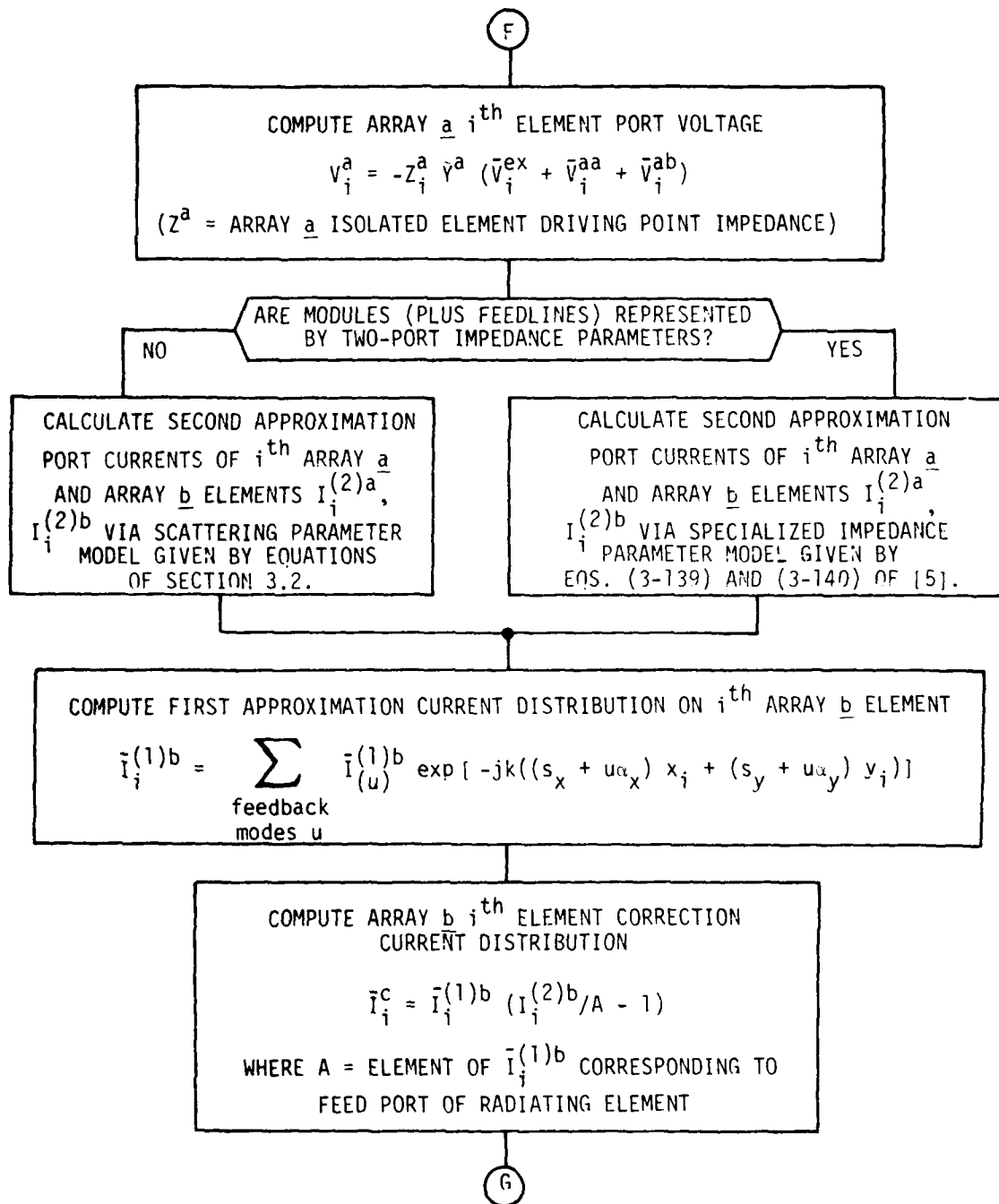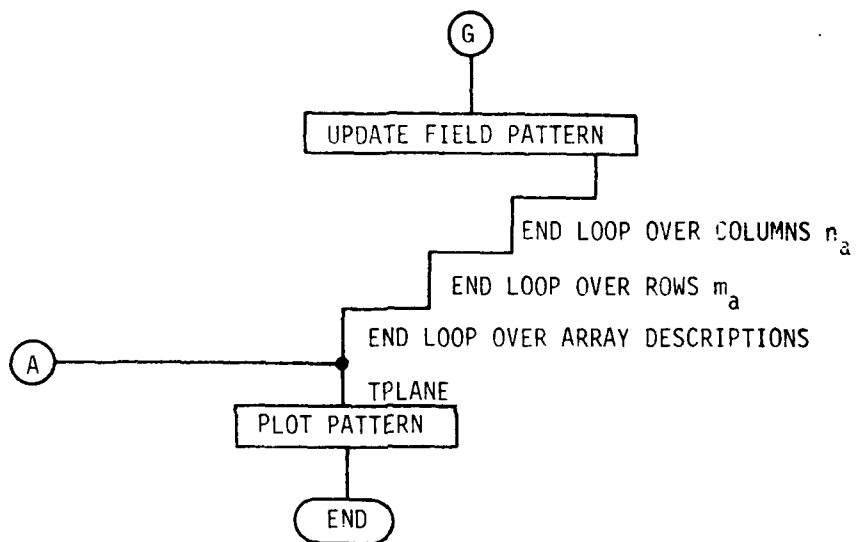
$$[R]^{\frac{1}{2}} ([U] + [S_0] + [z] ([U] - [S_0])) \, \bar{C}_0 = [z] \, \bar{I}_0^{sc}$$

where

$$[z] = \begin{bmatrix} z^a & 0 \\ & \\ 0 & z^b \end{bmatrix}$$

$$\bar{I}_0^{sc} = \begin{bmatrix} I_0^{ex} + I_0^{(1)aa'} + I_0^{(1)ab} \\ \\ \\ I_0^{(1)bb'} \end{bmatrix}$$

z^a and z^b are the array $\underline{a}$ and the array $\underline{b}$ isolated-element-above-a-ground-screen input impedances; and I_0^{ex}, $I_0^{(1)aa'}$, $I_0^{(1)ab}$, and $I_0^{(1)bb'}$ are the zero[th] element's short circuit port currents due to the illumination and first approximation currents on neighboring elements [5, Section 3.3.1].

3.3 Subprograms

The subroutine and function subprograms, typically not provided by a computer system, that are used in FAM and HAM are described below. The discussion follows closely the theoretical development of Section 2 and [5].

3.3.1 ZMATG

Subroutine ZMATG fills the moment matrices [Z] and [Z^{gs}] for planar arrays of general "out of plane" thin wire radiators with and without a perfect ground screen. The ground screen is located in the xy plane parallel to the array plane. Block Toeplitz symmetry allows reducing the number of computed matrix elements corresponding to interaction between segments on the same straight wire to the number of segments on that wire. (Toeplitz symmetry means $Z_{ij} = Z_{i+p,j+p}$ for p an integer.) Toeplitz symmetry generally is not exhibited by matrix elements corresponding to interaction between segments on different wires. Also Toeplitz symmetry generally is not present in the ground screen image interaction matrix [Z^{imag}] that subtracts from [Z] to yield [Z^{gs}]. However, significant computational savings usually is achieved since closely spaced segments usually require the most computation due to slowly converging plane wave expansions and closely spaced segments usually are located on the same wire.

The ijth element of the free space (ground screen absent) moment matrix [Z] is computed in OFFD for $i \neq j$ (off-diagonal element) as defined by (38). There, PSIGEN is invoked five times to approximate the five plane wave expansions

$$\psi(\alpha, \beta) = \sum_{q=-\infty}^{\infty} \sum_{p=-\infty}^{\infty} \psi_{pq}(\alpha, \beta) \qquad (49)$$

where $\alpha, \beta = i,j; \ i_a,j_a; \ i_a,j_b; \ i_b,j_a;$ or i_b,j_b. The i,jth element of [Z] is computed there according to

$$Z_{ij} = \frac{\eta}{2d_x d_y} \left[\Delta_i \Delta_j (\hat{\ell}_i \cdot \hat{\ell}_j) \ \psi(i,j) - \frac{1}{k^2} \ \psi(i_a,j_a) - \frac{1}{k^2} \ \psi(i_b,j_b) \right.$$

$$\left. + \frac{1}{k^2} \ \psi(i_a,j_b) + \frac{1}{k^2} \ \psi(i_b,j_a) \right] \qquad (50)$$

Equation (38) simplifies for diagonal elements of [z]. The ith diagonal element is computed in ZMATG directly via three plane wave expansions according to

$$z_{ii} = \frac{n(\Delta_i^2 - 2/k^2)}{2d_x d_y} \, \psi(i,i) + \frac{\eta}{2d_x d_y k^2} \, \psi(i_a, i_b) + \frac{\eta}{2d_x d_y k^2} \, \psi(i_b, i_a)$$

(51)

by invoking PSIGEN three times.

A flow diagram for ZMATG is given in Figure 15.

3.3.2 PSIGEN

Subroutine PSIGEN computes the ψ defined by (49) and (36) in determining the infinite array moment matrices. There are two types of ψ computations. One type sums over ψ_{pq} that contain both positive z and negative z traveling waves as defined by (36c). The other sums over ψ_{pq} that contain either all positive z traveling waves or all negative z traveling waves but not both as defined by (36a,b).

Let the vector $\vec{w}_{\alpha\beta}$ be the difference vector between one of the end points or center of the jth expansion segment and one of the end points or center of the ith test segment. The five possible forms for $\vec{w}_{\alpha\beta}$ are

$$\vec{w}_{ij} = \vec{r}_i - \vec{r}_j'$$

$$\vec{w}_{i_a j_a} = \vec{r}_i - \vec{r}_j' + \frac{\Delta_i}{2} \hat{\ell}_i - \frac{\Delta_j}{2} \hat{\ell}_j$$

$$\vec{w}_{i_b j_b} = \vec{r}_i - \vec{r}_j' - \frac{\Delta_i}{2} \hat{\ell}_i + \frac{\Delta_j}{2} \hat{\ell}_j$$

$$\vec{w}_{i_a j_b} = \vec{r}_i - \vec{r}_j' + \frac{\Delta_i}{2} \hat{\ell}_i + \frac{\Delta_j}{2} \hat{\ell}_j$$

$$\vec{w}_{i_b j_a} = \vec{r}_i - \vec{r}_j' - \frac{\Delta_i}{2} \hat{\ell}_i - \frac{\Delta_j}{2} \hat{\ell}_j$$

(52)

BEGIN

BEGIN j = 1, ns LOOP
OVER SOURCE SEGMENTS

BEGIN i = j, ns LOOP
OVER TEST SEGMENTS

TEST FOR TOEPLITZ SYMMETRY.
IF APPLICABLE, SET

$$[Z]_{i,j} = [Z]_{j,i}$$

$$[Z]_{j,i} = [Z]_{j-1,i-1}$$

AND BRANCH TO END OF i LOOP

BEGIN i,j INTERCHANGE LOOP:
ij = 1, 2, ONCE FOR $[Z]_{i,j}$
AND AGAIN FOR $[Z]_{j,i}$.
IF i = j COMPUTE ONLY $[Z]_{i,j}$.

PERP
DEFINE i^{th} SEGMENT
RADIUS VECTOR $\vec{a}_i$

DEFINE VECTOR BETWEEN CENTERS
OF jth SOURCE SEGMENT AND
i^{th} TEST SEGMENT
$\vec{rr} = \vec{r}_i' + \vec{a}_i - \vec{r}_j'$

CHECK FOR MATRIX SELF-ELEMENT
i = j?

SELF-ELEMENT
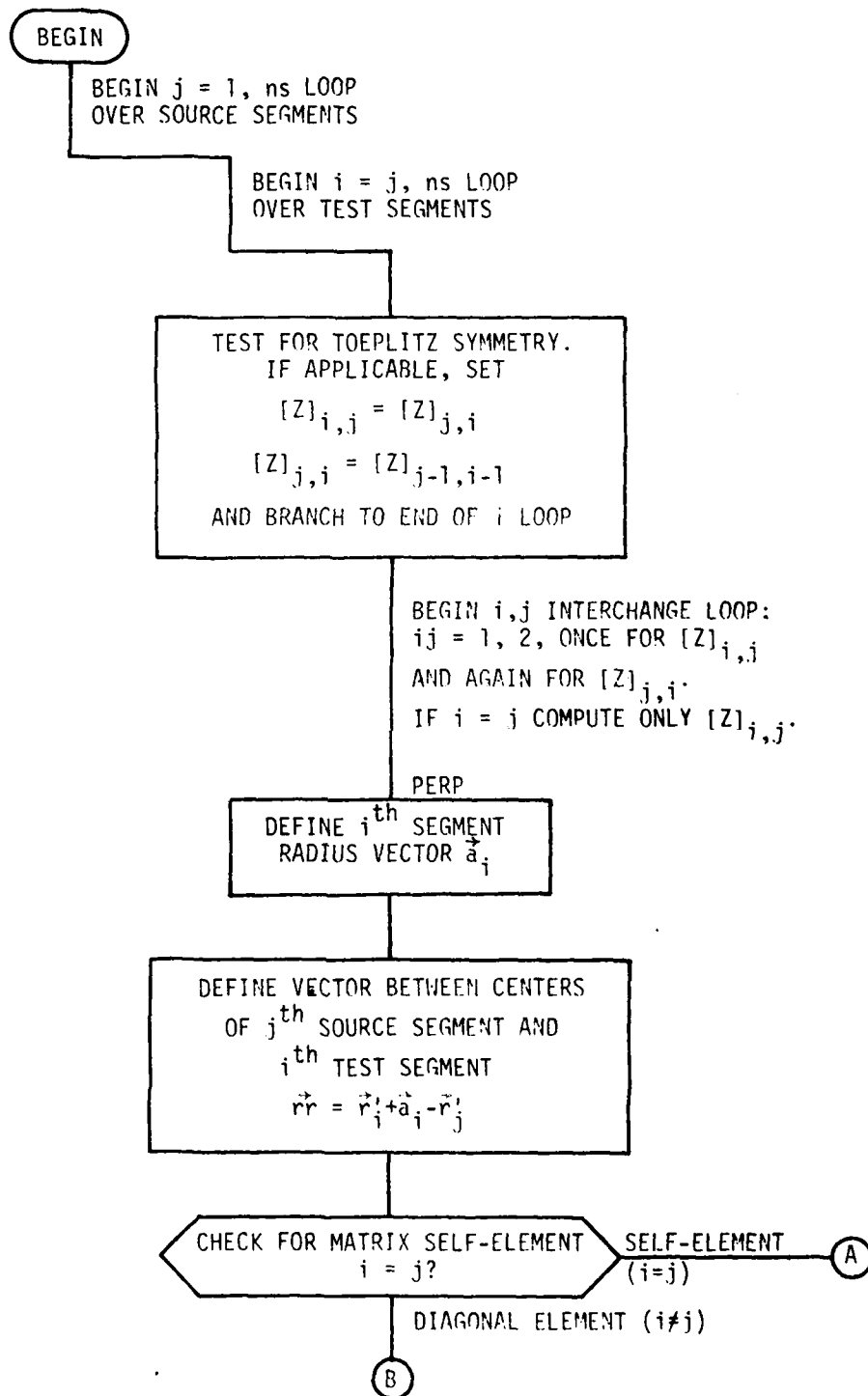(i=j)   Ⓐ

DIAGONAL ELEMENT (i≠j)
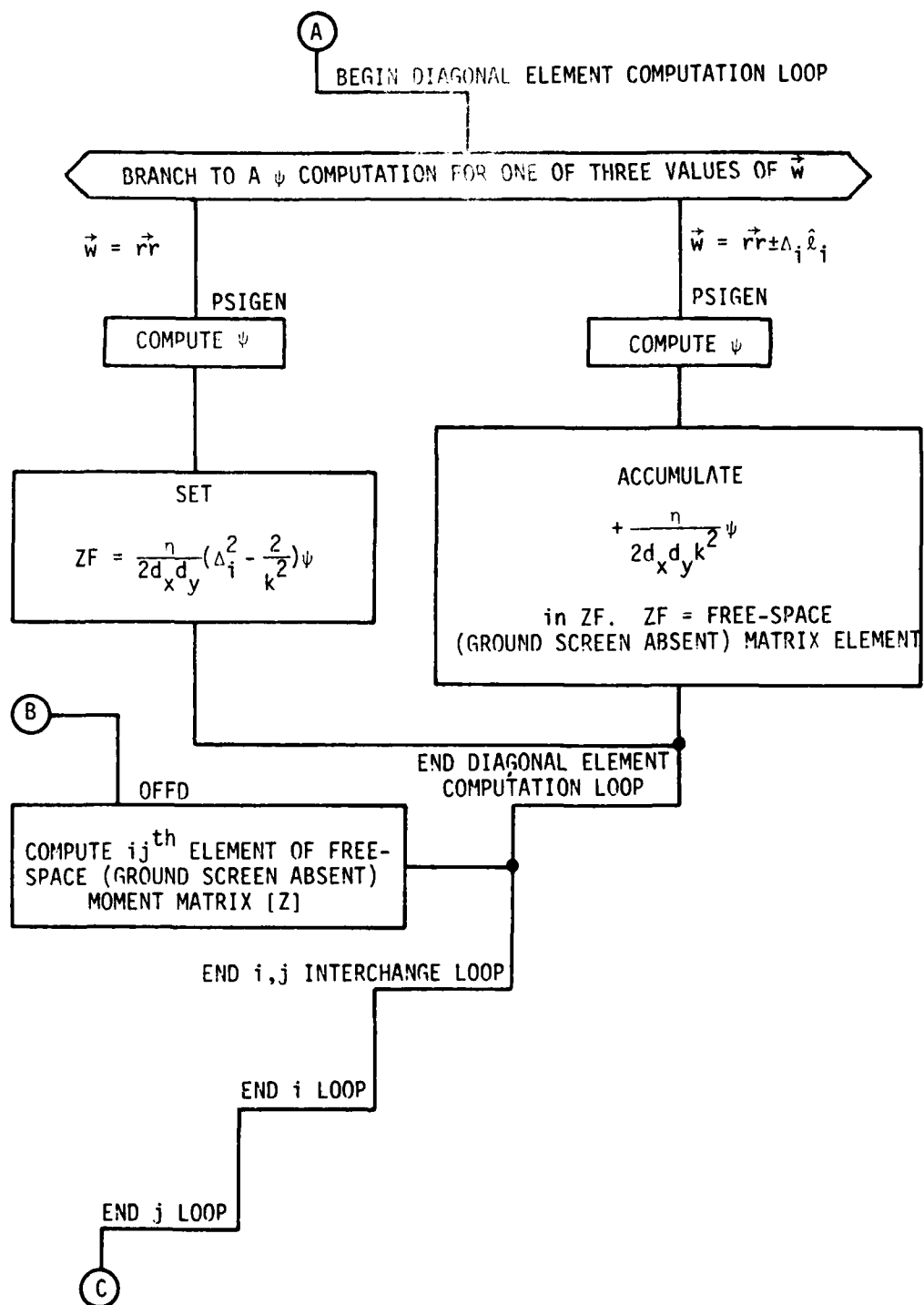
Ⓑ

Figure 15.   Flow Diagram for ZMATG
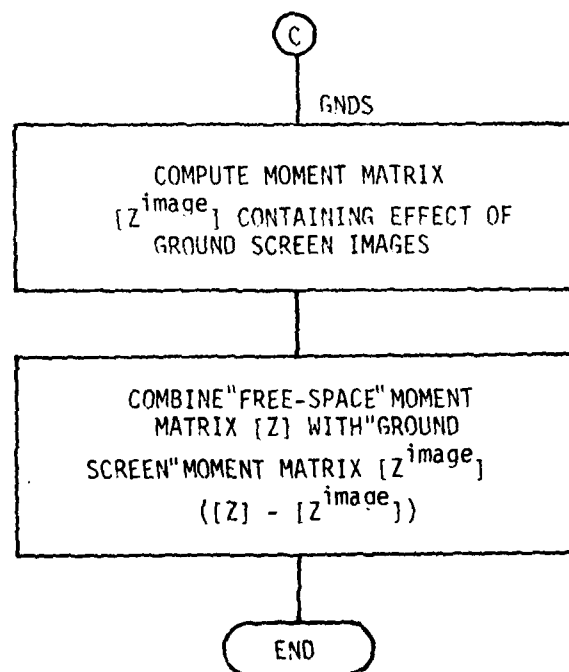
56

Figure 15. Continued

Figure 15. Concluded

58

where $\vec{r}_i = \vec{r}_i' + \vec{a}_i$. (The variables $\vec{r}_i$, $\vec{a}_i$, etc., are defined in the theory (Section 2.2).) The ψ computation is treated as involving both positive z and negative z traveling waves, and is performed in PSIGEN directly, if

$$|\vec{w} \cdot \hat{z}| < \frac{\Delta_j}{2} |\hat{\ell}_j \cdot \hat{z}| - 0.1 \, a_j$$

Otherwise, the ψ computation is treated as involving either positive z traveling waves only or negative z traveling waves only and is computed by invoking PSIA. The $0.1 \, a_j$ (tenth of the jth wire segment radius) assures that the more efficient PSIA computation will be performed whenever practicable.

The PSIGEN ψ computation is performed according to (49) where

$$\psi_{pq}(\alpha, \beta) = \frac{\pm 1}{jk\Delta_j} (A_\pm - B_\pm) \tag{53}$$

for $\hat{\ell}_j \cdot \hat{z} \gtrless 0$. In (53),

$$A_\pm = \frac{\exp[-jk(\vec{w}_{\alpha\beta} - \bar{\ell}\hat{\ell}_j) \cdot \hat{g}_+] - \exp[-jk(\vec{w}_{\alpha\beta} \pm \frac{\Delta_j}{2} \hat{\ell}_j) \cdot \hat{g}_+]}{g_z \hat{\ell}_j \cdot \hat{g}_+} \tag{54}$$

$$B_\pm = \frac{\exp[-jk(\vec{w}_{\alpha\beta} - \bar{\ell}\hat{\ell}_j) \cdot \hat{g}_-] - \exp[-jk(\vec{w}_{\alpha\beta} \mp \frac{\Delta_j}{2} \hat{\ell}_j) \cdot \hat{g}_-]}{g_z \hat{\ell}_j \cdot \hat{g}_-} \tag{55}$$

Since $\vec{w}_{\alpha\beta} - \bar{\ell}\hat{\ell}_j$ has no $\hat{z}$ component, the leading exponential terms in the numerators of (54) and (55) are equal.

If

$$|k(\bar{\ell} \pm \Delta_j/2) \, (\hat{\ell}_j \cdot \hat{g}_+)/2| << 1 \tag{56}$$

as may happen if $\hat{\ell}_j \cdot \hat{g}_+ \to 0$, $A_\pm$ is approximated by

$$A_\pm = \frac{\exp[-jk(\vec{w}_{\alpha\beta} - (\bar{\ell} \mp \Delta_j/2)\hat{\ell}_j/2) \cdot \hat{g}_+] \, jk(\bar{\ell} \pm \Delta_j/2)}{g_z} \tag{57}$$

Similarly, if

$$\left| k(\bar{\ell} \mp \Delta_j/2) \; (\hat{\ell}_j \cdot \hat{g}_-)/2 \right| << 1 \tag{58}$$

$B_\pm$ is approximated by

$$B_\pm = - \frac{\exp[-jk(\vec{w}_{\alpha\beta} - (\bar{\ell} \pm \Delta_j/2)\hat{\ell}_j/2) \cdot \hat{g}_-] \; jk(\bar{\ell} \mp \Delta_j/2)}{g_z}$$

Equation (57) (or (59)) can be derived by recasting $A_\pm$ of (54) (or $B_\pm$ of (55))
into the form

$$Y \, \frac{\sin X}{X}$$

Under the condition (56) *(or* (58)), $X \doteq 0$ and $Y \doteq A_\pm$ of (57) (or $B_\pm$ of (59)).

The pq looping between elliptical contours (circular contours in recip-
rocal lattice space) is described in the description for subroutine PSIA.

A flow diagram for PSIGEN is given in Figure 16.

3.3.3 PSIA

Subroutine PSIA computes $\psi(\alpha,\beta)$ of (49) with the $\psi_{pq}(\alpha,\beta)$ **given by**
(36 a,b) . The plane waves of (36a) are all positive z traveling waves, those
of (36b) are all negative z travelling waves. The case where the $\psi_{pq}(\alpha,\beta)$ are de-
fined by (36c) (combination of positive z and negative z traveling plane
waves) is handled in PSIGEN.

In PSIA, the $\psi_{pq}(\alpha,\beta)$ are computed from

$$\psi_{pq}(\alpha,\beta) = \frac{1}{jk\Delta_j g_z (\hat{\ell}_j \cdot \hat{g}_\pm)} \left(\exp[-jk(\vec{w}_{\alpha\beta} - \frac{\Delta_j}{2} \hat{\ell}_j) \cdot \hat{g}_\pm] \right.$$

$$\left. - \exp[-jk(\vec{w}_{\alpha\beta} + \frac{\Delta_j}{2} \hat{\ell}_j) \cdot \hat{g}_\pm] \right) \tag{59}$$

BEGIN

CHECK IF SOURCE INTEGRATION IS IN "ONE PART " i.e., PLANE WAVE EXPANSION CONTAINS EITHER ALL POSITIVE z TRAVELING WAVES OR ALL NEGATIVE z TRAVELLING WAVES BUT NOT A COMBINATION.

ONE PART INTEGRATION

TWO PART INTEGRATION

DEFINE CONSTANTS PRIOR TO pq LOOPS FOR COMPUTING ψ_{pq} VIA EQ. (52).

INTERCHANGE SOME CONSTANTS IF SOURCE SEGMENT REFERENCE DIRECTION ($\hat{\ell}_j$) HAS A NEGATIVE z COMPONENT.

BEGIN p LOOP

SET UP pq LOOP BOUNDS ACCORDING TO ELLIPTICAL RING INCREMENTING (CIRCULAR CONTOURS IN RECIPROCAL LATTICE SPACE).

BEGIN pq LOOPS

DEFINE $g_\pm$ AND OTHER CONSTANTS.

DECIDE COMPUTATIONAL FORM OF $A_\pm$.
IS $|(k(\hat{\ell} \pm \Delta_j/2)(\hat{\ell}_j \cdot \hat{g}_+)/2)| < 0.001$?

NO

YES

DETERMINE A_+ BY EQ. (53) AND ACCUMULATE IN ψ.

DETERMINE A_+ BY EQ. (56) AND ACCUMULATE IN ψ.

A

CHECK WHETHER PLANE WAVES ARE POSITIVE z OR NEGATIVE z TRAVELING BY TESTING w_z.
WHERE w_z IS THE z COMPONENT OF THE VECTOR.

$$\vec{w} = \begin{cases} \vec{r}_i - \vec{r}_j & (i \neq j) \\ \vec{r}_i - \vec{r}_j' \pm \frac{\Delta_i}{2}\hat{\ell}_i \pm \frac{\Delta_j}{2}\hat{\ell}_j & (i \neq j) \\ \vec{r}_i - \vec{r}_i' \pm \Delta_i \hat{\ell}_i & (i = j) \end{cases}$$

AS DEFINED IN THE CALLING PROGRAMS OFFD AND ZMATG.

POSITIVE z ($w_z > 0$)

NEGATIVE z ($w_z < 0$)

SET FLAG = TRUE

SET FLAG = FALSE

INCREASE w_z TO A MINIMUM VALUE, IF NECESSARY TO SPEED PLANE WAVE EXPANSION CONVERGENCE

DECREASE w_z (w_z IS NEGATIVE) TO A MAXIMUM VALUE, IF NECESSARY, TO SPEED PLANE WAVE EXPANSION CONVERGENCE

PSIA

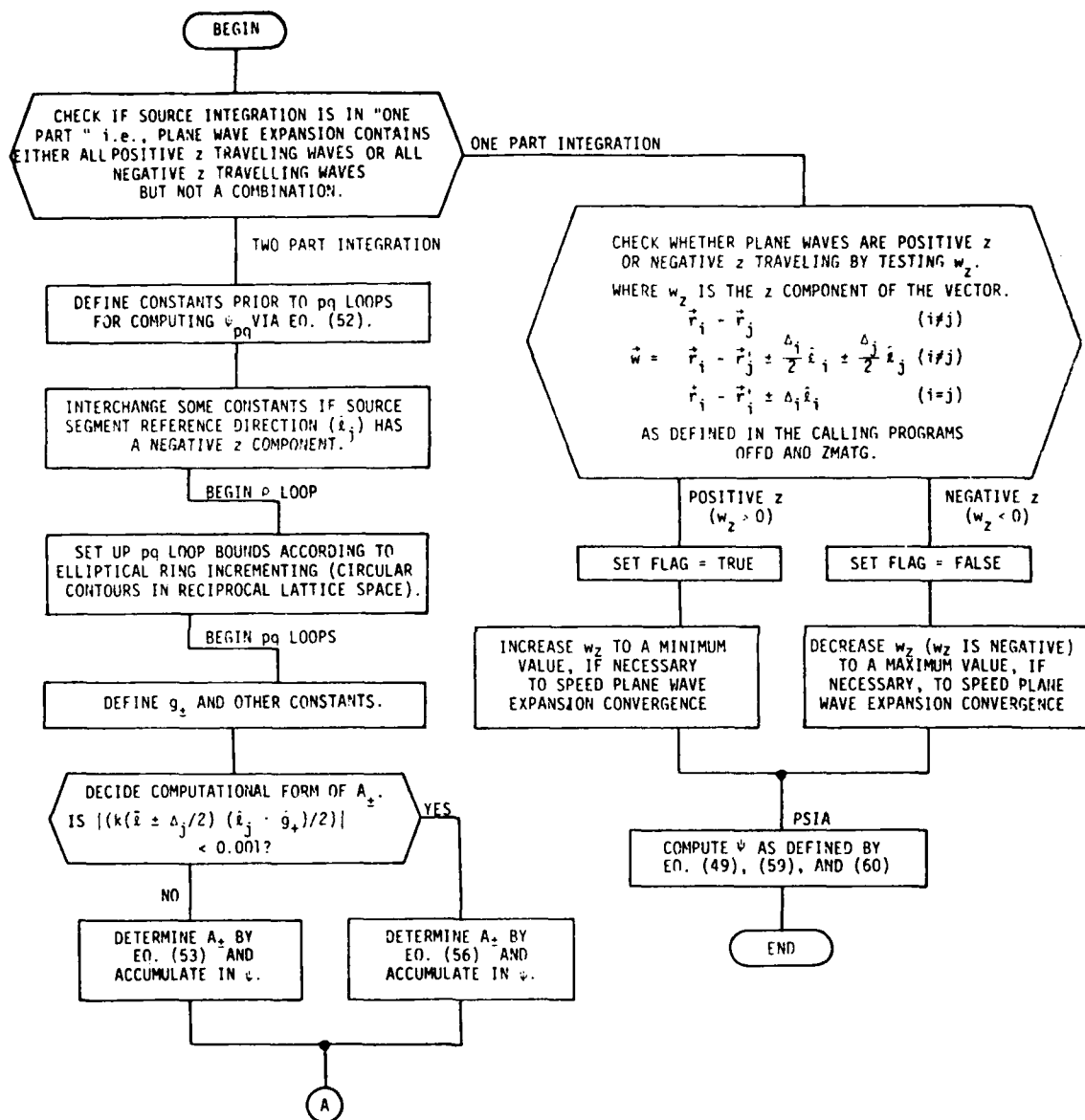COMPUTE ψ AS DEFINED BY EQ. (49), (59), AND (60)
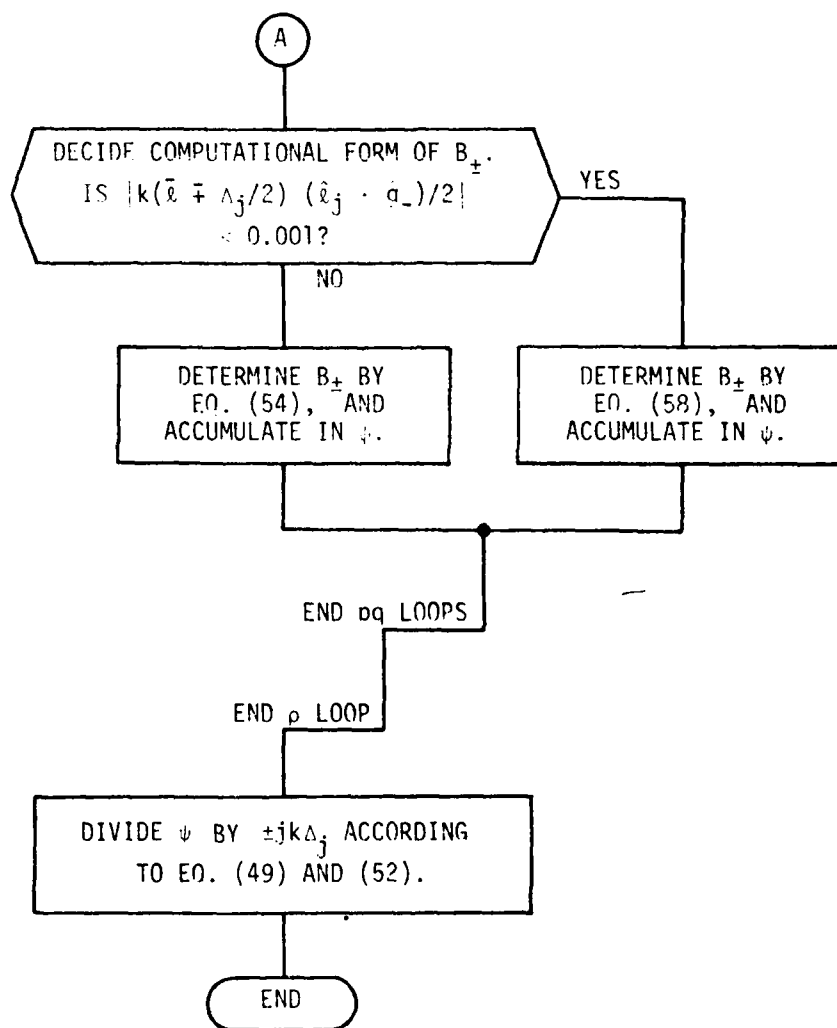
END

Figure 16. Flow Diagram for PSIGEN

61

Figure 16. Concluded

for $\vec{w}_{\alpha\beta} \cdot \hat{z} \gtrless 0$ where $\vec{w}_{\alpha\beta}$ is determined from one of the five forms of (52).

If $|k(\hat{\ell}_j \cdot \hat{g}_\pm) \Delta_j/2| << 1$, however $\psi_{pq}(\alpha,\beta)$ is computed according to the approximation

$$\psi_{pq}(\alpha,\beta) = \frac{1}{g_z} \exp[-jk\vec{w} \cdot \hat{g}_\pm] \tag{60}$$

The doubly infinite pq summations in (49) are, of course, approximated by finite summations. The area in pq space containing the points over which the summation is performed is chosen to be elliptical. The reason for chosing ellipses is that a characteristic factor of the ψ_{pq} functions has the form

$$F = \frac{\exp[-jk\vec{R} \cdot \hat{g}_\pm]}{g_z}$$

for $R_z \gtrless 0$ where $\vec{R}$ is a spatial vector with z component R_z. For p and/or q sufficiently large, $g_\pm$ is approximated by

$$\hat{g}_\pm \doteq \rho_x \hat{x} + \rho_y \hat{y} \mp j\rho$$

where

$$\rho = \sqrt{\rho_x^2 + \rho_y^2}$$

$$\rho_x = s_x + \frac{p\lambda}{d_x} + q \frac{\lambda \Delta y}{d_x d_y}$$

$$\rho_y = s_y + q \frac{\lambda}{d_y}$$

Then

$$|F| \doteq \frac{\exp[-k|R_z|\rho]}{\rho}$$

Contours of constant $|F|$ are, therefore, circles of radii ρ in ρ_x, ρ_y space and ellipses in p,q space. (The space defined by the coordinates ρ_x and ρ_y is typically called "inverse lattice space".)

63

The summations in (49) are performed by adding contributions in p,q space corresponding to the area between circular contours in ρ_x, ρ_y space. A maximum radius ρ_{max} is chosen by the user, and, to monitor convergence, a "minimum" radius ρ_{min} and incremented radius $\Delta\rho$ also are chosen. The summation over the ψ_{pq} is performed by first including all values corresponding to points within the ρ_{min} circular contour. The contribution from points within the ρ_{min} and $\rho_{min} + \Delta\rho$ circles then are added to the summation and so on until the contribution corresponding to all points within the ρ_{max} circle is determined. The value of ψ at each step in the process can be recorded as a means for observing convergence. For each step in the process, the elliptical contours in pq space that correspond to the circular contours in ρ_x, ρ_y space are determined. Thus the computer code has a "ρ" loop which takes on the values $\rho = \rho_{min}$, $\rho_{min} + \Delta\rho$, $\rho_{min} + 2\Delta\rho$, ... , ρ_{max} and, for each ρ, p and q loops where the bounds on p and q are the ellipses corresponding to circles in ρ_x, ρ_y space of previous ρ value and present ρ value radii.

Large values of ρ_{max} are required for small values of $k|R_z|$. When

$$|R_z| \leq a_j$$

where a_j = radius of jth segment, the user supplied value of ρ_{max} ($\rho_{max} = \rho_u$) is used. Otherwise, ρ_{max} is computed in PSIA according to

$$\rho_{max} = \rho_u a_j / |R_z| \tag{61}$$

The parameters ρ_{min} and $\Delta\rho$ also are adjusted if necessary, and ρ_{max} is set to a minimum value (usually = 5) if ρ_{max}, as computed by (61), should be less than 5.

The ψ computation in PSIGEN always uses $\rho_{max} = \rho_u$ since the characteristic factor is

$$F = \frac{1}{g_z}$$

and the series in (49) is absolutely divergent. The terms in the series oscillate, however, and the series appears to converge conditionally.

64

A flow diagram of PSIA is given in Figure 17.

3.3.4 OFFD

The ij^{th} off-diagonal element of the ground screen absent moment matrix $[Z]$ or the ij^{th} element of the ground screen "image" matrix $[Z^{image}]$ is computed in OFFD. The equation that is implemented is discussed in the ZMATG description. A flow diagram of OFFD is given in Figure 18.

3.3.5 GNDS

Subroutine GNDS computes the matrix $[Z^{image}]$. The ij^{th} element of $[Z^{image}]$ is the interaction between the jth segment ground screen image and the ith segment. Toeplitz symmetry, even applied to a straight wire, is not generally exhibited in $[Z^{image}]$. Thus all ij elements are computed individually. The generally wide separation between wire segments and images, however, results in rapid convergence of (49) and fast computation times. A flow diagram is given in Figure 19.

3.3.6 VIDCJ

This subroutine computes the generalized voltage excitation column vector $\bar{V}_i^{aa}$ (or $\bar{V}_i^{bb}$) of the ith element of an array due to the jth neighboring radiating element current distribution in the region of influence. Each segment of the jth element current distribution is approximated as a Hertzian dipole. The voltage is accumulated in $\bar{V}_i^{aa}$ (or $\bar{V}_i^{bb}$) as VIDCJ is called for each radiating element in the region of influence.

A flow diagram of VIDCJ is given in Figure 20.

3.3.7 AOFI

This subroutine computes region of influence boundaries for the ith radiating element in a higher approximation computation. All radiating elements within the region of influence will be included in the higher approximation computation of $\bar{V}^{aa}$ (or $\bar{V}^{bb}$) corresponding to the ith element. Lens face elements are tested for location within the region of influence by looping over all cells and considering each cell array description individually. All array descriptions are considered "regular" for this computation,

BEGIN

DEFINE CONSTANTS PRIOR TO pq LOOPS FOR COMPUTING ψ_{pq} VIA EQ. (59) AND (60).

ADJUST PLANE WAVE SERIES TRUNCATION (ρ LOOP BOUNDS)

BEGIN ρ LOOP

SET UP pq LOOP BOUNDS ACCORDING TO ELLIPTICAL RING INCREMENTING (CIRCULAR RINGS IN RECIPROCAL LATTICE SPACE)

BEGIN pq LOOPS

DEFINE $\hat{g}_{\pm}$ ACCORDING TO:

g_{+} IF POSITIVE z TRAVELING WAVES ONLY (FLAG = TRUE)

g_{-} IF NEGATIVE z TRAVELING WAVES ONLY (FLAG = FALSE)

DECIDE COMPUTATIONAL FORM OF ψ_{pq}. IS $|k(\hat{\ell}_j \cdot \hat{g}_{\pm}) \Delta_j/2| < 0.001$?

YES

NO

DETERMINE ψ_{pq} ACCORDING TO EQ. (59) AND ACCUMULATE IN ψ.

DETERMINE ψ_{pq} ACCORDING TO EQ. (60) AND ACCUMULATE IN ψ.

END pq LOOPS

END ρ LOOP

END

Figure 17. Flow Diagram for PSIA

BEGIN

BEGIN ij^{th} ELEMENT COMPUTATION LOOP

BRANCH TO A ψ COMPUTATION FOR ONE OF FIVE VALUES OF $\vec{w}$.

$\vec{w} = \vec{rr}$

$\vec{w} = \begin{cases} \vec{rr} + \dfrac{\Delta_i}{2}\hat{\ell}_i - \dfrac{\Delta_j}{2}\hat{\ell}_j \\ \vec{rr} - \dfrac{\Delta_i}{2}\hat{\ell}_i + \dfrac{\Delta_j}{2}\hat{\ell}_j \end{cases}$

$\vec{w} = \begin{cases} \vec{rr} + \dfrac{\Delta_i}{2}\hat{\ell}_i + \dfrac{\Delta_j}{2}\hat{\ell}_j \\ \vec{rr} - \dfrac{\Delta_i}{2}\hat{\ell}_i - \dfrac{\Delta_j}{2}\hat{\ell}_j \end{cases}$

PSIGEN

COMPUTE ψ

PSIGEN

COMPUTE ψ

PSIGEN

COMPUTE ψ

SET ZF = $\Delta_i \Delta_j (\hat{\ell}_i \cdot \hat{\ell}_j)\psi$

ACCUMULATE $-\dfrac{1}{k^2}\psi$ in ZF

ACCUMULATE $+\dfrac{1}{k^2}\psi$ in ZF

END ij^{th} ELEMENT
COMPUTATION LOOP

FREE-SPACE (GROUND SCREEN ABSENT) MATRIX OFF-DIAGONAL ELEMENT
OR GROUND SCREEN "IMAGE" MATRIX ELEMENT COMPUTED AS

$$\frac{n}{2d_x d_y} ZF$$

END

Figure 18. Flow Diagram for OFFD

67

```
                        ┌─────────┐
                        │  BEGIN  │
                        └────┬────┘
                             │
                  BEGIN i=1,ns LOOP OVER TEST SEGMENTS
                             │
                        PERP │
            ┌────────────────┴──────────────┐
            │ DEFINE i^th SEGMENT           │
            │ RADIUS VECTOR $\vec{a}_i$     │
            └────────────────┬──────────────┘
                             │
                  BEGIN j=1,ns LOOP OVER IMAGE SEGMENTS
                             │
```

DEFINE VECTOR BETWEEN CENTERS OF jth IMAGE SEGMENT AND i^{th} TEST SEGMENT

$$\vec{rr}\cdot\hat{x} = (\vec{r}_i' + \vec{a}_i - \vec{r}_j')\cdot\hat{x}$$
$$\vec{rr}\cdot\hat{y} = (\vec{r}_i' + \vec{a}_i - \vec{r}_j')\cdot\hat{y}$$
$$\vec{rr}\cdot\hat{z} = (\vec{r}_i' + \vec{a}_i + \vec{r}_j')\cdot\hat{z}$$

DEFINE j^{th} IMAGE SEGMENT UNIT VECTOR

$$\hat{\ell}_j''\cdot\hat{x} = \hat{\ell}_j\cdot\hat{x}$$

$$\hat{\ell}_j''\cdot\hat{y} = \hat{\ell}_j\cdot\hat{y}$$

$$\hat{\ell}_j''\cdot\hat{z} = -\hat{\ell}_j\cdot\hat{z}$$

OFFD

COMPUTE ij^{th} ELEMENT OF GROUND SCREEN "IMAGE" MATRIX $[Z^{image}]$

END LOOP OVER IMAGE SEGMENTS

END LOOP OVER TEST SEGMENTS

```
                        ┌─────────┐
                        │   END   │
                        └─────────┘
```

Figure 19.   Flow Diagram for GNDS

68

```
                         ┌─────────┐
                         │  BEGIN  │
                         └─────────┘
                              │  LOOP OVER iᵗʰ RADIATING
                              │  ELEMENT'S SEGMENTS
         ┌────────────────────┴─────────────────────┐
         │  ADJUST mᵗʰ SEGMENT'S UNIT VECTOR,        │
         │  POSITION VECTOR, AND LENGTH              │
         └────────────────────┬─────────────────────┘
                              │  LOOP OVER jᵗʰ ELEMENT'S SEGMENTS
         ┌────────────────────┴─────────────────────┐
         │  ADJUST nᵗʰ SEGMENT'S UNIT VECTOR,        │
         │  POSITION VECTOR, AND LENGTH              │
         └────────────────────┬─────────────────────┘
                              │  LOOP OVER nᵗʰ SEGMENT AND ITS IMAGE
                              │  ZIMPS
         ┌────────────────────┴─────────────────────┐
         │  COMPUTE "HERTZIAN DIPOLE INTERACTION"    │
         │  BETWEEN nᵗʰ AND mᵗʰ SEGMENTS            │
         └────────────────────┬─────────────────────┘
              ┌───────────────┴────────────────┐
              │  COMPUTE AND ACCUMULATE         │
              │  VOLTAGE ON mᵗʰ SEGMENT         │
              └───────────────┬────────────────┘
     ABSENT ╱────────────────────────────────────╲
       ◄────┤  TEST FOR PRESENCE OF GROUND SCREEN  │
            ╲────────────────────────────────────╱
                              │  PRESENT
              ┌───────────────┴────────────────┐
              │  ADJUST UNIT VECTOR AND POSITION│
              │  VECTOR OF nᵗʰ SEGMENT'S IMAGE  │
              └───────────────┬────────────────┘
                              │  END IMAGE LOOP
                              ●
                              │  END jᵗʰ ELEMENT SEGMENT LOOP
                              │  END iᵗʰ ELEMENT SEGMENT LOOP
                         ┌─────────┐
                         │   END   │
                         └─────────┘
```

Figure 20.   Flow Diagram for VIDCJ

i.e., the array boundaries are parallel to the cell lattice coordinates. Judicious choice of IARY (L,2) by the user when defining cells by array descriptions (as done for FAM) is called for. Note that for irregular arrays IARY (L,3) $\neq$ IARY (L,5), the user may choose IARY (L,2) equal to neither IARY (L,3) or IARY (L,5). Since only IARY (L,2) is used by AOFI in determining the region of influence, several elements in an irregular array would not be tested for location within the region of influence (an irregular array is "regularized"). The user must be aware of this.

A flow diagram of AOFI is given in Figure 21.

3.3.8 CELPAT

This subroutine computes the radiation pattern of a cell described in terms of several arrays. The coding follows the theory of [5, Section 3.4] where "regular" and "irregular" shaped arrays are discussed. The θ and ϕ (global system) components of $\vec{E}$-field that results are normalized by exp $[-jkR]/(4\pi R)$.

A flow diagram of CELPAT is given in Figure 22.

3.3.9 MUTUAL

The array b to array a ground screen penetration mutual impedance z^{ab} is computed in subroutine MUTUAL. The induced short circuit current distribution on the array a reference element also is computed. The coding follows closely the theory in the latter part of Section 2.2. The good conducting screen approximation, $g^t_- = -\hat{z}$, is employed. A flow diagram is given in Figure 23.

3.3.10 ZIMPS

Subroutine ZIMPS computes the moment matrix for an isolated thin wire radiating element over a perfect ground screen. This matrix is needed in the higher approximation method (HAM). An option for removing the ground screen from the computation exists by setting IGSC = 0. The user must not exercise this option, however, in a HAM computation.

The thin wire moment method code, upon which ZIMPS is based, is the code WRSMOM available from NAPS [7]. Since WRSMOM assumes geometry data in

70
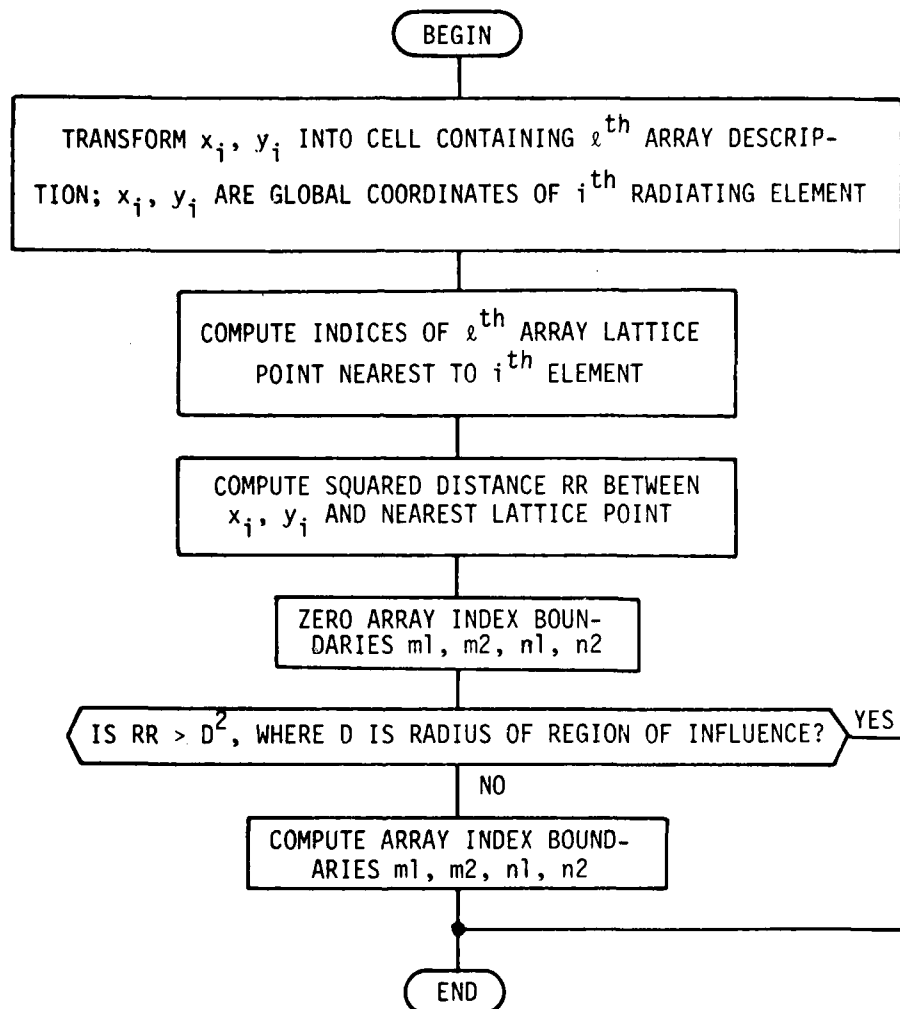
Figure 21.   Flow Diagram for AOFI
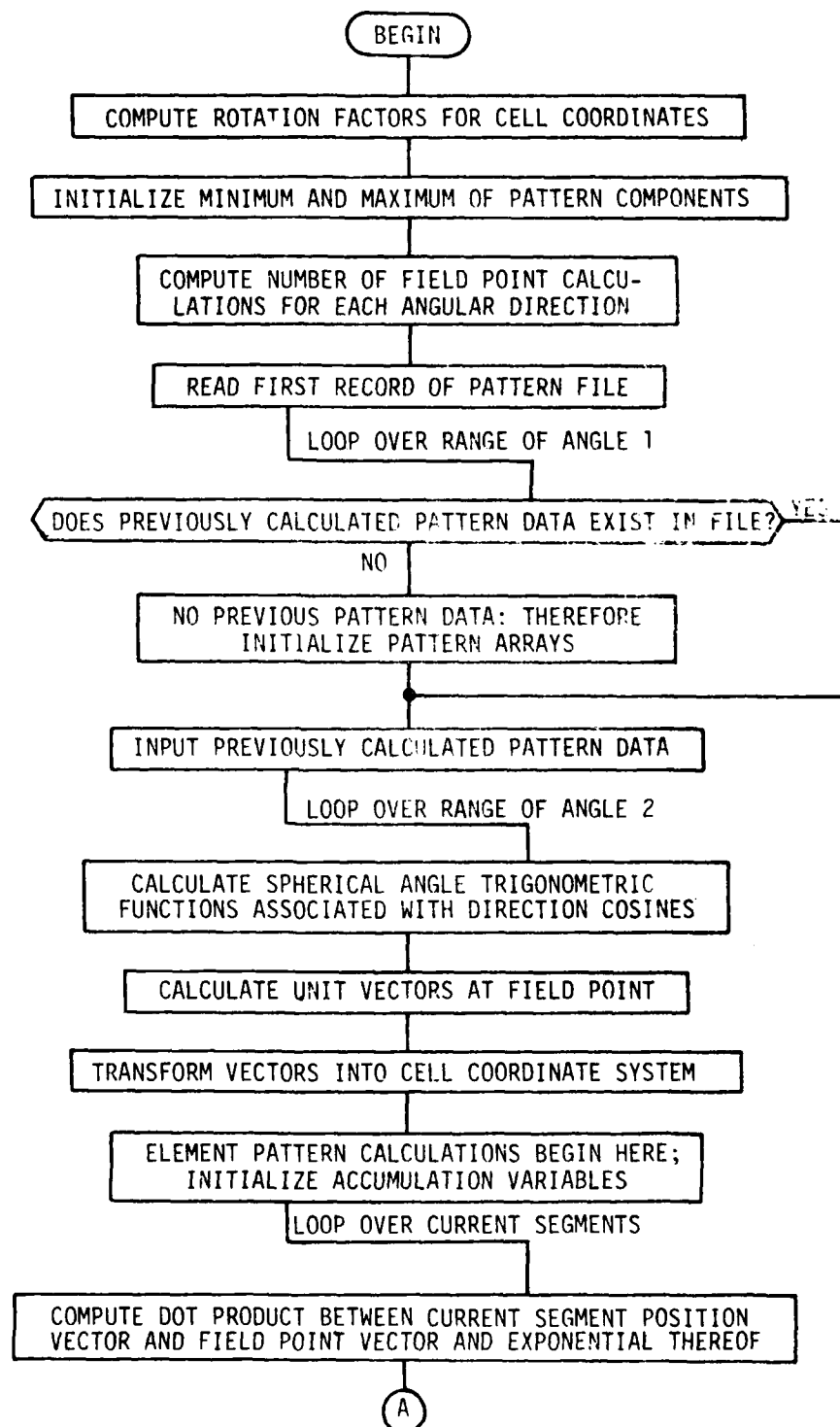
Figure 22. Flow Diagram for CELPAT

Figure 22. Continued

73
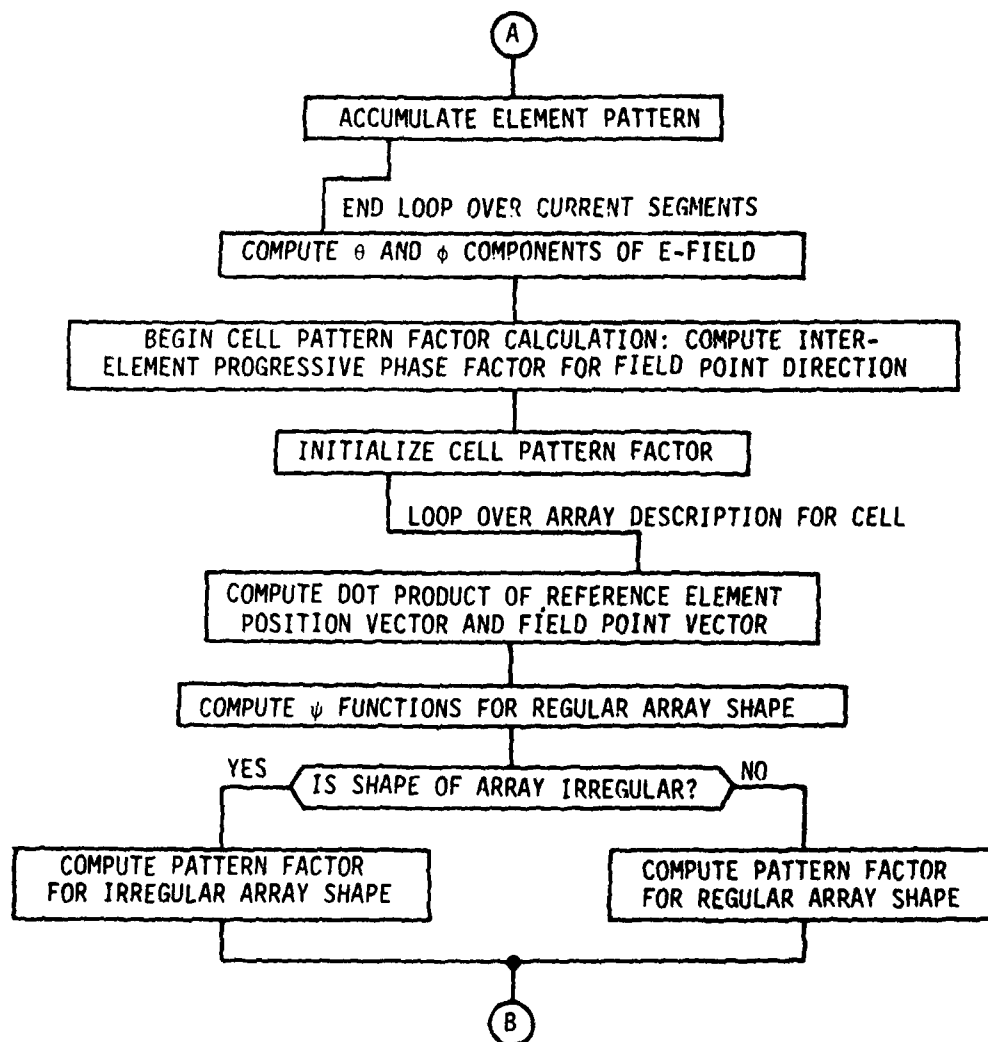
```
                    (B)

        ┌─────────────────────────────────┐
        │  ACCUMULATE CELL PATTERN FACTOR  │
        └─────────────────────────────────┘

              END LOOP OVER ARRAY DESCRIPTIONS
     ┌──────────────────────────────────────┐
     │  STORE FIELD VALUES IN PATTERN ARRAYS │
     └──────────────────────────────────────┘

                END LOOP OVER RANGE OF ANGLE 2
       ┌────────────────────────────────────┐
       │  STORE FIELD VALUES IN PATTERN FILE │
       └────────────────────────────────────┘

                 END LOOP OVER RANGE OF ANGLE 1
      ┌─────────────────────────────────┐
      │  SET FLAG TO INDICATE THAT FILE  │
      │  NOW CONTAINS PATTERN DATA       │
      └─────────────────────────────────┘

                    ( END )
```
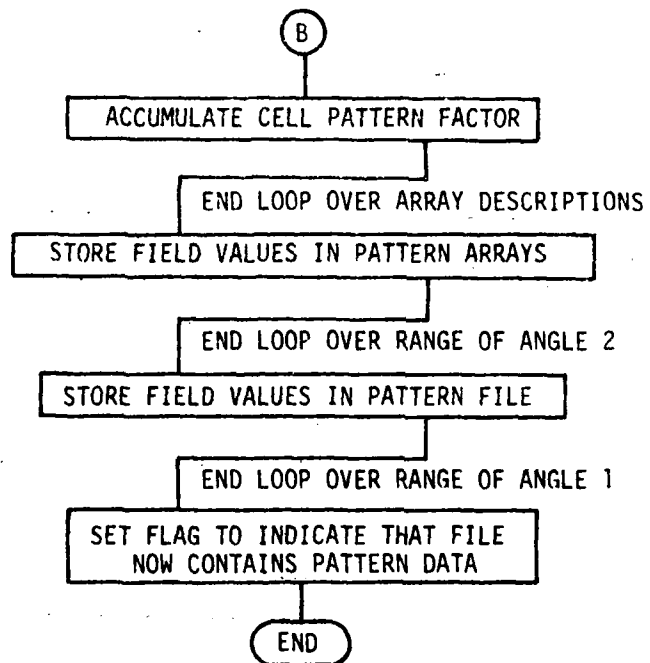
Figure 22. Concluded

74
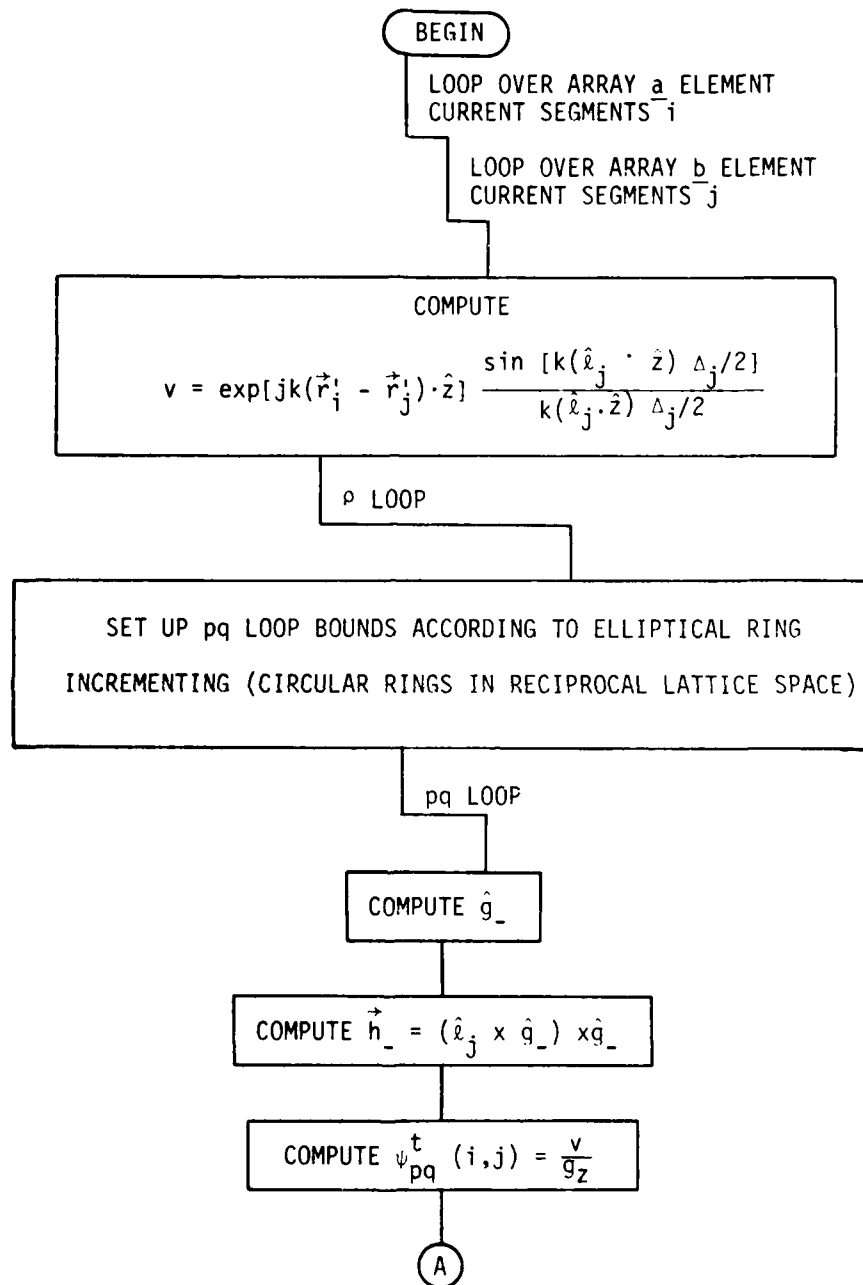
Figure 23. Flow Diagram For MUTUAL
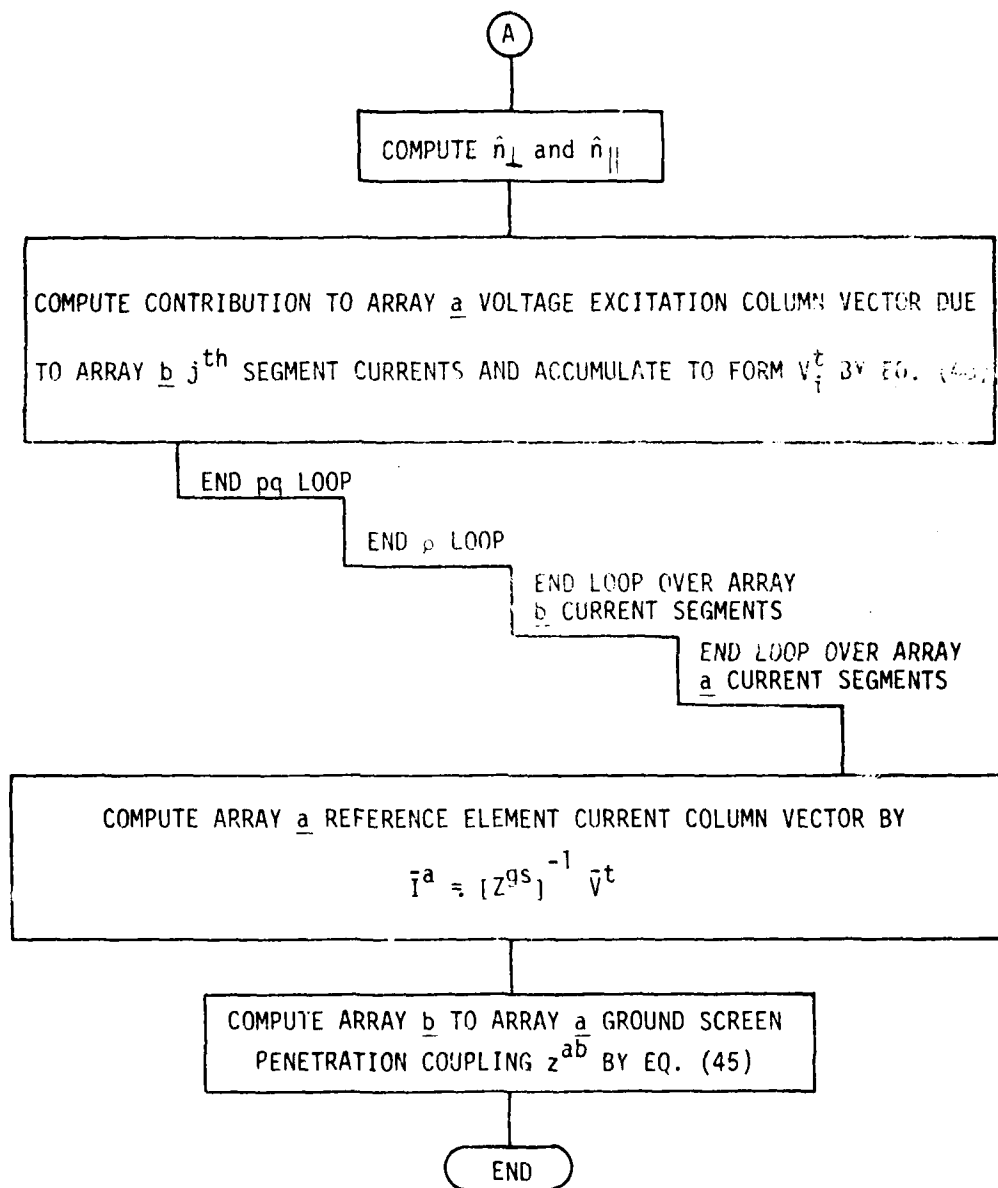
Figure 23. Concluded

wavelengths, this data is converted to wavelengths in ZIMPS. The matrix elements then are computed by calls to subroutines ZIMP2 or ZIMP3. A flow diagram is given in Figure 24.

3.3.11 LENSIN, CELLIN, ARAYIN, GEOMET, TPIN

These subroutines control the input data defining the lens structural and electrical characteristics, lens illumination, software control parameters, and radiation pattern plot format. A user interactive manner is established whereby the program queries the user for each data input.

Subroutine LENSIN requests:

- existence of a radiation pattern file. If "yes", the logical variable FILFG is set equal to TRUE, and pattern data computed is superimposed on the existing pattern data.

- direction cosine limits of pattern calculation. If "12", the y axis direction cosine will vary most rapidly. If "21", the x axis direction cosine will vary most rapidly. Input of the x axis direction cosine minimum, maximum, and increment are followed by those for the y axis direction cosine.

- boom length.

- ground screen transmission coefficients for $\vec{E}$-field perpendicular and parallel to plane of incidence.

Subroutine CELLIN, for each cell, calls ARAYIN and GEOMET and also requests:

- cell ID number, number of plane waves in illumination, and number of feedback modes to be considered in analysis.

- reciprocal lattice space (ρ_x, ρ_y space) minimum, maximum, and incremental radii (ρ_{min}, ρ_{max}, $\Delta\rho$) used in the $\psi(\alpha,\beta)$ summations.

- cell coordinate system origin.

- cell coordinage system rotation relative to global system.

- lattice parameters d_x, d_y, Δ_y.

- cell area via array description (call to ARAYIN).

- characteristics of modules and feedlines to form limited scattering parameter or impedance parameter models.

- array $\underline{a}$ and array $\underline{b}$ radiating element data (call to GEOMET).

Subroutine ARAYIN requests:

- number of array descriptions.

- each array description in terms of number of columns (elements along line parallel to lattice e coordinate), number of rows (elements along line parallel to y coordinate), number of elements in first column (set=0 if array is regular [5, Section 3.4])
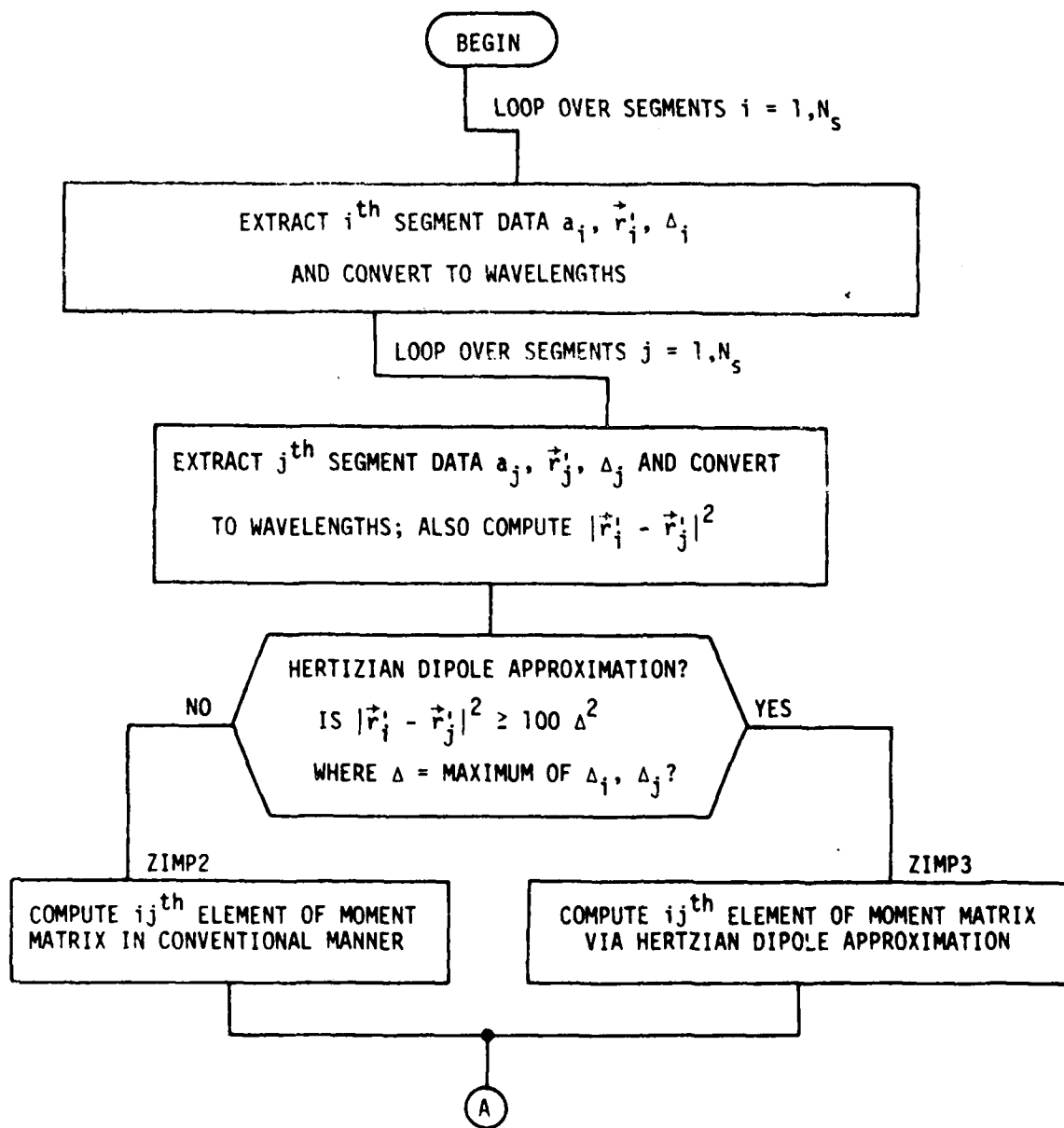
Figure 24. Flow Diagram for ZIMPS
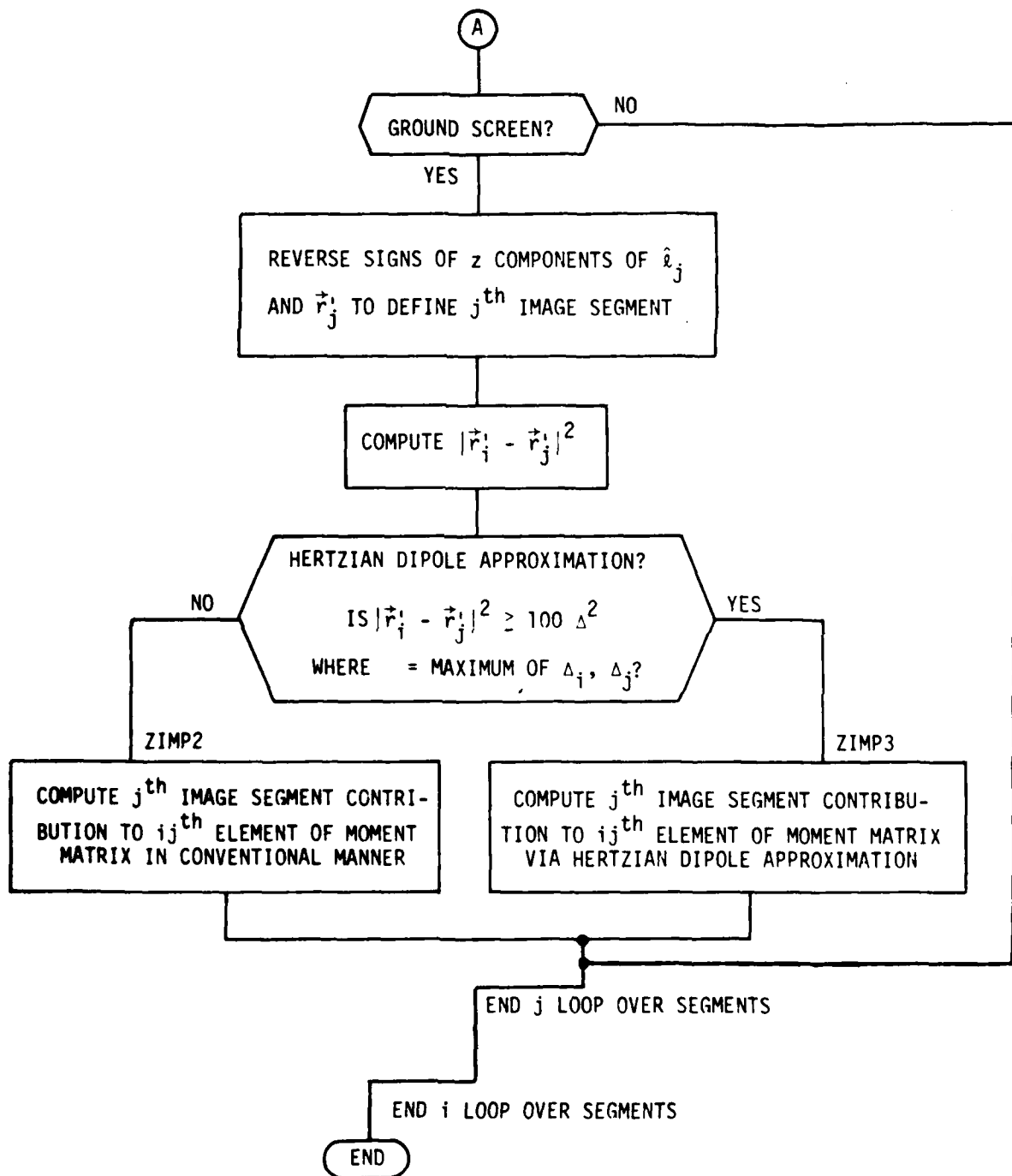
Figure 24. Concluded

number of elements in last column, and sum-subtract code = 1
or -1 (not used in present versions of FAM or HAM).

- cell coordinates of array reference element (must be the "lower
  left hand corner" [5, Figure 3-16]).

- array lattice parameters (may differ from cell lattice param-
  eters d_x, d_y, Δ_y when describing elements for which a higher

  approximation analysis is sought (HAM)).

Subroutine GEOMET requests:

- frequency.

- folded dipole model control parameter ("yes" or "no"). If
  "yes", then folded dipole length and characteristic impedance
  of transmission line mode are entered.

- radiator geometry as a collection of straight wires (follow
  closely [7]). The user provides the number of wires and, for
  each wire, beginning and end point coordinates, radius, con-
  nection code, number of feed points (0 or 1 for present ver-
  sion of FAM - one feed point per radiator), and location of
  feed points. The user must take care that the numbers of
  segments per wire and wire lengths yield nearly uniform seg-
  ment lengths throughout any nondisjoint collection of wires.
  Segment length variations greater than ~1.5:1 are discouraged.
  Also, the algorithm the program uses to segment a wire depends
  somewhat on connection code. If L is the wire length, N_s the
  number of segments, and Δ the segment length then:

no connection:	$\Delta = L/(N_s + 1)$	
one connection:	$\Delta = L/(N_s + 0.5)$	
two connections:	$\Delta = L/N_s$	

  The connection code for a wire that touches the ground screen
  must indicate a connection at that end of the wire.

Subroutine TPIN request, for T-plane radiation pattern plot:

- x axis direction cosine limits.

- y axis direction cosine limits.

- minimum level of field value to be assigned a distinguishing
  plot notation ("FLOOR") and field level increment between
  distinguishing notations.

Subroutine CELLIN computes module progressive phase settings to ac-
commodate beam scanning and focusing. Subroutine GEOMET computes
wavelength, wave number, reference element segment position vectors
(to the segment centers), and segment unit vectors.

80

3.3.12 FEED

Subroutine FEED computes the plane wave illumination of a cell according to

$$\vec{E} = \frac{e^{-jkr}}{r} \left(\frac{\eta P_e}{4\pi}\right)^{\frac{1}{2}} (P_x \hat{x} + P_y \hat{y} + P_z \hat{z})$$

where

x_g, y_g are the global coordinates of the cell coordinate origin (date input)

η = free space wave impedance

P_e = effective radiated power (data input)

L = boom length (data input)

$r = \sqrt{x_g^2 + y_g^2 + L^2}$

P_x, P_y = x and y polarization components (data input)

P_z = z polarization component computed according to

$$P_z = -\frac{P_x s_x + P_y s_y}{s_z}$$

to assure polarization orthogonal to propagation direction. Here, s_x, s_y, s_z are the propagation direction cosines computed according to $s_x = x_g/r$, $s_y = y_g/r$, $s_z = L/r$.

3.3.13 SCAN

Subroutine SCAN computes the scan (active) impedance of an array over a perfect ground screen. Here, the array moment matrix $[Z^{gs}]$ is inverted via LINEQ, the element $y = [Z^{gs}]^{-1}_{i_s, i_s}$ corresponding to the feed port segment i_s is extracted, and the active impedance is given by $z = y^{-1}$.

3.3.14 SCIA, EX

Subroutine SCIA computes, for a cell, the array a reference element short circuit current distribution. All array a ports are short circuited

and the ground screen is present. The excitation is the plane wave illumination as defined in FEED.

Subroutine EX is called by SCIA to compute the voltage excitation, column vector $\overline{V}^{ex,gs}$ according to (40). The reference element short circuit current distribution is then computed by solving (41) with $\overline{V}$ removed. The matrix $[Z^{gs}]$ has been inverted in SCAN via LINEQ. The reference element short circuit port current I_{i_s} is extracted.

3.3.15 PERP

Subroutine PERP computes the ith segment radius vector $\vec{a}_i$ according to the discussion following (38). It the segment is oriented normal to the array plane ($\hat{\ell}_i = \pm\hat{z}$) the double cross product relation for $\vec{a}_i$ is not defined. The $\vec{a}_i$ then is chosen to be $\vec{a}_i = a_i\hat{x}$.

3.3.16 ZCOL

Subroutine ZCOL extracts a specified column from a square matrix.

3.3.17 LINEQ

Subroutine LINEQ inverts a complex matrix.

3.3.18 CEXP, TAN

These function subprograms compute e^x where x is complex (CEXP) and tan (θ) where θ is in radians (TAN). If the real part of $x \leq -70$, e^x is set to zero. If cos (θ) = 0, tan (θ) is set to 10^{32}.

3.3.19 ZIMP2, ZIMP3, HAMPSI

Subroutines ZIMP2 and ZIMP3 and function HAMPSI are minor modifications of coding in the isolated element moment method program WRSMOM [7].

3.3.20 XYGCS

Subroutine XYGCS transforms x, y cell coordinates to lens system (global) coordinates.

3.3.21 TPLANE

Subroutine TPLANE plots the radiation pattern versus x and y directional cosines. Printer characters are used to denote field levels. This routine was written by R. Hancock [8].

SECTION 4

RESULTS

The pulse expansion-point matching-finite difference operator moment method derived in Section 2.2 was applied to the infinite rectangular lattice array of straight halfwave dipoles previously analyzed by Chang [9]. The lattice parameters were $d_x = 0.25\lambda$, $d_y = 1.2\lambda$, and $\Delta y = 0$ (rectangular lattice). The E-plane and H-plane scan active admittances are shown in Figure 25. The excellent agreement compares well with the previous comparison between Chang's results and the pulse expansion-pulse matching moment method originally employed in the lens simulator [5, Figure 5-3]. The finite difference operator method is considerably more efficient also; only 13 segments subdivided a dipole for the finite difference results whereas 21 were required for the pulse matching results. A ρ_{max} of 100 (Section 3.3.3) were used in obtaining the Figure 25 results.

Active impedances and current distributions of infinite arrays of straight and "swept back" dipoles on equilateral triangular lattices also were computed using the lens simulator finite difference moment method discussed in this report. Figure 26 shows a straight halfwave dipole array radiating element (y polarized) a quarter wavelength in front of a perfect ground screen. All dipoles were assumed to be fed through perfect baluns. The radiating nature of the feedlines, then, was that of parasitic scatterers not physically connected to the dipole feed ports. The two types of feedline scatterers modeled are shown in Figure 26. One was a 0.2λ straight feedline and the other a 0.275λ bent feedline. Both feedlines lay parallel to the yz plane (coordinate system of Figure 2 applies). All array elements were located on the equilateral triangular lattice defined by Figure 4 with

$d_x = 0.715\lambda$

$d_y = 0.826\lambda$

$\Delta y = 0.413\lambda$

The H-plane scan active impedance for the array without feedline scatterers is plotted in Figure 27. The effect of the H-plane grating lobe singularity occurring at 23.49° is evident. The ground screen removes the infinity that would otherwise occur at an H-plane grating lobe singularity for straight
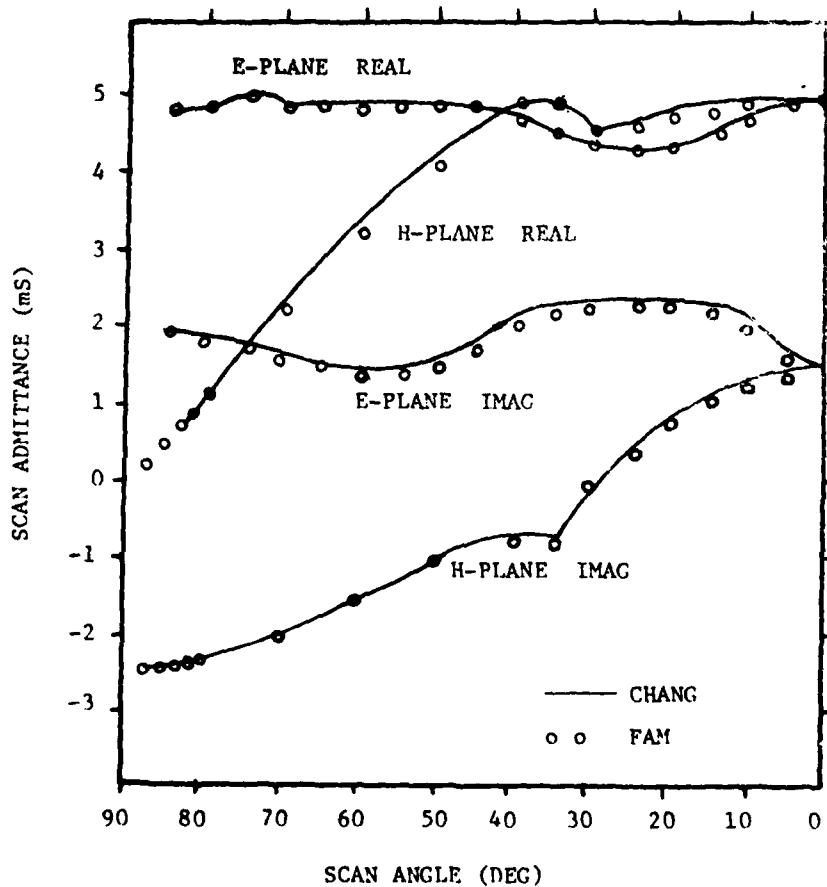
83

Figure 25. Reference Element Active Admittance
for a $\lambda/2$ Dipole Array 0.25λ Above
a Perfect Ground Screen. The Dipole
Radii Are 0.007022λ. The Lattice
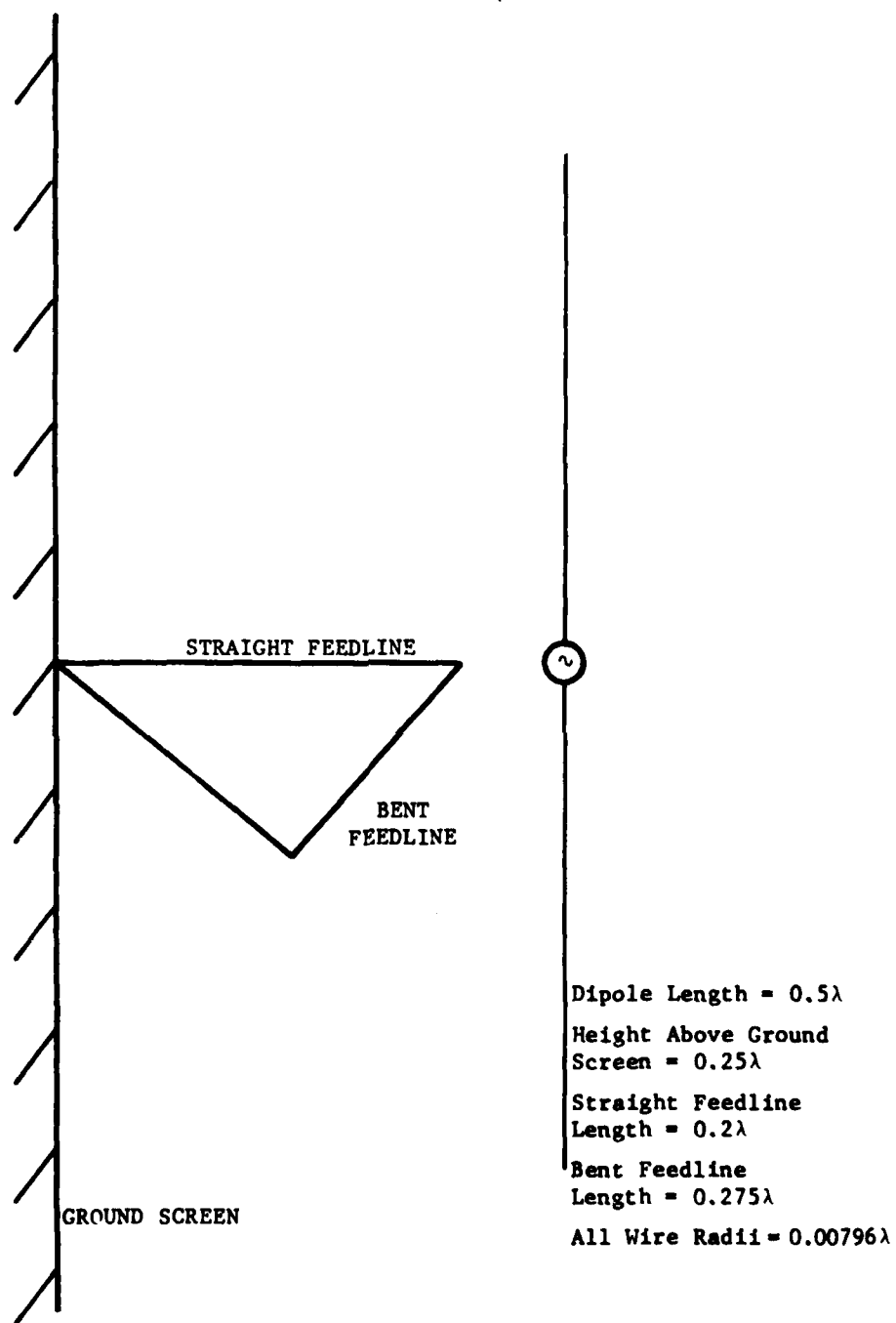Parameters Are $d_x = 0.25\lambda$, $d_y = 1.2\lambda$,
$\Delta y = 0$

STRAIGHT FEEDLINE

BENT
FEEDLINE

GROUND SCREEN

Dipole Length = 0.5λ

Height Above Ground
Screen = 0.25λ

Straight Feedline
Length = 0.2λ

Bent Feedline
Length = 0.275λ

All Wire Radii = 0.00796λ

Figure 26.   Straight Dipole Array Element Above a Perfect
Ground Screen With Either a Straight Feedline
Scatterer or a Bent Feedline Scatterer

85
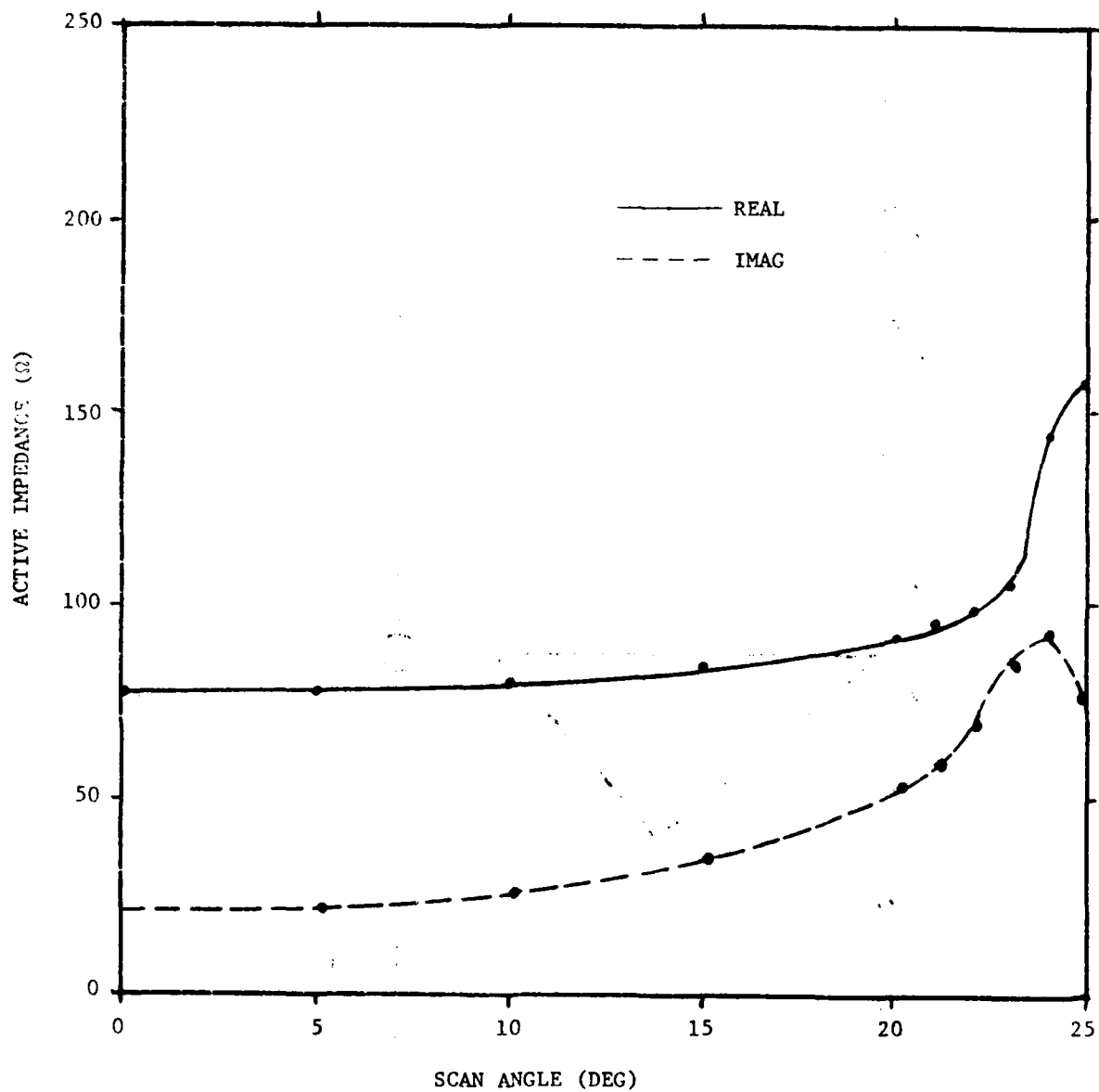
Figure 27. H-Plane Active Impedance of Straight
Dipole Array Without Feedlines

86

dipoles. A similar plot for straight-dipole array with straight feedline scatterers differed very little from Figure 27. The absence of a stronger singularity effect at 23.49° scan likely is a consequence of H-plane scanned $\vec{E}$-field radiated by the dipoles along the array plane being cross polarized with respect to the feedlines.

The E-plane scanned active impedances for the straight-dipole array for the three cases: feedlines absent, straight feedlines, and bent feedlines, are shown in Figure 28. The feedline absent and bent feedline cases appear strongly effected by the E-plane grating lobe singularity occurring at 29.22°. The straight feedline case exhibits rapid impedance variation in the vicinity of 22° scan. The reference element current distributions plotted in Fig- ures 29, 30, and 31 also bear out this behavior. The reactive current on the straight feedline swings widely from capacitive to inductive in scanning from 20° to 25° (Figure 30). The bent feedline current does not demonstrate this behavior.

E-plane scan results for the Figure 32 dipole array without feedlines and with straight feedlines are shown in Figures 33 and 34. Without feedlines, the swept back dipole array active impedance varies less with E-plane scan than does that of the straight-dipole array. The effect of straight feed- lines on the E-plane active impedance is at least as pronounced for the swept back-dipole array as it is for the straight-dipole array.

A ρ_{max} of 50 (Section 3.3.3) was used in obtaining the equilateral lattice results. Sampled computations with ρ_{max} = 100 were within ∿10 per- cent of the ρ_{max} = 50 results. Also 9 segments subdivided the dipoles and 5 segments the feedlines.
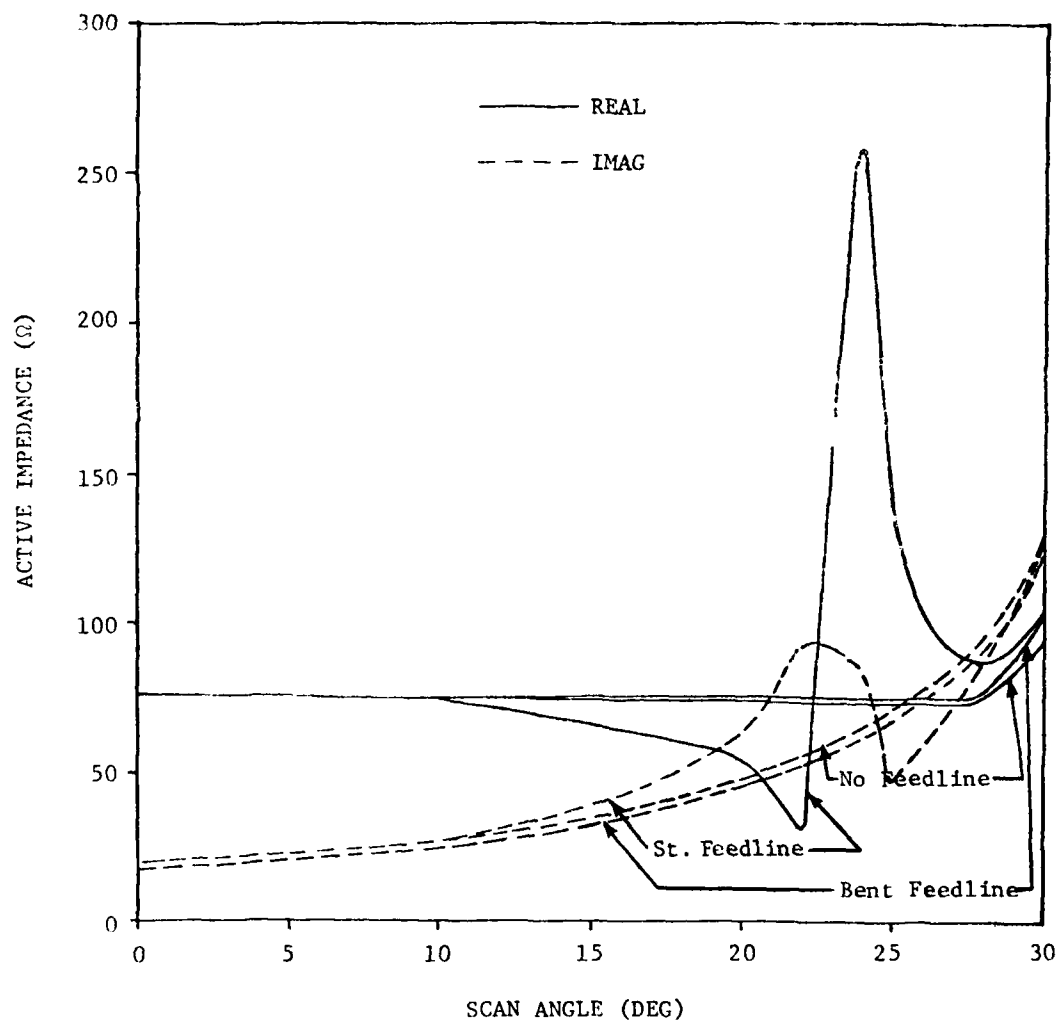
Figure 28. E-Plane Active Impedances of Straight
Dipole Array Without Feedlines, With
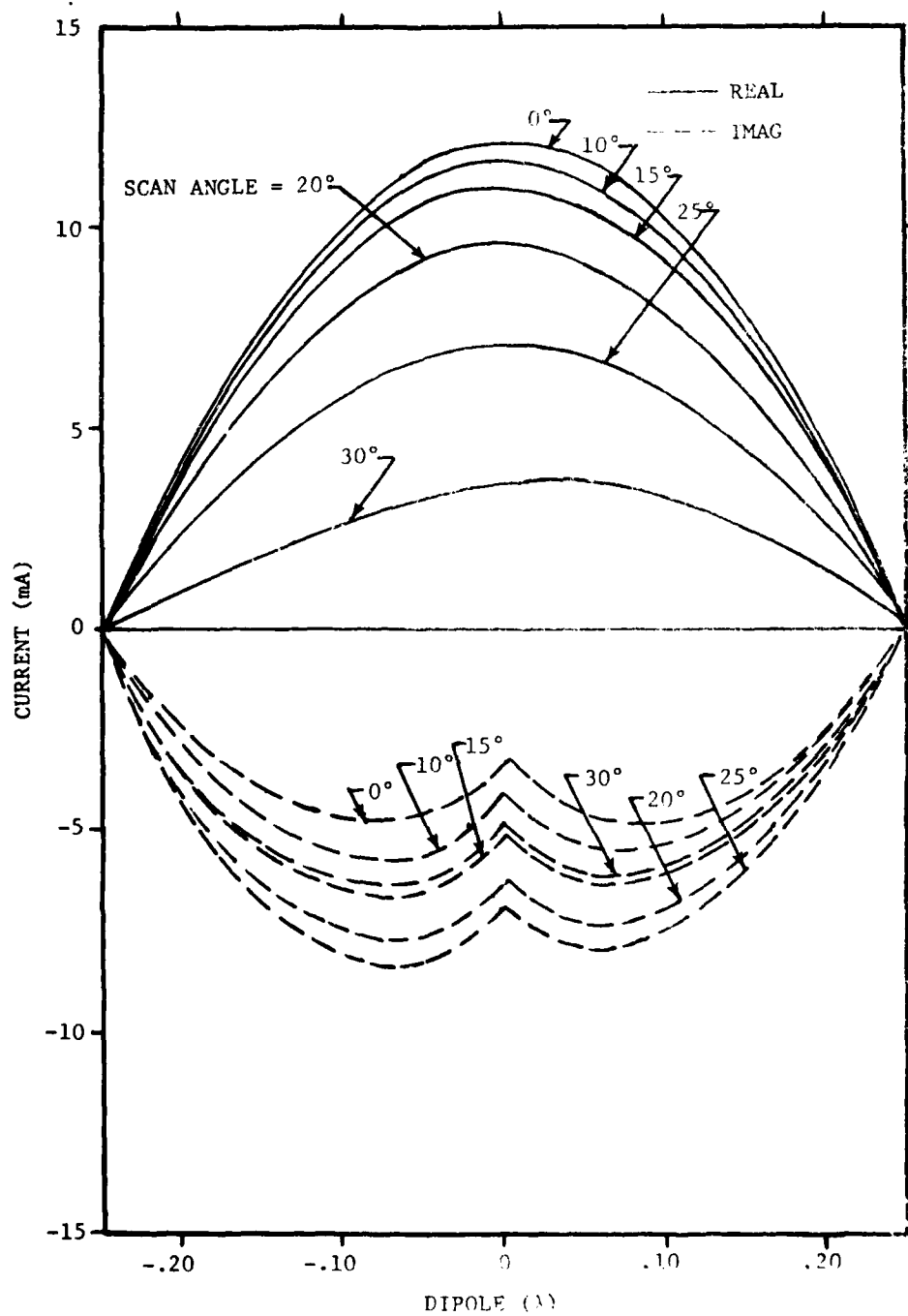Straight Feedlines and With Bent Feed-
lines

Figure 29. Straight Dipole Array Reference Element
Current Distribution: 1 V Source, No
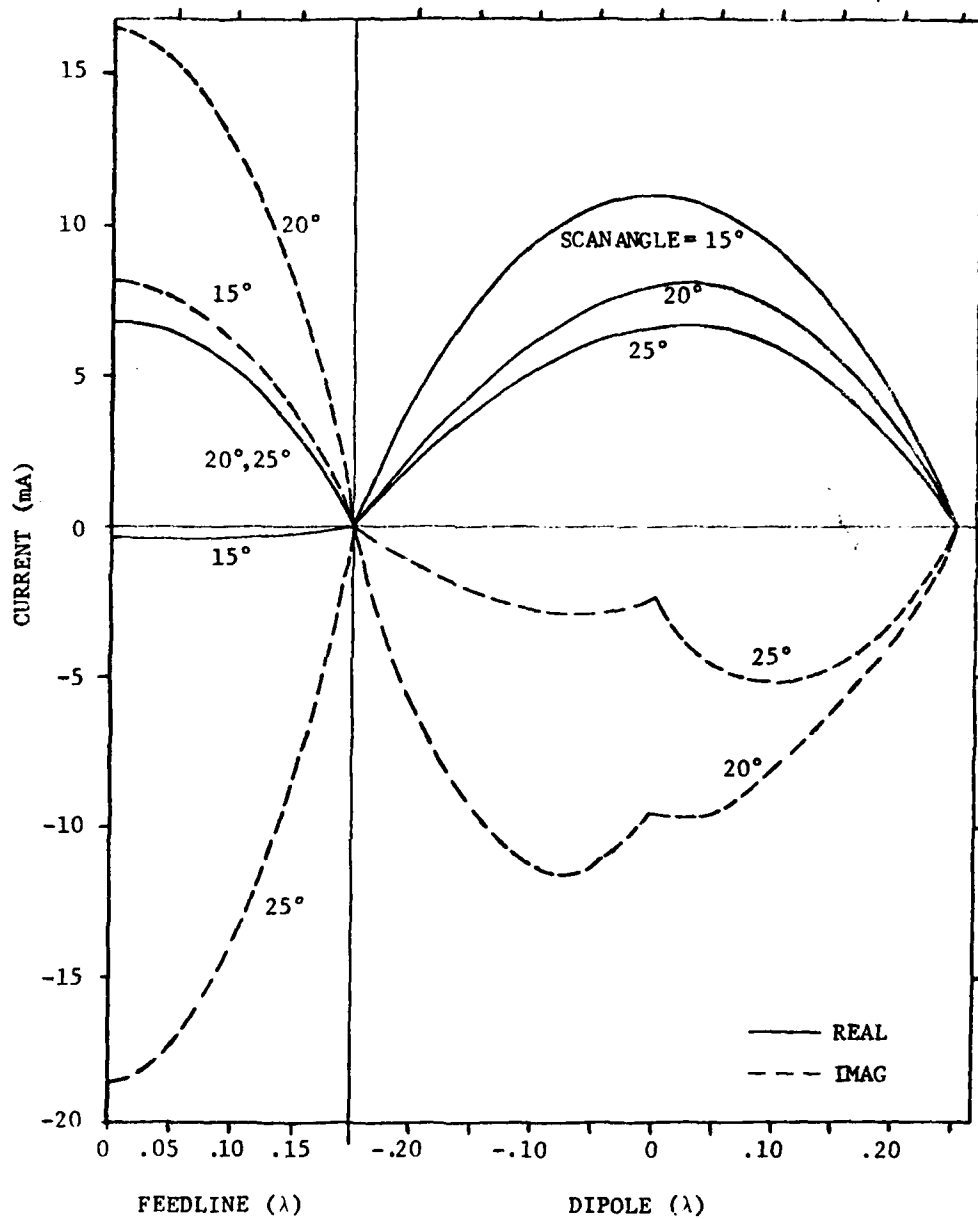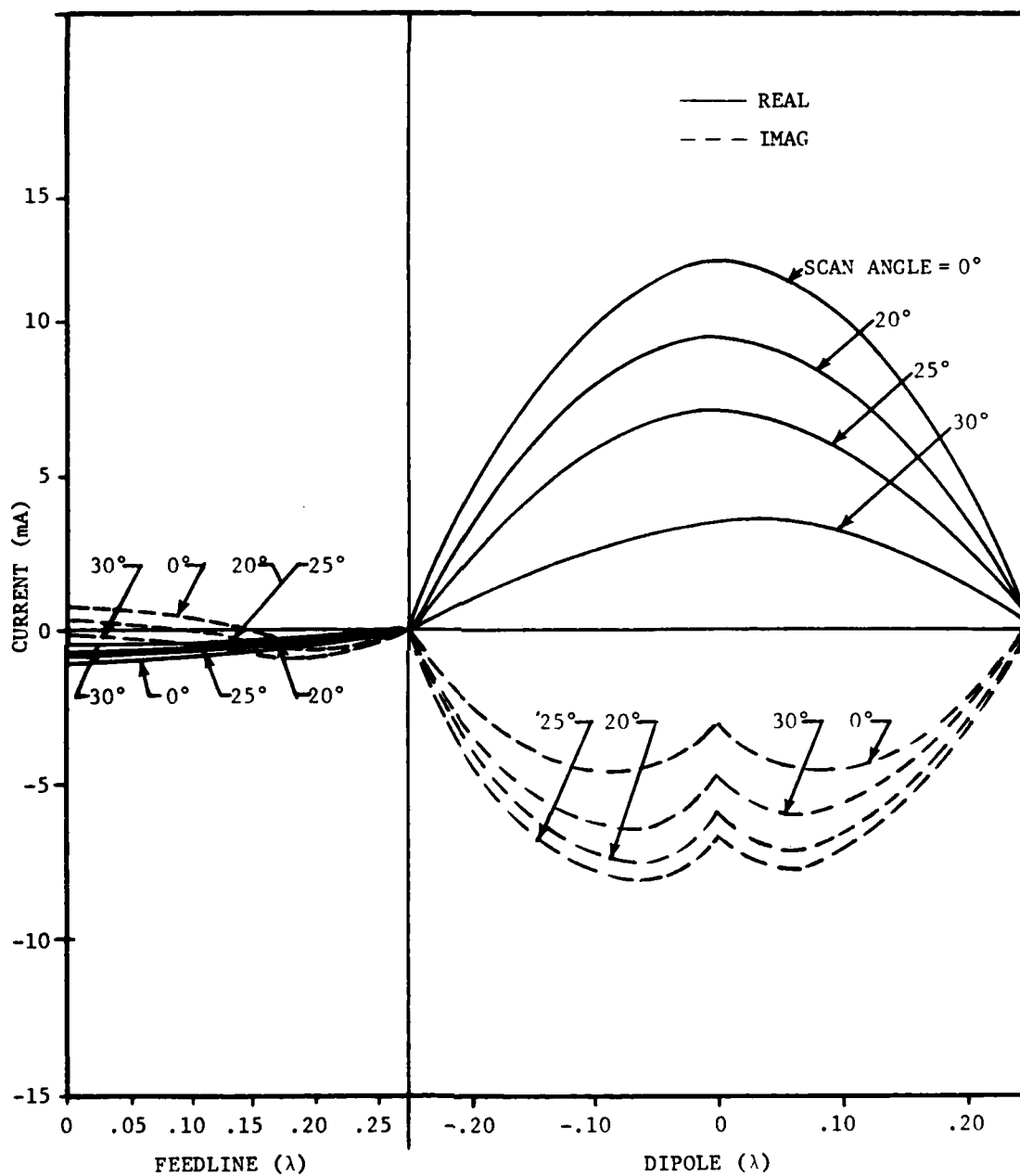Feedlines

Figure 30. Straight Dipole Array Reference Element
Current Distribution: 1 V Source,
Straight Feedlines

Figure 31.   Straight Dipole Array Reference Element Current
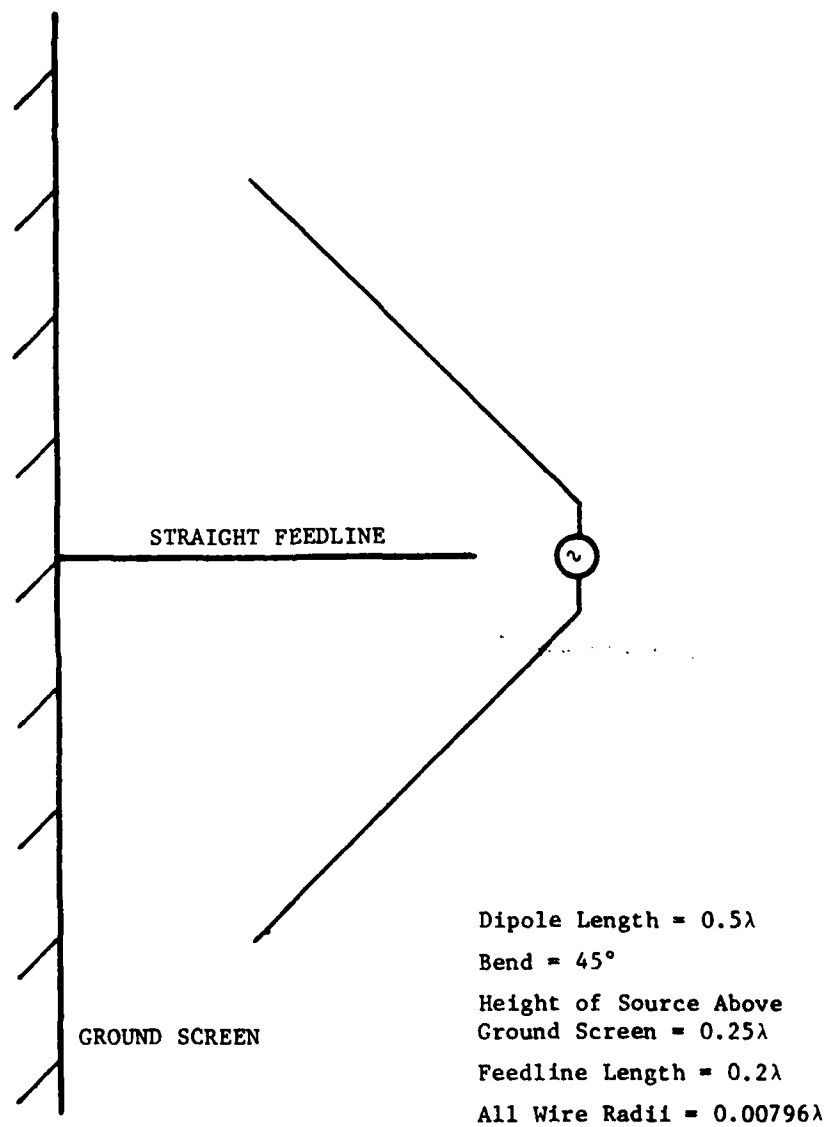Distribution: 1 V Source, Bent Feedlines

91

STRAIGHT FEEDLINE

GROUND SCREEN

Dipole Length = 0.5λ

Bend = 45°

Height of Source Above
Ground Screen = 0.25λ

Feedline Length = 0.2λ

All Wire Radii = 0.00796λ

Figure 32.   Swept Back Dipole Array Element Above a
Perfect Ground Screen With a Straight
Feedline Scatterer
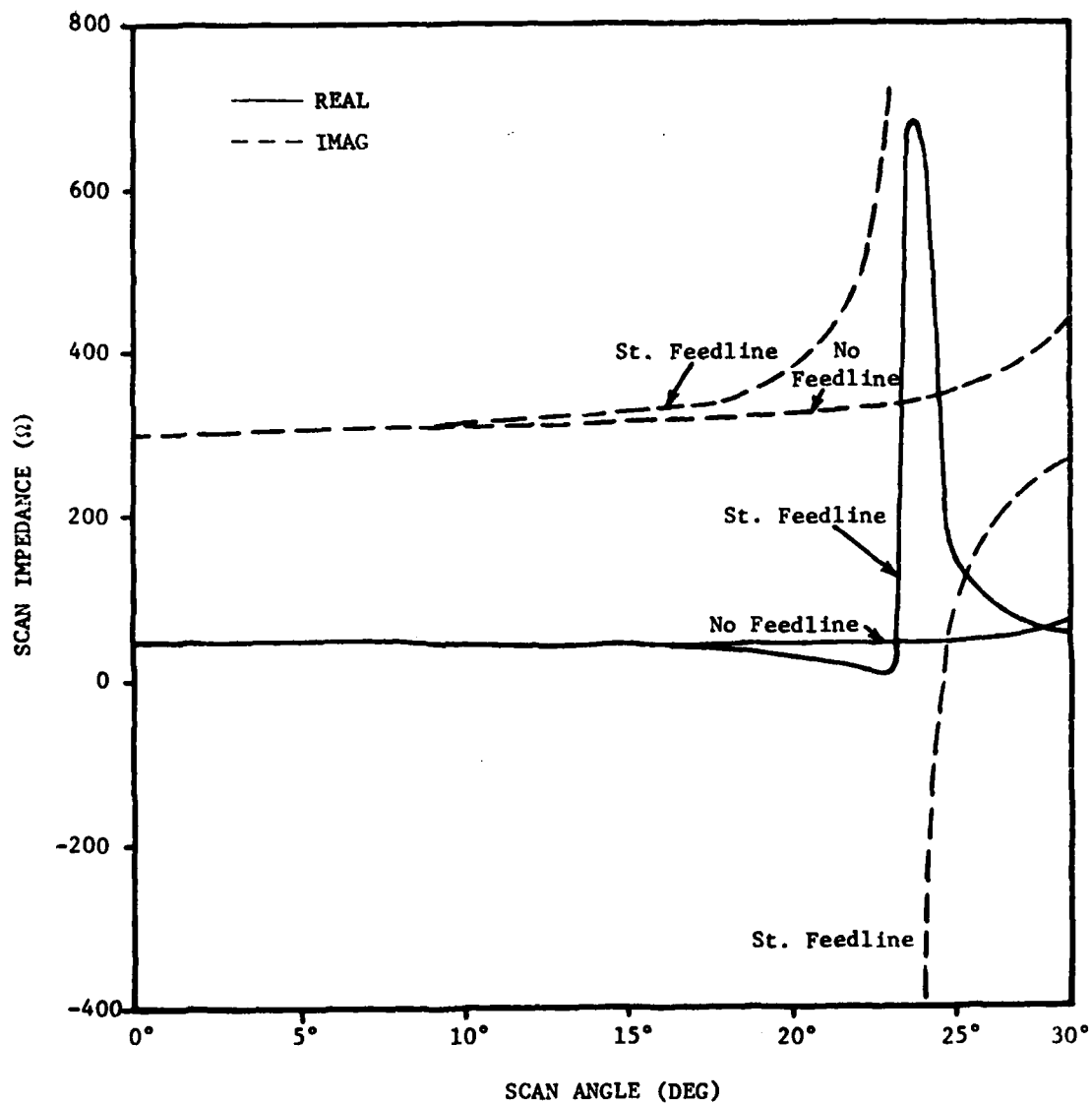
Figure 33.   E-Plane Active Impedances of Swept Back Dipole
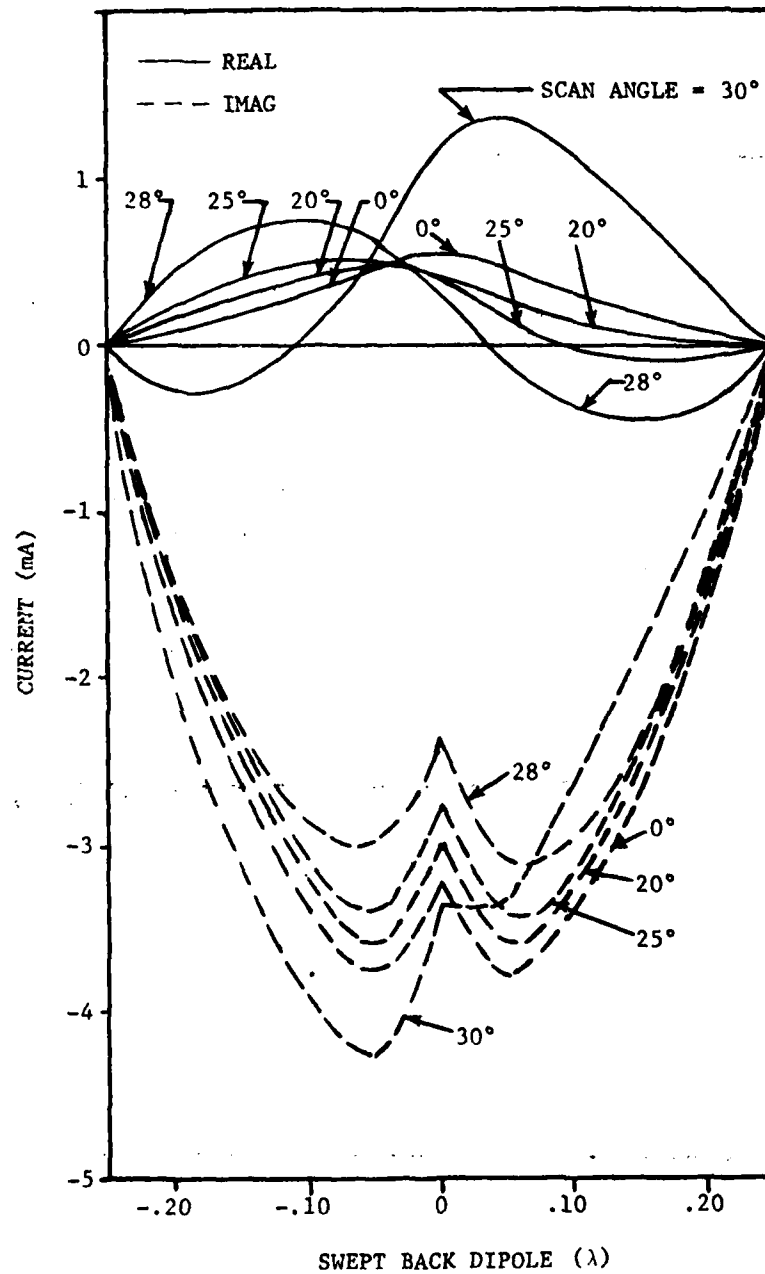Array Without Feedlines and With Straight Feedlines

93

Figure 34. Swept Back Dipole Array Reference
Element Current Distribution: 1 V
Source, No Feedline

94

SECTION 5

REFERENCES

1. B. A. Munk and G. A. Burrell, "Plane-Wave Expansion for Arrays of Arbitrarily Oriented Piecewise Linear Elements and its Application to Determining the Impedance of a Single Linear Antenna in a Lossy Half-Space," IEEE Trans. on Antennas and Propagation, Vol. AP-27, No. 3, pp. 331-343, May 1979.

2. R. F. Harrington, Field Computation by Moment Methods, Macmillian, 1968.

3. R. F. Harrington, Time Harmonic Electromagnetic Fields, McGraw-Hill, 1961, pp. 60-61.

4. T. W. Kornbau, Application of the Plane Wave Expansion Method to Periodic Arrays Having a Skewed Grid Geometry, AFAL-TR-77-112, October 1977.

5. H. Schuman, D. Pflug, L. Thompson, Space-Based Radar Array System Simulation and Validation, Interim Technical Report, Rome Air Development Center, Griffiss AFB, New York, September 1980, RADC-TR-80-294 (A093493).

6. E. A. Wolff, Antenna Analysis, John Wiley and Sons, Inc., New York 1966.

7. D. E. Warren, et.al., "Near Electric and Magnetic Fields of Wire Antennas," (Computer Program Description), IEEE Trans. Ant. Propg., Vol. AP-22, No. 2, p 364, March 1974. (See also NAPS document 02221.)

8. R. Hancock, Simulation Technology Incorporated, P. O. Box 1314, Greenville, Texas 75401, Private Communication, 1981.

9. V. W. H. Chang, "Infinite Phased Dipole Array," Proc. IEEE, Vol. 56, No. 11, pp. 1892-1900, November 1968.

MISSION
of
Rome Air Development Center

RADC plans and executes research, development, test and selected acquisition programs in support of Command, Control Communications and Intelligence (C^3I) activities. Technical and engineering support within areas of technical competence is provided to ESD Program Offices (POs) and other ESD elements. The principal technical mission areas are communications, electromagnetic guidance and control, surveillance of ground and aerospace objects, intelligence data collection and handling, information system technology, ionospheric propagation, solid state sciences, microwave physics and electronic reliability, maintainability and compatibility.